ABSTRACT

Title of Dissertation:	AIR POLLUTION EMISSIONS FROM HIGHWAY VEHICLES: QUANTIFYING IMPACTS OF HUMIDITY, AMBIENT TEMPERATURE, AND COVID-19–RELATED TRAVEL RESTRICTIONS
	Dolly L. Hall-Quinlan, Doctor of Philosophy, 2022
Dissertation directed by:	Professor Russell R. Dickerson, Departments of Atmospheric and Oceanic Science and Department of Chemistry and Biochemistry

Air pollution adversely affects human health and climate at both local and regional scales. With vehicles representing the dominant source of several important air pollutants, more work is needed to improve our understanding of the factors impacting vehicular emissions to further reduce pollution levels. In this dissertation, I use ambient, near-road (NR) observations of nitrogen oxides (NO_x), carbon monoxide (CO), black carbon (BC), carbon dioxide (CO_2), and traffic to characterize vehicular emissions and the influence of weather and traffic patterns. The first part focuses on how vehicular emissions respond to ambient temperature. The second part investigates traffic pattern changes resulting from COVID-19 travel restrictions and the effects on mobile emissions.

Chapter 2 discusses the temperature and specific humidity sensitivity of vehicular NO_x, CO, and CO_2 emissions. Using NR (along Interstate 95) observations during the cold season, I calculated hourly $\Delta CO/\Delta NO_x$, $\Delta CO_2/\Delta NO_x$, and $\Delta CO_2/\Delta CO$ ratios to infer emissions ratios from vehicular exhaust. Chapter 3 builds on this work by extending the temperature analysis to BC emissions using $\Delta BC/\Delta CO$ and $\Delta BC/\Delta CO_2$. Results show a factor of two decrease in NO_x (−5°C to 25°C) and a ~50% increase in BC emissions (−5°C to 20°C). Combined with traffic observations, we trace this effect to diesel-powered trucks. The observed trends are then used to evaluate the temperature sensitivity in modeled mobile emissions. Important public policy decisions regarding air quality often depend on models that generate accurate emissions estimates from various sectors, including mobile sources. The US EPA estimates vehicular emissions for air quality models using the MOtor Vehicle Emissions Simulator (MOVES). Our analysis shows that MOVES underestimates the temperature effect in NO_x emissions and does not adjust BC emissions, indicating that more work is needed to improve the temperature sensitivity in the model.

Chapter 4 examines the impact of changing traffic patterns on I-95 in April 2020 on mobile emissions revealing ~60% fewer on-road cars and ~10% fewer trucks, resulting in faster highway speeds and less stop-and-go traffic. Coupled with an analysis of emission ratios, the results of this study suggest a significant decrease in BC emissions from diesel-powered trucks attributable to improved traffic flow.

AIR POLLUTION EMISSIONS FROM HIGHWAY VEHICLES: QUANTIFYING IMPACTS OF HUMIDITY, AMBIENT TEMPERATURE, AND COVID-19–RELATED TRAVEL RESTRICTIONS

by

Dolly L. Hall-Quinlan

Dissertation submitted to the Faculty of the Graduate School of the
University of Maryland, College Park, in partial fulfillment
of the requirements for the degree of
Doctor of Philosophy
2022

Advisory Committee:
Professor Russell R. Dickerson, Chair/Advisor
Research Scientist Xinrong Ren
Professor Ross J. Salawitch
Associate Professor Timothy Canty
Assistant Research Professor Hao He

Dean's Representative:
Professor Akua Asa-Awuku

Dedication

I dedicate this dissertation to my parents, my husband, and the best group of emotional support animals a human could ever dream of: Waffles, Pancakes, Muffin, and an endless count of hamsters. I am so grateful for their endless support, love, and words of wisdom (or meows) that have guided me every step of the way.

Acknowledgements

First, I want to thank my academic advisor, Russ Dickerson, and all of my research advisors, Xinrong Ren, Ross Salawitch, Tim Canty, and Hao He, for their guidance, support, and dedication to my success in graduate school. Thank you to Jennifer Hains, Acefaw Belay, Joel Dreessen, Ryan Auvil, Aaron Ryan, and Cory Martin for their help with the measurements and analysis. Thank you also to the agencies who have financially supported my work over the years, including the Maryland Department of the Environment and the National Institute of Standards and Technology.

I want to acknowledge the many more people that have been helped me along this journey. Thank you to Huiting Mao and William Winter at the SUNY College of Environmental Science and Forestry for their endless mentoring and guidance that made me want to pursue graduate school in the first place. Thank you to my amazing friends and colleagues at UMD, including Sandra Roberts, Laura McBride, Pamela Wales, Maggie Marvin, Linda Hembeck, Sayantan Sahu, and Doyeon Ahn, for always supporting me. Thank you to my amazing parents, Manuela and Michael, and my husband, Dan Quinlan, for your endless love and encouragement at every step of the way. And lastly, I want to thank my amazing cats, Waffles, Pancakes, and Muffin, for always lending a listening ear…and giving their occasional words of wisdom at dinner time.

Table of Contents

List of Tables

List of Figures

List of Abbreviations and Acronyms

NO_x – Nitrogen Oxides
CO – Carbon Monoxide
BC – Black Carbon
$PM_{2.5}$ – Particulate Matter 2.5
NEI – National Emissions Inventory
US EPA – United States Environmental Protection Agency
NAAQS – National Ambient Air Quality Standards
CAP – Criteria Air Pollutant
DPF – Diesel Particulate Filter
O_3 - Ozone
BWR – Baltimore Washington Region
MOVES – MOtor Vehicle Emissions Simulator
TDC – Top Dead Center
BDC – Bottom Dead Center
CI – Compression Ignition
A/F – Air-to-Fuel Ratio
SI – Spark-Ignited
SCR – Selective Catalytic Reduction
EGR – Exhaust Gas Recirculation
DPF – Diesel Particulate Filter
PFI – Port Fuel Injection
GDI – Gasoline Direct Injection
GPF – Gasoline Particulate Filter
I-95 – Interstate-95
NR – Near-Road
AQS – Air Quality System
API – Advanced Pollution Instrumentation
IR – Infrared
GFC – Gas Filter Correlation
LGR – Los Gatos Research
ATR – Automatic Traffic Recorder
Mph - Miles Per Hour

Chapter 1: Introduction

Nitrogen oxides (NO_x; $NO_x = NO + NO_2$), carbon monoxide (CO), and black carbon (BC) are air pollutants that adversely impact human health (World Health Organization, 2022). Nitrogen oxides and CO also contribute to secondary ozone pollution in the urban (Haagen-Smit et al., 1953; Pusede and Cohen, 2012; Sather and Cavender, 2016) and remote atmosphere (P. J. Crutzen, 1973), and particulate formation (Ng et al., 2007; Xu et al., 2014). Black carbon, a component of fine particulate matter ($PM_{2.5}$) with an aerodynamic diameter of less than 2.5μm, also absorbs radiation and contributes to global warming (Ramanathan and Carmichael, 2008).

Nitrogen oxides, CO, and BC are commonly produced by combustion processes, both anthropogenically and naturally. According to the 2017 National Emissions Inventory (NEI), compiled every three years by the United States Environmental Protection Agency (US EPA), the dominant sources for all three pollutants are motor vehicles and wildfires (data available at https://www.epa.gov/air-emissions-inventories/2017-national-emissions-inventory-nei-data). Nitrogen oxides are also emitted naturally by microbial processes from vegetation and soils as well as lightning.

Ambient pollutants are regulated by the US EPA. Early federal regulation into air pollution began in 1955 with the enactment of the Air Pollution Control Act and was expanded to include air pollution control with the Clean Air Act of 1963 (US EPA, 2021a). Major revisions were implemented in the Clean Air Act of 1970,

including the development of the National Ambient Air Quality Standards (NAAQS) that set limits for key air pollutants. Since their initial enactment, the NAAQS have led to improvements in air quality within the US by reducing ambient concentrations of criteria air pollutants (CAPs). Currently, the national standard for the ambient NO_2 mixing ratio is set at 100 ppbv (one-hour average), for CO mixing ratios at 35 ppmv (one-hour average), and $PM_{2.5}$ concentrations at 12.0 μg m^{-3} (annual mean averaged over three years; US EPA, 2021b).

Reductions in the ambient concentrations of key air pollutants have occurred over the past several decades in response to widespread implementation of emission control measures (Hassler et al., 2016; McDonald et al., 2012). The use of catalytic converters in motor vehicles has led to significant reductions in NO_x, volatile organic compounds (VOCs), and CO emissions, while the installation of low-NO_x burners in stationary sources has also decreased NO_x production. Control strategies specifically targeting $PM_{2.5}$ include electrostatic precipitators and PM cyclones on stationary sources, and diesel particulate filters (DPF) in motor vehicles (Tucker, 2000). The trend in the national-average ambient NO_2, CO, and $PM_{2.5}$ levels over the past several decades is shown in Figure 1.1; national-average NO_2 and CO decreased by 64% from 1980 to 2020, while $PM_{2.5}$ decreased by 41% from 2000 to 2020 (Figure 1.1). Although most of the US is well below the NAAQS set for CO, ambient NO_2 and $PM_{2.5}$ abundances still have the potential to reach unhealthy levels near major sources, such as highways.

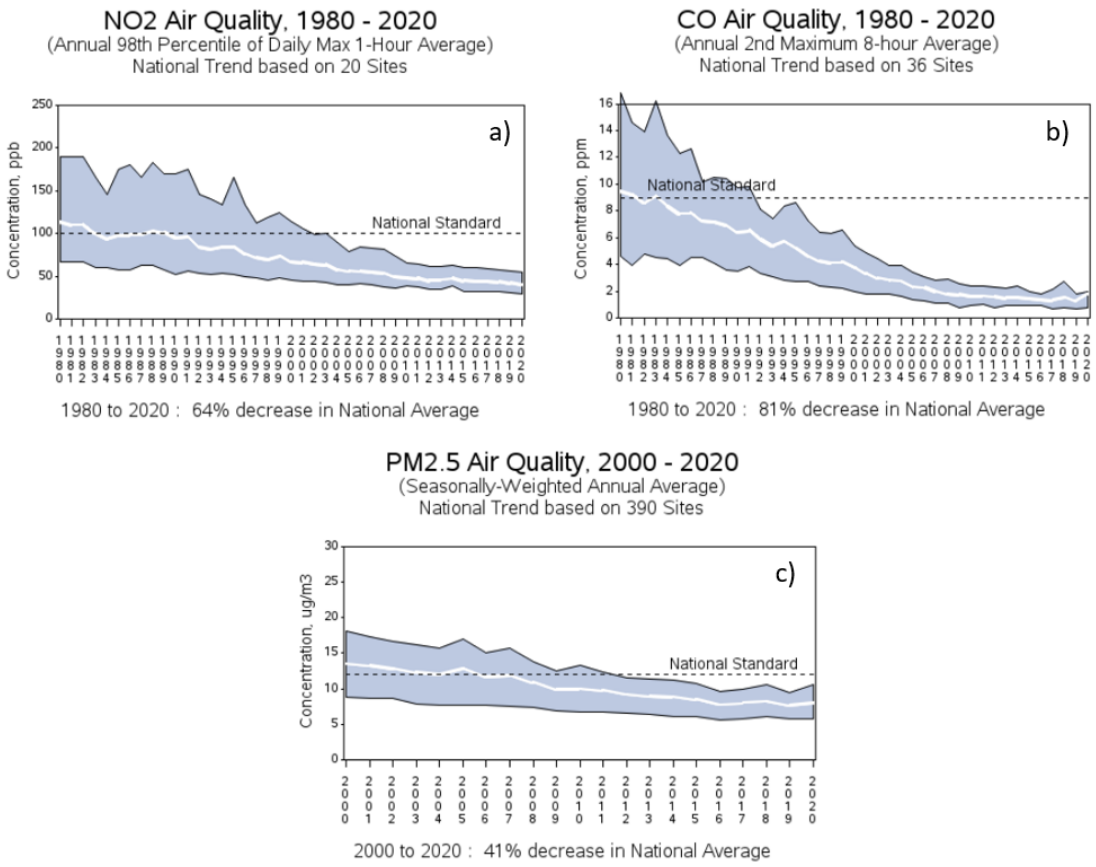

Figure 1.1. Historic trends in the national-average surface-level abundance of ambient NO_x (a), CO (b), and $PM_{2.5}$ (c). Figures available at https://www.epa.gov/air-trends.

Tropospheric ozone (O_3), one of the seven criteria air pollutants regulated by the US EPA for its adverse impacts on public health, is produced secondarily through chemical reactions in the atmosphere. Both CO and NO_x are precursors to surface-level O_3 formation. While reductions in its precursors have generally led to a decline in ambient O_3 levels across the US (H. He et al., 2013; Sather and Cavender, 2016; US EPA, 2021c), some cities and areas, including parts of Maryland, continue to struggle with attainment of the current 70 ppbv NAAQS set

for eight-hour average O_3. These areas are classified as being in nonattainment of the standard and must devise plans to reach attainment.

Ambient concentrations of air pollutants including O_3 are simulated using computer models, such as the EPA Community Multiscale Air Quality (CMAQ) model. These models rely on accurate emissions estimates from a variety of sectors, including vehicular emissions. As detailed below, recent studies suggest that there is a discrepancy in measured and modeled NO_x and BC emissions. With mobile sources representing the largest emitter of anthropogenic NO_x and BC, inconsistencies between the NEI and observations warrant further investigation into emissions from the mobile sector.

In the remainder of this chapter, I will first provide an overview of the motivation for the research in this dissertation, then focus on mobile emissions and the mechanisms that produce and control air pollutant emissions from vehicles. Next, I will describe the observations used in this dissertation and how mobile emissions are inferred from ambient air measurements. The last section of the Introduction provides an overview and discussion of the scope of the dissertation.

1.1. Motivation

1.1.1 Ambient Temperature and Mobile Emissions

The NEI is developed using pollutant emissions data provided by state and local agencies for various sectors including fires and stationary area, point, nonpoint, on-road, and non-road sources. The Sparse Matrix Operator Kernel Emissions

(SMOKE) modeling system is used to apportion emissions data from the NEI and Canadian, Mexican, and offshore inventories, into spatially and temporally gridded emissions by chemical species used by air quality models (Reff et al., 2020).

The dependability of air quality simulations and forecasts depends on the accuracy of the emissions input. Recent studies reveal substantial discrepancies in measured and modeled mobile NO_x emissions; the NEI appears to have overestimated mobile NO_x emissions compared to observations, especially in the summer (Anderson et al., 2014; Li et al., 2018; Mao et al., 2018; McDonald et al., 2012; Qin et al., 2019; Travis et al., 2016; Wang et al., 2019). In contrast to these findings, wintertime observations in the Baltimore Washington Region (BWR) showed good agreement in NO_x emissions with the NEI (Salmon et al., 2018).

In addition to the inconsistencies in NO_x emissions reported in the literature, ambient BC levels have previously been found to be underestimated by CMAQ in the summer and consistent with observations in the winter (Appel et al., 2008). While seasonal concentrations of BC are affected by several factors including changing planetary boundary layer height, they may also be impacted by variations in the strength of sources and sinks. Contrary to the general seasonal cycle of other air pollutants also emitted by vehicles, ambient BC concentrations measured at Fort Meade, MD, a site influenced by vehicular emissions, showed no discernible seasonal cycle (Chen et al., 2001). Studying co-variations in pollutants, such as through emission ratios, is a useful way to minimize the effects of changing planetary boundary layer heights on atmospheric species. Chen et al. (2001) also examined inferred $\Delta BC/\Delta CO$ emission ratios and found the highest emission ratios

at the warmest temperatures and during the summer, and lowest emission ratios at the coolest temperatures and during the winter. The authors attributed the absence of a seasonal cycle in BC concentrations and higher summertime ΔBC/ΔCO emission ratios to greater BC source strength in the summertime, possibly by diesel vehicles (Chen et al., 2001). Diesel exhaust is a significant source of ambient BC and a temperature sensitivity in vehicular BC may contribute to the underestimation of modeled summertime BC concentrations.

The seasonal variability in the overestimation of NO_x and the underestimation of BC suggests that the discrepancies may be seasonally, and thus temperature, sensitive. With motor vehicles representing the largest anthropogenic source of BC and NO_x according to the 2017 NEI, vehicles are a likely source for the disagreement between measured and modeled BC.

On- and off-road vehicular emissions within the NEI are estimated using a tool that integrates the MOtor Vehicle Emissions Simulator (MOVES) into SMOKE. Neither the current version (MOVES3) or the previous version (MOVES2014) of MOVES (when employed as recommended) incorporates a temperature sensitivity for hot-running (engine properly warmed up) NO_x emissions. While MOVES3 lacks a temperature adjustment for running BC emissions, MOVES2014b, the version used for the 2017 NEI, only incorporates a slight adjustment for gasoline vehicles of model year 2004 and earlier. This provides us motivation to investigate the impact of temperature on mobile emissions of CO, NO_x, and BC inferred from NR observations. The temperature sensitivity of

vehicular NO_x, CO, and BC emissions will be explored in greater detail in Chapters 2 and 3.

1.1.2 Traffic Impacts Resulting From the COVID-19 State of Emergency

Vehicular emissions depend on a variety of factors. The type, number, and speed of vehicles driving on roads, as well as the amount of traffic congestion and type of exhaust aftertreatment used by vehicles, affect emissions of pollutants by the vehicle fleet. Emergency measures were implemented in March 2020 to curtail the spread of COVID-19. In Maryland, a mandatory telework order for non-essential employees went into effect on 13 March 2020 and a stay-at-home order was issued on 30 March 2020. These events led to strong reductions in the total number of vehicles driving on roads, and inadvertently provided researchers with an interesting scenario to examine how vehicular emissions respond to sudden decreases in on-road traffic. Such studies, including the work presented in Chapter 4 of this dissertation, can provide guidance for future policy decisions on how to further reduce air pollution from a major source: vehicles.

1.2. Production and Control of Emissions from Motor Vehicles

The focus of this dissertation is to investigate vehicular emissions and how they respond to various factors such as temperature, vehicular speed, and traffic flow. In the following sections I will discuss how motor vehicles operate and how their emissions are both produced and controlled in compression- and spark-ignited vehicles.

1.2.1. The Four-Stroke Internal Combustion Engine

Motor vehicles are driven by an internal combustion engine that contains one or several engine cylinders. Each of these cylinders acts as an internal combustion chamber in which the movement of a piston, crankshaft, and many other parts and gears work in harmony to drive a vehicle. The number of cylinders within an engine depend on the power demand of the vehicle. Gasoline cars generally have four to six cylinders, while diesel trucks have six to eight. Power that drives most vehicles is produced through the four-stroke cycle, discussed here. In sequence, these four strokes are intake, compression, power, and exhaust.

The cycle begins with the piston located at the top of the combustion chamber in a position called top dead center (TDC). The intake valve is opened at the beginning of the intake stroke so that as the piston moves downward, air or an air-fuel mixture enters the combustion chamber. Once the piston is at its lowest position in the chamber, called bottom dead center (BDC), the intake valve closes and the compression step begins. With the intake and exhaust valves closed and the piston moving towards TDC, air is compressed within the chamber. The ignition of fuel, whether diesel or gasoline, happens when the piston is near the top of the chamber and the air (or air-fuel blend) has been compressed. Details on the two types of fuel ignition, compression and spark, are discussed in the following sections.

The actual energy that drives the vehicle is produced in the third part of the cycle, called the power stroke. Here, the pressure created by the gases produced from combustion pushes the piston down to BDC. Finally, the exhaust valve opens

so that combustion gases are pushed out of the chamber by the piston on its way up to TDC. The cycle repeats once the piston is back at TDC and the exhaust valve has been closed (de Nevers, 2010).

1.2.2. Compression-Ignited Vehicles

Vehicles running on diesel fuel generally use the four-stroke mechanism and initiate combustion during the power stroke through compression-ignition (CI). Air enters the combustion chamber during the intake step and is compressed to 1/16 to $1/20^{th}$ of its initial volume. This level of compression results in a rapid increase in the air temperature above the autoignition point for diesel fuel (~ 400°F or 205°C), resulting in spontaneous ignition of the diesel fuel that is injected directly into the chamber during this step. Diesel fuel is typically composed of hydrocarbons (HC) containing between 8 and 25 carbon atoms ($C_8 – C_{25}$), while gasoline consists of HCs with 4 to 12 carbon atoms ($C_4 – C_{12}$). The larger HCs contained within diesel fuel lead to ~15 % more energy per unit volume of fuel than in gasoline, making diesel a suitable fuel for use in vehicles that require high power or long range (U.S. Department of Energy, 2021).

The air-to-fuel ratio (A/F) quantifies the mass of air relative to the mass of fuel within the combustion chamber. The stoichiometric ratio, or the ratio representing the ideal balance between air and fuel needed for complete combustion, varies depending on the number of carbon and hydrogen atoms in a hydrocarbon. Using Equation 1.1, the stoichiometric A/F ratio for an average formula representing

diesel fuel ($C_{12}H_{23}$) is 14.6, indicating that 14.6 grams of air are required to fully combust 1 gram of this diesel fuel (Equation 1.1).

$$C_{12}H_{23} + 17.75\ O_2 \rightarrow 12\ CO_2 + 11.5\ H_2O \quad \text{(Equation 1.1)}$$

Engines are said to run "fuel-lean" when there is an excess of air relative to fuel in the mixture, and "fuel-rich" when there is a deficit in air needed to fully combust the fuel.

The amount of energy produced in a diesel engine is controlled by adjusting the amount of fuel dispensed into the combustion chamber. Unlike gasoline engines, the amount of air entering the chamber is relatively constant, causing diesel engines to operate fuel-lean. The combined effect of higher compression and A/F ratios yield a higher thermal efficiency (the amount of useable energy produced relative to the amount of energy contained within a given amount of fuel) in diesel engines compared to gasoline engines (discussed in the next section), and higher tailpipe NO_x emissions if left uncontrolled.

Despite the number of benefits, including higher fuel and thermal efficiency compared to gasoline vehicles, diesel engines struggle with high NO_x and BC emissions. Nitrogen oxide (NO) is produced during combustion following the simplified Zeldovich mechanism below (Zeldovich, 1946):

$$O_2 + N_2 \leftrightarrow 2NO \quad \text{(Equation 1.2)}$$

The production of thermal NO is dependent on peak combustion temperature and increases rapidly for peak temperatures greater than 2000°F (1093°C; de Nevers, 2010). These high temperatures are conducive for the formation of O and N radicals (Equations 1.3 and 1.4) that go on to produce NO with N_2 and O_2 (Equations 1.5 and

1.6). The amount of NO produced in an IC engine also depends on the amount of O_2 relative to fuel in the combustion chamber (AF ratio), as a fuel-lean mixture leads to higher NO production (Equations 1.5-1.6). The high AF ratio (fuel-lean) in CI engines is one of the reasons why NO formation is higher in CI vehicles than in spark-ignited (SI) vehicles.

$$N_2 \leftrightarrow 2N \quad \text{(Equation 1.3)}$$
$$O_2 \leftrightarrow 2O \quad \text{(Equation 1.4)}$$
$$2N + O_2 \leftrightarrow 2NO \quad \text{(Equation 1.5)}$$
$$2O + N_2 \leftrightarrow 2NO \quad \text{(Equation 1.6)}$$

Black carbon is a byproduct of incomplete combustion produced in higher quantities by CI engines than SI engines. Since fuel in a CI engine is injected directly into the compressed air, the fuel does not have the chance to thoroughly mix with the compressed air before combustion. This results in fuel-rich pockets forming within the combustion chamber that produce elevated BC emissions relative to premixed air-fuel mixtures.

Vehicle acceleration is known to impact BC emissions from CI vehicles, including trucks. Heavy traffic congestion, with frequent acceleration, produces higher tailpipe BC emissions than driving at highway speeds (Giakoumis and Zachiotis, 2021; Rakopoulos and Giakoumis, 2009). During acceleration, more fuel is needed to supply sufficient power to the vehicle. Most compression-ignited vehicles contain a turbocharger used to quickly compress and pump additional air into the engine to balance the excess fuel that is required to provide more power (Figure 1.2). Higher engine-out air pressure, resulting from combustion with increased fuel, drives a turbine in the turbocharger that also spins a turbine in the air

intake and compresses the incoming air. A momentary lag, known as turbocharger lag, results from the difference in the time excess fuel is added to the cylinders and the time when enough engine-out air pressure has built up to supply additional air to the engines. Turbocharger lag results in excess BC emissions because of the addition of extra fuel to already fuel-rich pockets within the combustion chambers.

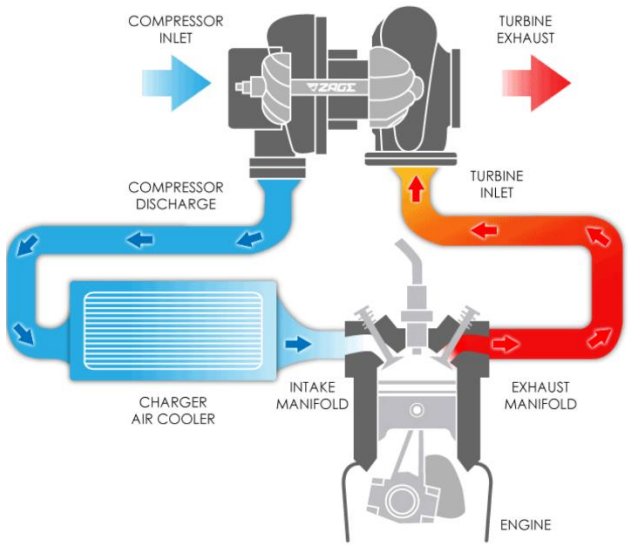

Figure 1.2. A simplified diagram of a typical turbocharger on a spark ignited engine. Image from https://www.turbodynamics.co.uk/technical/understanding-turbochargers/.

Several control strategies exist to reduce the amount of air pollutants released by CI vehicles. Pollutants may be reduced during combustion, post-combustion, and through changing the fuel composition (ultra-low-sulfur diesel fuel, for example). Reducing emissions during combustion often requires altering the conditions under which the fuel combustion occurs. An example of a control method used to reduce NO_x in the combustion chamber is exhaust gas recirculation (EGR). In this method, a portion of the exhaust gas, low in O_2 and relatively high in CO_2, N_2O, and N_2, is

recirculated back into the air intake for the engine cylinders. Because thermal NO production is sensitive to the amount of O_2 present, less O_2 in the combustion chamber results in lower NO formation.

Vehicles also utilize control strategies that target engine-out emissions before they leave the tailpipe. Examples of these methods in CI vehicles include diesel oxidation catalysts, selective catalytic reduction (SCR), lean NO_x traps, and diesel particulate filters (DPF). Oxidation catalysts in diesel engines contain a honeycomb structure coated with a platinum-based (or similar) catalyst mixture that oxidizes CO and HCs to CO_2 and H_2O with an efficiency of 10-60% for CO and 40-75% for HCs (US EPA, 2010a). Some of the engine-out NO may oxidize to NO_2, however the SCR method works to remove NO_2 from the exhaust stream. For this reason, the oxidation catalyst is often located upstream of the SCR system. Nitrogen oxides are removed from the exhaust stream using SCR in CI engines. The process involves spraying diesel exhaust fluid (DEF) containing ammonia or urea over a catalyst, typically vanadium-based, into the exhaust stream. Selective catalytic reduction works to remove NO_x from the exhaust stream by reducing NO, or NO_2, into inert N_2. Equations 1.7, 1.8, and 1.9 represent several of the reactions, among others, that occur within the SCR system (de Nevers, 2010).

$$6NO + 4NH_3 \rightarrow 5N_2 + 6H_2O \quad \text{(Equation 1.7)}$$
$$4NO + 4NH_3 + O_2 \rightarrow 4N_2 + 6H_2O \quad \text{(Equation 1.8)}$$
$$2NO_2 + 4NH_3 + O_2 \rightarrow 3N_2 + 6H_2O \quad \text{(Equation 1.9)}$$

Selective catalytic reduction in diesel engines depends on several factors including the type of catalyst used and the exhaust temperature, and can reach efficiencies of >90% when properly warmed up (Wang et al., 2021). In addition to SCR, oxidation

catalysts, and lean NO_x traps, diesel vehicles also utilize DPF technology to reduce particulates including BC. The DPF works to remove most particles, including BC, from the exhaust stream with an efficiency of >90%, depending on the type and age of the filter material (Barone et al., 2010).

1.2.3. Spark-Ignited vehicles

Most SI engines use the same four-stroke mechanism detailed in the prior section, but with several key differences compared to a CI engine. In terms of fuel, SI vehicles use gasoline, a type of fuel blend consisting of compounds that each contain between 4 and 12 carbon atoms. One of the key differences is how the fuel enters the combustion chamber in the intake step. Spark-ignited engines equipped with port-fuel injection (PFI) differ from CI engines in that the fuel is pre-blended into a homogeneous mixture with air before entering the cylinders, resulting in better control of the AF ratio. Modern SI engines also utilize gasoline direct injection (GDI), which offers better fuel economy and reduced CO_2 emissions compared to PFI. In GDI, fuel is injected at high-pressure directly into the combustion chamber instead of mixing with the intake air prior to entering the cylinder. The GDI mechanism leads to a cooling effect due to the evaporation of fuel in the chamber, reducing NO_x emissions and allowing the use of a higher compression ratio which further increases the thermal efficiency of the engine (Huang et al., 2021). The US EPA estimates that ~ 50% of on-road SI vehicles in the US are equipped with GDI technology (US EPA, 2020a).

Conditions inside SI engines are sometimes kept oxygen deficient (fuel-rich), indicating that the AF ratio is typically below the stoichiometric ratio (~ 14.8) needed for complete combustion (de Nevers, 2010). Running the engine fuel-rich produces more power but lowers the overall fuel efficiency because there is not enough oxygen to fully combust the fuel.

Spark-ignited engines typically attain a compression ratio of between 1/8 to $1/10^{th}$ of the initial volume during the compression stroke. If the compression ratio is too high in a spark-ignited engine, the air-fuel mixture may ignite prematurely in the cylinder and cause a loud knock, an event that is appropriately called engine knock. In general, the lower compression ratio in SI engines results in lower thermal and fuel efficiencies compared to CI engines because less of the fuel is combusted in the fuel-rich environment, however SI engines equipped with GDI rather than PFI lead to less engine knock and higher thermal efficiency than their PFI counterparts (Huang et al., 2021).

One of the most important differences between CI and SI engines is how the air-fuel mixture is ignited during the combustion phase. As the name suggests, spark-ignited engines use a spark plug to ignite the mixture, while compression-ignited engines use the heat of compression to ignite the mixture. When the piston is near TDC, a spark is produced by the spark plug at the top of the cylinder, initiating the combustion process. The exhaust gases are then pushed out of the combustion chamber in the exhaust stroke in the same manner as in CI engines.

Differences in engine mechanism affect the relative amount of air pollutants produced during combustion. The fuel-rich environment in SI engines leads to

higher levels of engine-out CO and HCs relative to CI engines. Carbon monoxide and HCs are the products of incomplete combustion of fuel and are formed within fuel-rich pockets in the combustion chamber or when there is insufficient oxygen for complete combustion. Spark-ignited engines tend to produce more CO and HC because the formation of CO is highest in a fuel-rich environment with a low compression ratio and at high temperatures, such as during combustion. Spark-ignited vehicles also generate NO_x, but the amount produced is less than from CI vehicles. This is because the combustion chamber in SI engines is often oxygen deficient and attains a lower peak temperature than in CI engines. Gasoline direct injection-equipped SI vehicles produce more BC than PFI-equipped vehicles because the gasoline is directly injected into the cylinders with GDI. However, the difference in engine-out BC emissions between GDI and PFI is significantly smaller than the difference between the average CI and SI engine; while GDI-equipped SI vehicles emit ~ 5 times more BC than PFI-equipped vehicles (Saliba et al., 2017; Zimmerman et al., 2016), CI engines produce up to 50 times more BC than the average SI engine (Ban-Weiss et al., 2008; Dallmann et al., 2013). To combat higher BC emissions, SI vehicles with GDI also contain a gasoline particulate filter used to remove particles including BC, from the exhaust.

The primary emission control strategy used in modern SI engines is the three-way catalytic converter. An earlier version of the catalytic converter was the two-way converter, which only targeted HC and CO emissions. The newer three-way catalytic converter, shown in Figure 1.3, reduces emissions of NO_x, CO, and HCs by up to ~ 95% using a ceramic monolith in the shape of a honeycomb coated with a

catalyst mixture containing rhodium and either platinum or palladium (de Nevers, 2010). Catalytic converters work by reducing NO_x to inert N_2 and O_2, and oxidizing CO and HCs to CO_2 and H_2O. These reactions are typically slow in the atmosphere, however the presence of catalysts works to lower the activation energy and speed up the reactions. The catalysts do not function well until they are properly heated, resulting in high tailpipe concentrations of NO_x, CO, and HC if the vehicle and emission control devices are not properly warmed up such as during a cold start. As will be discussed in later chapters, emission control equipment that has not been properly warmed up may lead to higher tailpipe emissions of certain pollutants including NO_x.

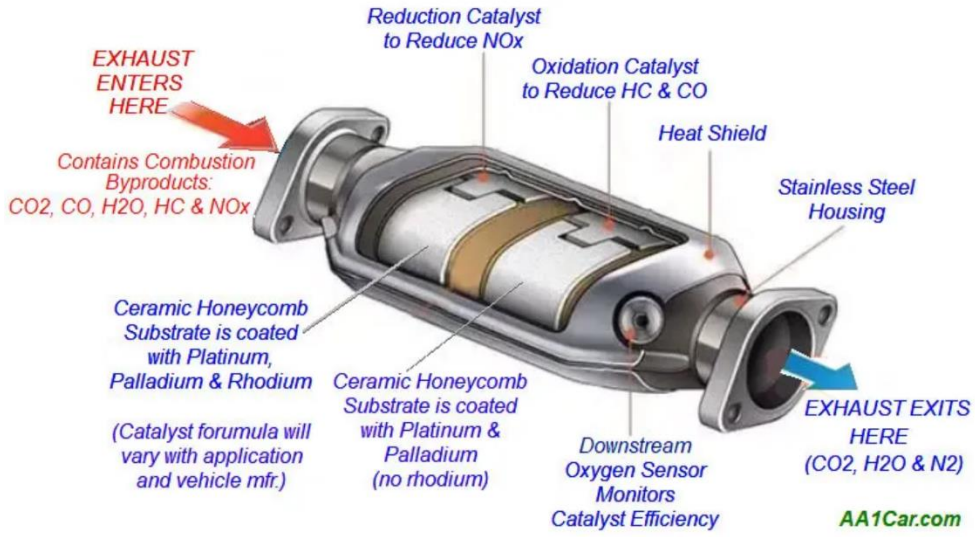

Figure 1.3. Diagram of the structure of a three-way catalytic converter. Image from https://aa1car.com/library/converter.htm.

1.3. Measurements

The ambient observations used in this research were collected at a stationary near-road (NR) monitoring site located at a rest area along Interstate-95 (I-95) southbound, midway between Baltimore and Washington, DC (Figure 1.4). Traffic measurements, including hourly total vehicle counts and speed information, were collected ~ 8 km (~5 miles) north of the NR site (Figure 1.5). The observations used in this work span from late 2016 through April 2020. Together, the ambient and traffic observations are used in this dissertation to study patterns and sensitivities in mobile emissions.

Figure 1.4. Ambient monitoring site located along I-95 in the Baltimore-Washington DC area. Images from Google Earth (https://earth.google.com/).

Figure 1.5. Close-up view of the I-95 traffic counter used in this study.

1.3.1. Near-Road Measurements

The I-95 NR site is part of a greater network of thousands of ambient monitoring sites located through the US, as part of the US EPA Air Quality System (AQS). The variables measured at each site varies, however typical measurements include airborne CAPs, hazardous air pollutants (HAPs), meteorological data, among others. The location of each site is carefully chosen to meet certain objectives, such as measuring highest concentrations, population exposure, and background levels. The I-95 NR site used in this study is designated as a source-oriented monitor to measure highest concentrations of a variety of air pollutants, including CO, $NO/NO_2/NO_x$, BC, PM, and various volatile organic compounds.

The work in this dissertation utilizes NR measurements of BC, CO, NO_x, CO_2, and meteorological variables. As part of the AQS network, the analyzers are held to specific standards set forth in the Code of Federal Regulations 40, Subchapter C, Part 58 (see https://www.ecfr.gov/for more information). The discussion presented below highlights key aspects of the principles of operation for each analyzer, while more in-depth estimates of analyzer specifications are provided in Chapters 2-5.

Meteorological variables including temperature, pressure, relative humidity, wind speed, and wind direction are measured above the NR trailer using a Vaisala WXT 520 instrument.

Black carbon concentrations are measured with a filter-based, optical technique using a Magee Scientific TAPI M633 (AE33) Aethalometer. Intake air with a volumetric flow rate (calculated from a mass flow meter at a specific

temperature and pressure) is passed through a filter inside of the analyzer, allowing aerosols to be collected on the filter. The light attenuation (Equation 1.10) is then measured at seven distinct wavelengths (ranging from 370 to 950 nm) and combined with the spot size, the time interval (1-minute in the NR observations), the volumetric flow rate, and wavelength-specific mass cross sections to calculate the mass concentration of BC (Grimes and Dickerson, 2021; Magee Scientific, 2018).

$$\text{Attenuation} = -100 \cdot \ln\left(\frac{I}{I_0}\right) \quad \text{Equation 1.10.}$$

Here, I represents the light intensity through a filter covered with particles, while I_0 represents the reference light intensity through a clean portion of the filter.

The typical wavelength used to report BC concentrations is 880 nm so we can minimize interferences from other light-absorbing aerosols such as brown carbon, which can interfere with the BC signal at lower wavelengths (Olson et al., 2015). A problem arising in this filter-based method is non-linearity in the analyzer response at high concentrations due to the spot-loading effect, in which the instrument signal becomes less sensitive as the aerosol loading on the filter surface increases. To address this issue, the Aethalometer is equipped with Dual-Spot technology, in which two filters, rather than one, are used to simultaneously measure BC concentrations. Intake air passes through one of the filters at a faster flow rate than through the other, leading to different amount of aerosol that are collected on the two filters. The Aethalometer estimates a loading compensation parameter from the reported BC concentrations on each filter spot, then uses this parameter to

minimize the spot-loading effect and calculate the adjusted BC concentration (Magee Scientific, 2018).

Near-road CO levels are measured using a Teledyne Advanced Pollution Instrumentation (API) model 300U. The CO analyzer operates on the principle of infrared (IR) energy absorption and measures the amount of energy at 4,700 nm transmitted through a measurement cell.

Due to interferences at this wavelength by gases other than CO, including water vapor, a Nafion Dryer® is placed at the instrument inlet to remove water vapor. To further minimize potential interfering gases, the analyzer is equipped with a Gas Filter Correlation (GFC) wheel in the measurement chamber. The wheel has two sealed cavities, one housing a high concentration of only CO (reference cell) and the other containing inert N_2 gas (measurement cell). During the reference cycle, dried intake air is first passed through a CO scrubber before entering the measurement chamber. The GFC wheel turns so that the IR beam passes through the cell containing high levels of CO that absorbs much of the energy at 4,700 nm, leaving significantly less energy left to be absorbed by gases within the air sample (API, 2017). In the measurement cycle, the IR beam passes freely through the inert N_2 measurement cell and any absorbing gases within the air sample will absorb some of the IR energy. The concentration of CO is then estimated from the ratio of the measured signal and the reference signal using a look-up table (API, 2017).

Ambient $NO/NO_2/NO_x$ is sampled using a Teledyne API 200U analyzer through chemiluminescence. In the presence of O_3, NO may react via Equations

1.11 and 1.12 to produce an excited NO_2 molecule that generates a detectable light signal in its return to ground state (API, 2018; Fontijn et al., 1970).

$$NO + O_3 \rightarrow NO^*_2 + O_2 \quad \text{(Equation 1.11)}$$

$$NO^*_2 \rightarrow NO_2 + hv \quad \text{(Equation 1.12)}$$

Because NO_2 would not chemiluminesce with O_3 within the reaction chamber, any NO_2 present in the air sample is first converted to NO before reacting with O_3 to measure total the total NO_x concentration. The nitrogen dioxide concentration is then calculated as the difference between the amounts of NO_x and NO. To switch between NO and NO_x measurements, air entering the analyzer alternates between flowing directly into the reaction cell or passing through a cartridge filled with a catalyst before reacting with O_3. When air flows directly into the reaction chamber, only NO in the sampled air reacts with O_3, thus the data is sensitive to the amount of NO in the air. When the intake air passes through the cartridge, however, any NO_2 present in the air is catalytically converted to NO with the aid of hot molybdenum at 315°C (Equation 1.14**;** API, 2018**)**.

$$xNO_2 + yMo \rightarrow xNO + M_yO_z \quad \text{(Equation 1.13)}$$

The latter process results in the sum of NO and NO_2, or NO_x, being measured in the reaction cell, so that the difference between this measurement and the prior measurement represents the abundance of NO_2 in the sampled air. Other reactive nitrogen species, including nitric acid and alkyl nitrates, that are present in air may also be converted to NO in the molybdenum converter (Dickerson et al., 2019; Dunlea et al., 2007; Fehsenfeld et al., 1987), and we assume these are detected along with fresh tailpipe emissions in the NO_x measurements at the NR site.

The ambient CO_2 abundances prior to 2020 were measured using a Los Gatos Research (LGR) Fast Greenhouse Gas Analyzer with the Enhanced Performance option (Los Gatos Research, 2013). This instrument uses a type of laser absorption spectroscopy that depends on Beer's Law (similar to Equation 1.11) to calculate the amount of a CO_2 in the sampled air. As air enters the optical cavity, a tunable laser emits a beam at ~ 1650 nm into the optical cavity. The beam is then reflected many times within the cavity by highly-reflective mirrors to produce an effective optical pathlength of several kilometers (Los Gatos Research, 2013). The enhanced performance model employs Off-Axis Integrated-Cavity Output Spectroscopy to lengthen the effective pathlength within the absorption cell, leading to a higher sensitivity for CO_2 than the base model (Los Gatos Research, 2018). The presence of CO_2 in the optical cavity leads to absorption of some of the IR energy, thus reducing the intensity of the beam as it exits the cavity. Since March 2020, near-road ambient CO_2 levels have been measured with a Picarro Model G2301 CO_2/CH_4 analyzer. Like the LGR, the Picarro uses a modified type of laser absorption spectroscopy to calculate CO_2 concentrations from the absorption of IR energy within an optical cavity. To do so, the Picarro uses its patented cavity ring-down spectroscopy with a three-mirror cavity that produces an effective path length of up to 20 km (Picarro, 2019). Unlike the LGR which detects the intensity of light exiting the cavity, the cavity ring-down system calculates the CO_2 concentration from the time it takes for an initial light intensity to make it through the cavity, based on the reference time without any CO_2 in the cavity. Even with these differences in

operation, the CO_2 measurements taken by each analyzer agree very well and will be discussed further in Chapter 3.

The observations collected at the NR site represent ambient, rather than direct emissions, measurements. The emission of a particular gas into the atmosphere is typically taken to be the enhancement above background level. In the absence of a background site located directly upwind of the NR site, here I use emission ratios to infer mobile emissions from the air measurements. Unlike absolute concentrations, emission ratios are useful in studying mobile emissions because tropospheric abundances of BC, CO, NO_x, and CO_2 co-vary under changing atmospheric conditions including the boundary layer height. Changes in the types of vehicles passing the NR site, however, reflect in the mobile emissions and provide insight into the vehicle fleet composition. More details on how emission ratios are inferred from the ambient observations are provided in Chapters 2-3.

1.3.2. Traffic Observations

The I-95 traffic sensor is part of a network of 87 automatic traffic recorders (ATR) that are operated by the Maryland State Highway Administration. The counter used in this study (ATR #39) is located 8 km north of the NR monitoring site and is embedded within I-95. The sensor classifies vehicles by type and speed, counting the total number of hourly vehicles in each of 13 vehicle and 12 speed bins. To distinguish vehicles, the site uses a combination of inductive loops that determine the presence of a metal object above them, and piezo sensors that act as pressure, or axle, sensors (Briedis et al., 2010). The site uses a loop-piezo-loop configuration to

determine the type and speed of a passing vehicle from the number of and spacing between the axles. Figure 1.6 shows the groups of vehicles distinguished by the counter. The speed bins are each five miles per hour (mph) apart, except for the slowest (0 to 30 mph, or 0 to ~ 48 km hr^{-1}) and the fastest (greater than 30 mph, or ~ 48 km hr^{-1}) speed bin.

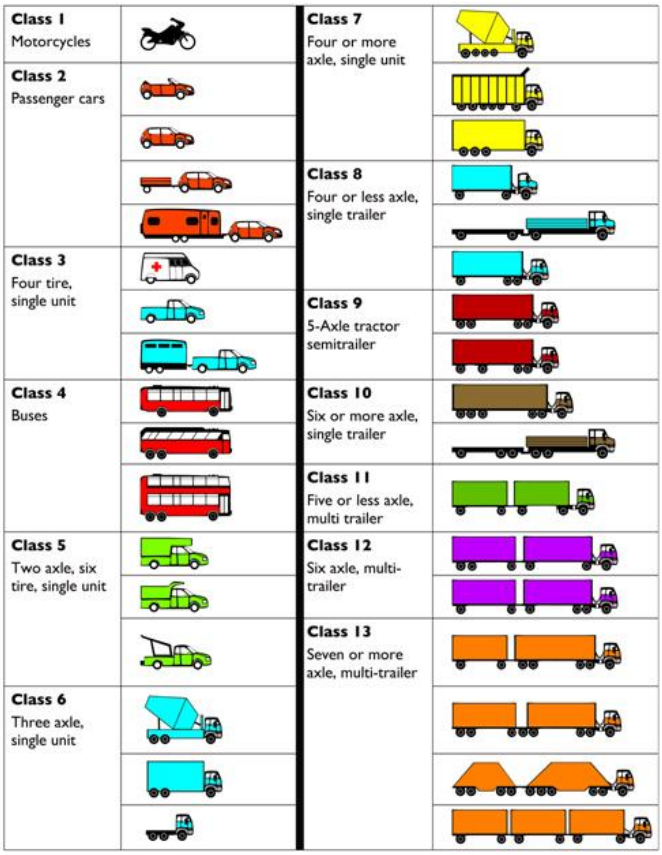

Figure 1.6. Federal Highway Administration vehicle classification scheme. Image from https://www.fhwa.dot.gov/policyinformation/tmguide/tmg_2013/vehicle-types.cfm.

The overall accuracy of the traffic counter depends on a number of conditions, including the type and condition of the sensors and, for some types of sensors, daylight and weather (Briedis et al., 2010; US Department of Transportation Federal Highway Administration, 2006). The counter located at I-95 consists of

inductive loops that are used to count the total hourly number of passing vehicles and classify each vehicle into one of 13 FHWA-designated vehicle types and 16 vehicle speed bins. Inductive loop sensors are the most widely employed class of traffic counter and are often used as a reference when evaluating new traffic technology due to their high accuracy, long-term use, and consistency across different types of weather (Bellucci and Cipriani, 2010; Briedis et al., 2010; US Department of Transportation Federal Highway Administration, 2006). Provided the traffic counter and pavement are in good condition, as is the case at the I-95 site, the accuracy of total vehicle counts by inductive loops generally exceeds 95% (Briedis et al., 2010). One challenge faced by traffic sensors is the classification of individual vehicles into the 13 FHWA vehicle types. For instance, due to the similarities between passenger cars (class 2) and passenger pick-up trucks (class 3), the accuracy of classified vehicle counts can be increased from ~79% to 96% by grouping classes 2 and 3 together (Georgia Department of Transportation, 1995). To improve the overall accuracy of the classified traffic observations used in this dissertation, vehicle classes with similar traits have been placed into four distinct vehicle families, and these are passenger vehicles (classes 1-3), buses (class 4), single-unit trucks (class 5-7), and combination-unit trucks (classes 8-13).

1.4. Overview of This Dissertation

The goal of this work is to improve our understanding of the factors that influence vehicular emissions, thereby providing useful guidance on how to further regulate mobile emissions. Since vehicular emissions account for the majority of

CO, NO_x, and BC emissions in the U.S., the work discussed in this dissertation provides useful guidance for policy decisions aimed at improving air quality. A summary of the measurements and instruments used in this dissertation is provided in Table 1.1. Using emission ratios ($\Delta CO/\Delta NO_x$, $\Delta CO_2/\Delta NO_x$, and $\Delta CO_2/\Delta CO$), I first investigate how mobile emissions of NO_x, CO, and CO_2 respond to ambient temperature and specific humidity using observations collected along a NR site (Chapter 2). The observed temperature and humidity sensitivity is then compared to output from MOVES, the model used by the US EPA to simulate mobile emissions. A potential source for this sensitivity is traced using traffic measurements, and more specifically, the split between gasoline and diesel vehicles by time-of-day and weekday. This work was published in April 2020 in the scientific journal of *Atmospheric Environment*.

To further explore the impact of temperature on mobile emissions, Chapter 3 investigates the response of vehicular BC emissions to ambient temperature. A detailed investigation of traffic information and observed emission ratios by weekday and hour-of-day, combined with the fact that diesel trucks emit most of the BC in the NR environment, is then used to determine the types of vehicles most likely to exhibit a temperature sensitivity. The observed sensitivity is compared to emissions output from the newest version of MOVES, MOVES3. Together with the work in Chapter 2, the results from Chapter 3 provide insight into how observed vehicular emissions respond to changes in ambient temperature and how well this sensitivity is represented in the US EPA's mobile emissions modeling efforts.

Changes in traffic patterns, such as the amount of traffic congestion and the types and number of vehicles driving on roads, also influence on-road vehicular emissions. Chapter 4 provides a detailed examination of observed emission ratios and how COVID-19 travel restrictions imposed in early 2020 impacted vehicular emissions of BC, CO, NO_x, and CO_2 at the NR site. To better estimate the relative contribution of cars and trucks to changes in CO, NO_x, and BC in April 2020, I investigate the weekday/weekend and time-of-day differences in emission ratios and traffic composition (the split between car and truck vehicle counts) in April 2020 relative to prior years. Chapter 4 also provides an analysis of how traffic patterns, specifically the amount of stop-and-go traffic and the average vehicle speed, changed in April 2020 compared to prior years. Using this information, I identify an important mechanism driving the changes in the observed emission ratios in April 2020. The work in Chapters 3 and 4 is currently in preparation for submission to *Atmospheric Environment*.

The last chapter, Chapter 5, presents conclusions from the work in Chapters 2, 3 and 4 and suggestions for future research projects.

Variable	Measurement Technique/ Analyzer	Accuracy
CO	Infrared Energy Absorption Teledyne API 300U	2.3%
$NO/NO_2/NO_x$	Chemiluminescence Teledyne API 200U	4.7%
BC	Filter-based, optical measurement technique Magee Scientific TAPI M633 (AE33) Aethalometer	~ 5% (Grimes et al., 2021)
CO_2 (2016-2018)	Laser Absorption Spectroscopy Los Gatos Research Fast Greenhouse Gas Analyzer	0.089%
CO_2 (2020)	Laser Absorption Spectroscopy/Cavity Ring-down Picarro Model G2301	0.025%
Classified Traffic Counts	Inductive loops and piezo sensors	~ 5% (Briedis et al., 2010)
Temperature/Pressure/ Relative Humidity/ Wind Speed/ Wind Direction	Vaisala WXT 520	T: 0.3°C P: 0.5-1 hPa RH: 3-5% WS: 3-5% WD: 3° *Manufacturer specifications

Table 1.1. Ambient observations measured at the I-95 NR site in Maryland. Traffic information collected along I-95, 8 km north of the NR site. More details on the accuracies listed above are provided in Chapters 2-4.

Chapter 2: Using Near-Road Observations of CO, NO_y, and CO_2 to Investigate Emissions from Vehicles: Evidence for an Impact of Ambient Temperature and Specific Humidity

The work in this chapter was published under the same title in the journal of *Atmospheric Environment*. The article was made available online on April 27, 2020 as part of Volume 232. I am the first author of this paper and collaborated with eight co-authors from the University of Maryland and the Maryland Department of the Environment. Numbered references within this chapter have been adjusted to reflect the numbering system of the larger dissertation. Supplemental material from this article is provided in Appendix A and referenced within this chapter.

2.1 Introduction

Emissions of carbon monoxide (CO) and nitrogen oxides (NO_x = NO+NO_2) from mobile sources have steadily declined over the past decade throughout the United States (US) due to the implementation of emission control technologies (see also https://www.epa.gov/air-emissions-inventories/air-pollutant-emissions-trends-data; Bishop and Stedman, 2008; Hassler et al., 2016; He et al., 2013; Krotkov et al., 2016; McDonald et al., 2012; Parrish et al., 2014; Silvern et al., 2019). Nonetheless, CO and NO_x remain major precursors of ozone (O_3) pollution in the troposphere (P. J. Crutzen, 1973; Haagen-Smit et al., 1953; Pusede and Cohen, 2012; Sather and Cavender, 2016) and contribute to the formation of fine particles.

The National Emissions Inventory (NEI) compiled by the EPA every three years provides detailed emission data of criteria, precursor, and hazardous pollutants from various sectors, including mobile and point sources. According to the 2014 NEI, mobile sources account for 56% of the total (including wildfires) national emissions of CO and for 59% of the total emissions of NO_x. Within Maryland, mobile sources are estimated to account for 81% of CO and 74% of NO_x emissions (data available at https://www.epa.gov/air-emissions-inventories/air-pollutant-emissions-trends-data).

Long-standing discrepancies between measured and modeled mixing ratios of NO_y ([NO_y] or total reactive, oxidized nitrogen, including NO, NO_2, HNO_3, HONO, NO_3, peroxyacetyl nitrates (PAN), and alkyl nitrates) suggest more work is needed to improve the accuracy of the anthropogenic emissions of NO_x (Canty et al., 2015; Castellanos et al., 2011; Souri et al., 2016; Yu et al., 2012). For example, measured [NO_y] at surface sites in urban areas is consistently lower than indicated by simulations conducted using the EPA-approved Community Multiscale Air Quality (CMAQ) model, driven by emissions from the NEI (Castellanos et al., 2011; Souri et al., 2016). Similar overestimation of [NO_y] by CMAQ has also been observed in comparison to aircraft data (Yu et al., 2012). Canty et al. (2015) used observations of tropospheric column NO_2, a component of NO_y, from the National Aeronautics and Space Administration (NASA) Ozone Monitoring Instrument (OMI) to show that CMAQ overestimates the urban-to-rural NO_2 ratio over the Eastern US.

Anderson et al. (2014) demonstrated that the NEI appears to substantially overestimate total emissions of NO_x during the summer of 2011 for the mid-Atlantic region of the Eastern US, most likely due to mobile sources. Using satellite and aircraft

observations from the NASA Deriving Information on Surface COnditions from Column and VERtically Resolved Observations Relevant to Air Quality (DISCOVER-AQ) field mission over the Baltimore, MD and Washington, DC area (Crawford, 2010), Anderson et al. (2014) found a modest overestimate in the abundance of CO simulated by CMAQ (~15%) while simulated levels of NO_y were nearly twice as high as observed. The generation of CO from isoprene oxidation may be underestimated in the study by Anderson et al. (2014), but the substantial excess of NO_y is robust. The authors also evaluated point-source emissions of NO_x by comparing reported values in the Continuous Emissions Monitoring System or CEMS (https://www.epa.gov/emc/emc-continuous-emission-monitoring-systems) to point-source NO_x emissions processed by the Sparse Matrix Operator Kernel Emissions (SMOKE) modeling system that prepares emissions inventories for use in CMAQ. This modeling system merges emission data of various source categories from databases including the NEI and the MOtor Vehicle Emissions Simulator (MOVES; US EPA, 2015a) to match the spatial and temporal resolution required as input for air quality models (https://www.cmascenter.org/smoke/documentation/4.0/html/). Anderson et al. (2014) found good agreement between point-source emissions of NO_x in the CEMS and the SMOKE modeling system. Therefore, they attributed the discrepancy between measured and modeled NO_y to an overestimate of mobile emissions of NO_x within MOVES2010.

The overestimate in mobile emissions of NO_x reported by Anderson et al. (2014) has been confirmed in various other studies, including one that used emissions derived from a fuel-based approach (McDonald et al., 2018, 2012). Travis et al. (2016)

confirmed these findings and demonstrated that the overestimate of NO_x emissions appears to apply to the entire contiguous US. Subsequent studies have also reported an overestimation of the emission of NO_x for the Southeast US from mobile sources (Mao et al., 2018) and non-stationary sources (Li et al., 2018). Kota et al. (2014) found that concentrations of NO_x and CO from on-road emissions using CMAQ run with MOVES were overestimated relative to measurements collected at urban and industrial sites in Southeast Texas. Tunnel studies suggest overestimation of NO_x (McDonald et al., 2012) and CO from vehicles (Fujita et al., 2012). A 2015 tunnel study in Baltimore, MD, observed higher NO_x emission factors in the wintertime than in the summertime, however the authors did not specifically correlate emission factors and temperature and the relationship between the ambient temperature inside and outside of the tunnel is unknown (Wang et al., 2019). In the Great Lakes area, a 30% reduction of modeled on-road mobile NO_x emissions yielded better comparison of CMAQ simulations to observations (Qin et al., 2019), but this is a lower limit to the necessary reduction because important NO_y species were not accounted for (Dickerson et al., 2019). A recent comparison of aircraft data acquired during the 2015 winter (as opposed to the summer season from DISCOVER-AQ) in the Baltimore-Washington Region (BWR) to the 2011 and 2014 NEI reported good agreement with the NO_x emission inventories, whereas CO emission rates inferred from observations were a factor of two lower than in the NEI (Salmon et al., 2018). These winter observations suggest that the discrepancy between observations of NO_x (or NO_y) and inventory estimates may be seasonally dependent, as most studies reporting an overestimate for NO_x emissions in the NEI were conducted during summer. Simon et

al. (2018) questioned the utility of using field experiments to evaluate emission inventories. However, their model runs also indicated good agreement with concentrations of CO and substantial overestimation of NO_y, a result consistent with the findings of Anderson et al. (2014) and numerous other studies.

Since most studies reporting an overestimate of emissions of NO_x in the NEI were conducted in the summer and NO_x emissions from stationary sources have been found to peak on hot, summer days (e.g., He et al., 2013), evaluating the temperature sensitivity of vehicular NO_x emissions becomes increasingly important. Saha et al. (2018) showed that emission factors of NO_x next to a highway in North Carolina were 20% higher in the winter than in the summer. The authors attributed much of this difference to slower dispersion of air pollutants in the winter. Two recent studies in Europe have shown that emissions of NO_x from light-duty diesel vehicles decrease with rising temperature, while gasoline vehicles do not show a significant temperature dependence (Grange et al., 2019; Weber et al., 2019), although Ko et al. (2019) and Prati et al. (2019) found the opposite effect for diesel vehicles. In the US, the fraction of NO_x emissions generated by diesel vehicles has been increasing and now probably exceeds that from spark-ignited vehicles (Dallmann and Harley, 2010; McDonald et al., 2018).

Emissions of pollutants from on-road vehicles within the NEI are estimated using MOVES; this model calculates pollutant inventories or emissions rates (e.g., grams $mile^{-1}$) on the county, state, and national scale using input parameters such as speed distribution, vehicle fleet composition, and meteorological data (US EPA, 2015a). Both MOVES2010 and MOVES2014 incorporate the effect of temperature

on cold-start CO, hydrocarbon (HC), and NO_x emissions (US EPA, 2015b, 2010b), however MOVES with the recommended settings does not adjust the hot-running exhaust (all engine processes besides engine-start, including vehicle idling) emissions of CO, NO_x, or HC for a direct temperature effect. Instead, these running emissions are impacted by a smaller, indirect effect of temperature due to air conditioning (AC). Emissions of NO_x within MOVES decrease with increasing specific humidity, the mass of water vapor per unit mass of moist air, due to quenching during combustion. Specific humidity does not impact direct running exhaust emissions of CO and CO_2 in MOVES. While users are free to adjust these factors, EPA documents (US EPA, 2015b) do not stipulate how these parameters should be changed. The default value of unity for the direct temperature effect results in hot-running exhaust emissions independent of ambient temperature for most air quality simulations.

In this study, we quantify vehicular emissions of CO and NO_x inferred from ambient measurements at a near-road (NR) site in the BWR and compare the results to output from the MOVES model. We examine CO_2, CO, and NO_x inferred from one-minute averaged observations at the NR site for their sensitivity to ambient temperature and specific humidity. Fleet composition impacts the emissions, with gasoline passenger cars emitting at a $\Delta CO/\Delta NO_x$ ratio of ~10 mol mol^{-1} and diesel trucks at a ratio less than 1 mol mol^{-1} (Bureau of Transportation Statistics, 2018). We study the temperature and humidity dependence using all hours and also for various times of the day. Additional analysis comparing NR CO and NO_x to CO_2 provides insight into the efficiency of emission control technologies of passing vehicles.

2.2 Methodology

2.2.1 Observational Data

Aircraft measurements of [CO] and [NO_y] were made aboard the NASA P3-B aircraft in July 2011 over the BWR during DISCOVER-AQ. In addition, the concentrations of NO, NO_2, HNO_3, peroxy nitrates, and alkyl nitrates were also measured (Day et al., 2002; Farmer et al., 2006; Ridley and Grahek, 1990; Wooldridge et al., 2010). As discussed in Anderson et al. (2014), measurements of [NO_y] were used in place of the mixing ratio of NO_x ([NO_x]) to account for the conversion of NO and NO_2 to other reactive nitrogen species in the several hours between emission and sampling. More details about the instruments can be found elsewhere (Anderson et al., 2014; Brent et al., 2015; Ridley and Grahek, 1990; Sachse et al., 1987).

Concentrations of trace pollutants were measured at a NR monitoring site within the BWR from November 1, 2016 to December 31, 2017. Details about the measurements and the analyzers are provided in section A2 of Appendix A. The analysis used here focuses exclusively on the colder months, hereby defined as November 1, 2016 through February 28, 2017 and November 1, 2017 through December 31, 2017, to minimize the impact of biospheric activity on mixing ratios of CO_2 ([CO_2]) and [CO]. The I-95 site, managed by the Maryland Department of the Environment, is located along the southbound leg of an eight-lane highway near a rest area in rural/suburban Laurel, Howard County, Maryland (39° 8’ 35.38” N, 76° 50’ 45.53” W) (Figure A1 in Appendix A). To isolate the impact of highway emissions on ambient measurements of [CO], [NO_x], and [CO_2], we only include measurements of

pollutants when winds blew from the adjacent highway, defined as 25° to 225°Compass (or clockwise from North) at the I-95 site (Figure A1). The site is located within ~12 m of this major highway, and thus measurements of ambient [CO] and [NO_x] are dominated by on-road vehicular emissions. Using the entire dataset, i.e., all wind directions, has little impact on our results and is discussed in section 2.3.2.1 and Appendix A. The very close proximity to the highway makes the NR site suitable for the analysis of mobile emissions.

Vehicle fleet composition and speed are measured hourly at an automatic traffic counter located ~8 km North of the NR site along I-95 and is operated by the Maryland State Highway Administration. A summary of the vehicle fleet composition passing this counter is given in Table A1**Error! Reference source not found.** in Appendix A and shows that passenger vehicles represent the majority of vehicles, although multi-axle trucks are common. A sample of observations of vehicle speeds at this counter for October 13 through November 17, 2016 showed that the average and median fractions of total vehicles driving at speeds faster than 81 km hr^{-1} were 86% and 98%, respectively, for all times of day.

EPA protocols for data quality were strictly followed and calibrations for [CO_2] were conducted with NIST-certified standards (Martin et al., 2017). The CO and NO_x analyzers follow quality control procedures as documented in the Code of Federal Regulations (CFR) 40 part 58: the measurement precision must be within ±10.1% for [CO] and ±15.1% for [NO_2] (guidelines available under Title 40, Part 58, Appendix A at http://www.ecfr.gov/cgi-bin/ECFR?page=browse). Quality control

checks were performed every 14 days to determine compliance with the precision standard.

Co-variations of [CO], [NO_x], and [CO_2] due to variability in meteorology and atmospheric dynamics, including boundary layer height, can be used to infer emission ratios, useful for studying air pollution plumes near sources (Ammoura et al., 2016; Crutzen et al., 1979). Emission ratios are traditionally derived from the ratio of the enhancement of two pollutants, defined as the background subtracted from a peak height. In the absence of a monitoring site upwind of the I-95 NR site to supply ambient pollutant background levels, we estimate the hourly emission ratios as the slopes of linear regressions of CO and NO_x, CO_2 and CO, and CO_2 and NO_x, effectively representing $\Delta CO/\Delta NO_x$, $\Delta CO_2/\Delta NO_x$, and $\Delta CO_2/\Delta CO$. Several techniques for testing the background confirm the robustness of the results and are discussed in section 2.3.2.1. We focus on the dependence of vehicular emissions (inferred from observed measurements) on ambient temperature and specific humidity.

2.2.2 Analysis of Emission Ratio Trends with Temperature and Specific Humidity

In this study we used the slope of a linear geometric mean regression fit to one-minute averaged measurements of [CO], [NO_x], and [CO_2], for all data acquired within an hour, to determine the hourly emission ratio ($\Delta CO/\Delta NO_x$, $\Delta CO_2/\Delta NO_x$, and $\Delta CO_2/\Delta CO$). This regression method minimizes the distance in the y-variable and the x-variable separately by computing the geometric mean of the slope parameters

estimated from the ordinary least-squares regressions of one-minute measurements of CO vs. NO_x and NO_x vs. CO. Since the one-minute averages may contain outliers that can affect the regression slope, i.e., the emission ratios, data farther than 2 standard deviations from the mean were excluded prior to calculating the geometric mean regression for each hour. To test the 2-σ criterion, we repeated this analysis using a definition of outliers based on the interquartile range, but the difference did not change the outcomes of our analysis. In addition, replacing the geometric mean regression with a robust regression, which places less weight on outliers when estimating a best-fit, also does not change our conclusions (see detailed results in Figure A6 and Figure **A7** of Appendix A). Only hours with more than 40 one-minute observations were used in the final analysis. Measurement uncertainties are not included in calculating the hourly linear regressions, however they are included in our calculations of the overall uncertainty in the temperature dependence of the emission ratios in section 2.3.2.2.

As a test of our method of determining the temperature dependence of hourly emission ratios, we present several alternative ways of calculating hourly emission ratios detailed in Appendix A and discuss these throughout Chapter 2. In addition to these methods, an alternate approach of estimating the temperature sensitivity of emissions from slope values of linear regressions performed every 10 minutes instead of every hour is presented in section A11 in Appendix A and mentioned in section 2.3.2.1.

The change in vehicle fleet composition throughout the day may impact the effect of temperature on the emission ratios inferred from observations. We performed the analysis for all hours of the day and for three individual time windows: 0:00 to

4:59, 5:00 to 10:59, and 15:00 to 20:59 Eastern Local Time (ET). The morning and afternoon rush hours (time periods starting at 5:00 and 15:00, respectively) were chosen to reflect periods with minimal changes in fleet composition, while the early morning window (0:00 to 4:59 ET) represents the time with the highest fraction of diesel fueled, compression-ignited vehicles (CIV) of the 24-hour cycle (Figure 2.1). The number of total vehicles is defined as the sum of the number of CIV and the number of spark-ignited gasoline fueled vehicles (SIV). The average percentage (±standard deviation) SIV to total vehicles in the early morning, morning rush hour, and afternoon rush hour time windows, respectively, were 74 ±10%, 88 ±3.8%, and 94±2.0% near the I-95 site. The split between diesel and gasoline-powered vehicles is important because NO_x emission factors (grams NO_x/kg fuel) are nearly a factor of ten higher from diesel vehicles than from gasoline vehicles in the continental US (McDonald et al., 2018), and even more per vehicle mile traveled. To minimize the influence of daily traffic trends on the temperature analysis, we also show the temperature sensitivity of the daily-averaged emission ratios as a function of the daily maximum temperature in section A10 in Appendix A.

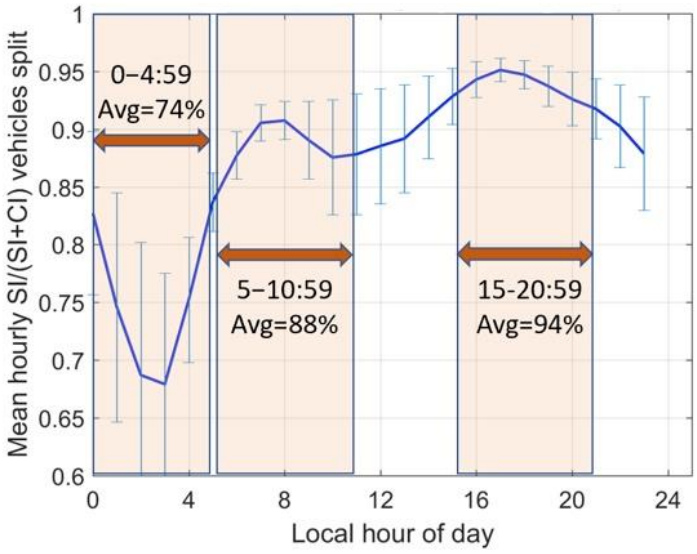

Figure 2.1. Vehicle fleet composition, represented by the fraction of spark-ignited vehicles (SIV) of total vehicles as a function of local time of day November 2016 and February, November, and December 2017 at the I-95 NR site. Highlighted are the three time windows used in the analysis. Midnight to 4:59 AM represents the early morning hours with the maximum CIV, 5:00 to 10:59 AM represents the morning rush hour, and 15:00 to 20:59 represents the evening rush hour. The split between SIV and compression-ignited vehicles (CIV) is important because CIV emit NO_x at ~ten or more times the rate of SIV per kg of fuel, and even more by vehicle miles traveled.

The statistical significance of each data trend (e.g., emission ratio as a function of temperature and specific humidity) was evaluated using the non-parametric Mann-Kendall trend test at a confidence level of 95% (Gilbert, 1987; Kendall, 1975; Mann, 1945). The uncertainty of the slope parameter of each trend was estimated using a Method of Maximum Likelihood, following Bevington and Robinson (2002).

2.2.3 Model Simulations

MOVES2014a was run for Howard County, MD for December 2014, the latest year for which all necessary model input data are available. December was chosen to

represent wintertime because the selection of month within MOVES is only used to alter the fuel type, and winter fuels are used from September through April in the model (US EPA, 2016). The direct effect of temperature on hot-running exhaust (all engine processes besides engine-start, including vehicle idling) emissions of hydrocarbons (HC), CO, and NO_x is estimated in MOVES by multiplicative adjustment factors calculated from polynomial functions. These adjustment factors are set to one for the baseline configuration of both MOVES2010 and MOVES2014, which means simulations run using this setting have no direct dependence of hot-running exhaust emissions of HC, CO, and NO_x on ambient temperature (US EPA, 2015b, 2010b). However, temperature does affect all modeled emissions indirectly, through a multiplicative air conditioning (AC) adjustment factor applied to running emission rates at higher temperatures for the baseline configuration. Temperature sensitivity for running emissions due to AC use is accounted for only at temperatures above ~20°C.

The direct temperature adjustment setting of unity and specific humidity settings for emissions of HC, CO, and NO_x within MOVES have not been updated between 2014, the year of the MOVES input data used here, and 2016-2017 when observations were made.

The MOVES model was run in emission rates mode at the county-level scale. This model run produced emission rates of CO, NO, NO_2, and CO_2 in grams per mile using county-specific inputs such as the fuel type, speed distribution, weekend/weekday split, vehicle age distribution, model year distribution, speed distribution, and all others that were available. The MOVES output is not specific to

any particular time scale, but rather is a function of temperature, humidity, vehicle type, fuel type, road type, model year, weekday or weekend, and speed. Ratios of emission rates were estimated by calculating average emission ratios weighted by the contribution of each speed and model year combination at each fuel, road, vehicle, emission, and day type. We tested for an impact of temperature in MOVES emission ratios by using a realistic temperature and relative humidity profile as meteorological input for MOVES derived from an exponential function fit to temperature and specific humidity observations at the I-95 site, following a method similar to Choi et al. (2010; Figure A2 in Appendix A). To test for the effect of specific humidity on emissions, we varied the humidity from 1 to 10 g kg^{-1} (H_2O to air by mass) for all temperatures in the range −5°C to 25°C, then averaged the emission rates over the temperature range at each specific humidity.

2.3 Results and Discussion

2.3.1 Aircraft Observations

Measurements of [CO] and [NO_y] from the 2011 DISCOVER-AQ field campaign were used to investigate the temperature dependence of inferred emissions of CO and NO_x (Anderson, 2016) for comparison to the EPA 2011 NEI. Aircraft observations downwind of cities integrate many sources, so comparison to the total emissions in these areas is appropriate. Because vertical profiles are used to evaluate $\Delta CO/\Delta NO_y$, we study this ratio as a function of potential temperature, θ, which remains constant as an air parcel moves vertically and adiabatically within the planetary boundary layer

(PBL). A discussion on the estimation of the PBL height during DISCOVER-AQ is given in Section A5 in Appendix A and the accompanying Figure A3 and Equation A1. The $\Delta CO/\Delta NO_y$ emission ratios from DISCOVER-AQ are defined as the calculated slope of the geometric mean regression of CO and NO_y mixing ratios in each spiral and transect within the PBL using a method similar to that developed by Crutzen et al. (1979). The potential temperature for each emission ratio used is the average of the potential temperature measured in each spiral and transect. Emission ratios from a total of 282 spirals and transects were used in our analysis.

Figure 2.2 depicts the temperature and specific humidity dependence of the inferred $\Delta CO/\Delta NO_y$ emission ratio for the vertical profiles of the DISCOVER-AQ campaign. The 25th, median, and 75th percentiles of the individual determinations of $\Delta CO/\Delta NO_y$ were calculated in bins that each contained an equal number of points. Between potential temperatures of 23.9°C and 26.6°C (the first three median values in Figure 2.2a) the average ratio was 8.7 mol mol^{-1}, whereas at higher potential temperatures between 32.4°C and 35.9°C (the last three median values in Figure 2.2a) the average emission ratio was 18.7 mol mol^{-1}. The value of $\Delta CO/\Delta NO_y$ increased by 114% for a rise in temperature of 8.7°C between 25.4°C and 34.1°C, the average values of these two temperature ranges, respectively. Below 28°C, $\Delta CO/\Delta NO_y$ was determined to be 8.3 mol mol^{-1}, similar to the $\Delta CO/\Delta NO_x$ emission ratio value of 7.5 mol mol^{-1} from the 2011 NEI for Maryland, averaged over all sources. Above ~29°C, the observed emission ratio was much higher than the 2011 NEI. The DISCOVER-AQ observations of [CO] and [NO_y] support the notion of a temperature dependence of emissions, not present in the NEI.

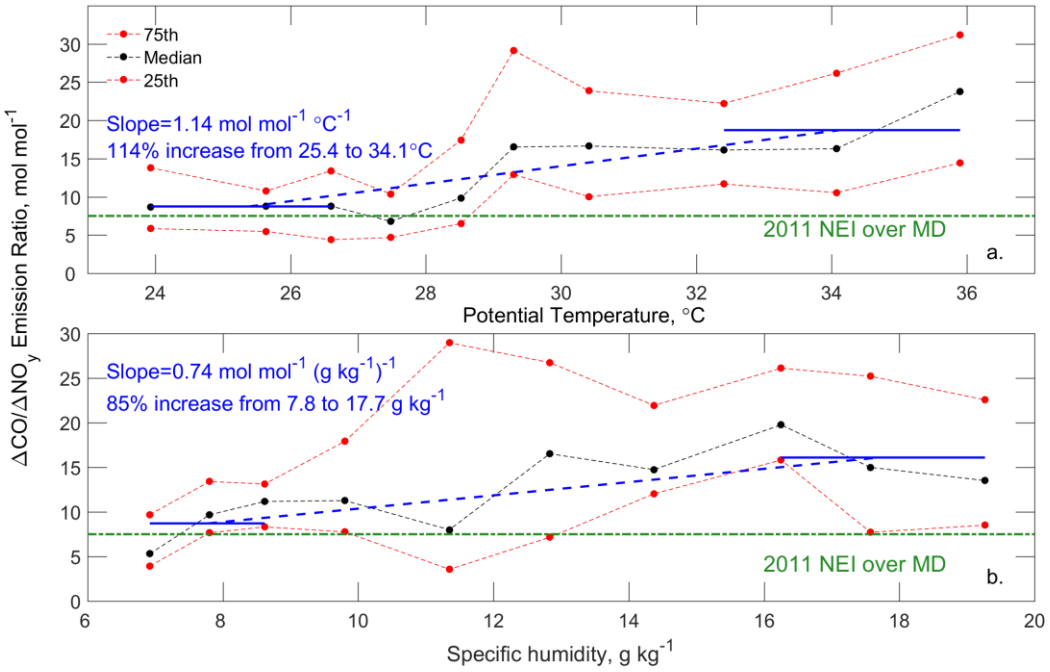

Figure 2.2. The $\Delta CO/\Delta NO_y$ emission ratio (inferred from observed [CO] and [NO_y] measurements) as a function of potential temperature (°C) and specific humidity (g_{H2O} kg^{-1}) for the entire July 2011 DISCOVER-AQ flight campaign over the Baltimore-Washington region. Data were split into bins with equal number of points. The black lines represent the median values and the red lines indicate the 25th and 75th percentiles of the binned observations. The leftmost solid blue lines represent the average of the emission ratios in the first three bins, while the rightmost solid blue lines represent the average of the ratios in the last three bins. The average temperature values of the first three and last three median points are connected by the dashed blue lines. The $\Delta CO/\Delta NO_y$ estimated from the 2011 NEI is shown by the dashed green lines. Potential temperature indicates the temperature a parcel of air would have if adiabatically compressed from the altitude of observation to near the surface (assumed to be 1000 hPa).

In a study by He et al. (2013), the authors found that summertime emissions of NO_x from stationary sources were sensitive to ambient temperature and peaked on hot, summer days. The temperature dependence observed in the DISCOVER-AQ data collected in the summer may indicate that emissions of NO_x from stationary sources become increasingly important relative to emissions from vehicles at higher temperatures in the summer.

The correlation between specific humidity and $\Delta CO/\Delta NO_y$ during the DISCOVER-AQ campaign is shown in Figure 2.2b. While there is a general increase in emission ratios with specific humidity, the rise is smaller than for temperature. At specific humidity values of 6.9 to 8.6 $gH_2O\ kg^{-1}$, the average $\Delta CO/\Delta NO_y$ is 8.7 mol mol^{-1}, while at humidity values between 16.3 and 19.3 $gH_2O\ kg^{-1}$ the average $\Delta CO/\Delta NO_y$ is 16.1 mol mol^{-1} (Figure 2.2b). This yields an increase in $\Delta CO/\Delta NO_y$ of 85% between 7.8 and 17.7 $gH_2O\ kg^{-1}$, the average of the two humidity ranges, less of a rise than the impact with temperature, but still an important consideration when analyzing emission ratios inferred from aircraft observations. Since temperature and specific humidity are coupled in the atmosphere (Figure A2 in Appendix A), part of the increase in $\Delta CO/\Delta NO_y$ with temperature should be due to the effect of humidity. However, there appears to be another contributor to the greater sensitivity of emission ratios to temperature than to humidity, which can be better explained with near-road observations.

The discrepancy between emissions of NO_x from the NEI and those inferred from DISCOVER-AQ suggests a sensitivity of vehicular emissions of NO_x to temperature and humidity. We analyze $\Delta CO/\Delta NO_x$, $\Delta CO_2/\Delta NO_x$, and $\Delta CO_2/\Delta CO$ from vehicles along a major highway to focus on the change in vehicular emissions of NO_x with ambient temperature and specific humidity. The DISCOVER-AQ campaign was conducted during July 2011, one of the hottest months on record for the Baltimore-Washington region (Figure A4 in Appendix A). The observed trend in the inferred $\Delta CO/\Delta NO_x$ emission ratio with increasing temperature (Figure 2.2a) suggests a strong response of vehicular emissions to ambient conditions. The latest version of

the 2011 NEI uses MOVES2014 to estimate highway emissions and does not apply a direct effect of temperature on running emissions of NO_x and CO in the default mode. This offers a possible explanation for the discrepancy between measured and modeled NO_y reported by Anderson et al. (2014) during the summer.

2.3.2 Near-Road Observations

Observations of [CO] and [NO_x] at a NR monitoring site along I-95 in the BWR were examined for an impact of temperature and humidity. Table 2.1 shows a summary of the data collected at the I-95 site for November 2016 and February, November, and December 2017, when measurements of [CO_2] were available. During this time, the median mixing ratios were 30.2 ppbv for [NO_x], 258 ppbv for [CO], and 443 ppmv for [CO_2]. These ambient pollutant levels are substantially elevated relative to regional background abundances, reflective of the close proximity of the NR site to the adjacent I-95.

Table 2.1. Statistics for [CO], [NO_x], and [CO_2] data collected at a NR site along I-95 for November 2016 and February, November, and December 2017.

I-95 Site one-min data	Number of valid data[#]	5th percentile	95th percentile	Median	Mean	Standard deviation
[CO] (ppbv)	110,237	140	571	258	296	146
[NO_x] (ppbv)	133,036	3.10	119	30.2	42.3	39.7
[CO_2] (ppmv)	118,862	414	504	443	449	30.5

[#]The numbers of observations of each variable differ slightly due to missing values

Ambient levels of [CO] and [NO_x] measured at the I-95 NR site reflect mobile emissions from vehicles traveling at ~81 km hr^{-1} (~50 miles per hour or mph) on the adjacent highway. Due to the proximity of the I-95 NR site to a rest area, cold starts or idling may represent a small fraction of the observations; however, we are not presently able to quantify directly the impact of cold starts on measurements of [NO_x], [CO], and [CO_2]. To minimize the effects of cold starts on the temperature and humidity analysis, we exclude observations collected when wind blew from non-highway angles. The adjacent highway represents angles between 25° and 225° Compass relative to the I-95 monitoring site (Figure A2 in Appendix A). The monitoring site is located ~100 m Southeast of the closest part of a rest area that holds parking spaces for 90 passenger vehicles and 50 large diesel-fueled trucks. There is a second, smaller rest area located ~200 m Southeast of the I-95 site on the other side of the highway, which holds parking spaces for 75

passenger vehicles and 20 large diesel-fueled trucks. Restricting the analysis to 25° to 225° Compass wind directions limits the influence of emissions coming from the rest area Northwest of the site but does not exclude emissions from the smaller rest area Southeast of the monitoring site. An analysis of [CO], [NO_x], and [CO_2] as a function of wind direction, however, shows that ambient levels were much higher when wind blew from the highway as opposed to from the rest area Northwest of the monitoring site, by 86% for [CO], 400% for [NO_x], and 8% for [CO_2] (Figure A5). Since this rest area has a greater vehicle parking capacity than the second area located Southeast of the monitoring site, and the average number of total vehicles passing the site along I-95 was roughly 8,430 vehicles per hour for the period of study, the impact of running emissions outweigh vehicle start or idling emissions from either rest area.

2.3.2.1 Influence of Temperature and Specific Humidity on Emissions at the Interstate-95 NR Site Using One-Minute Observations

The positive dependence of $\Delta CO/\Delta NO_x$ with ambient temperature and specific humidity found during DISCOVER-AQ can be further explored by analyzing emission ratios inferred from [CO], [NO_x], and [CO_2] observations at the I-95 NR site. The relationship between $\Delta CO/\Delta NO_x$, $\Delta CO_2/\Delta NO_x$, and $\Delta CO_2/\Delta CO$ and outdoor temperature is shown in Figure 2.3 for temperatures between –5°C and 25°C. The light gray dots represent the individual hourly emission ratios estimated from regressions of the one-minute observations, which have been sorted by temperature

into ten bins, each containing an equal number of data points. The black and light gray lines connect the median, 25th, and 75th percentiles of hourly emission ratios in the ten bins. An ordinary best-fit line to the median values is given by each red line. The positive relationship between $\Delta CO/\Delta NO_x$ and temperature shows a statistically significant increase of 113% over the temperature range from −5°C to 25°C (Figure 2.3a). We have also tested the sensitivity of the daily-averaged hourly $\Delta CO/\Delta NO_x$, $\Delta CO_2/\Delta NO_x$, and $\Delta CO_2/\Delta CO$ to the daily maximum temperature, in an attempt to minimize the impact of daily traffic trends on the analysis, which shows an increase in both $\Delta CO/\Delta NO_x$, $\Delta CO_2/\Delta NO_x$ with rising temperature similar to Figure 2.3 (Figure A8 in Appendix A). An alternative method of estimating the impact of temperature on $\Delta CO/\Delta NO_x$, $\Delta CO_2/\Delta NO_x$, and $\Delta CO_2/\Delta CO$, based upon the slope values of linear regressions conducted for every 10 one-minute set of observations, results in a similar positive trend in $\Delta CO/\Delta NO_x$ and $\Delta CO_2/\Delta NO_x$ and is shown in Figure A9 in Appendix A.

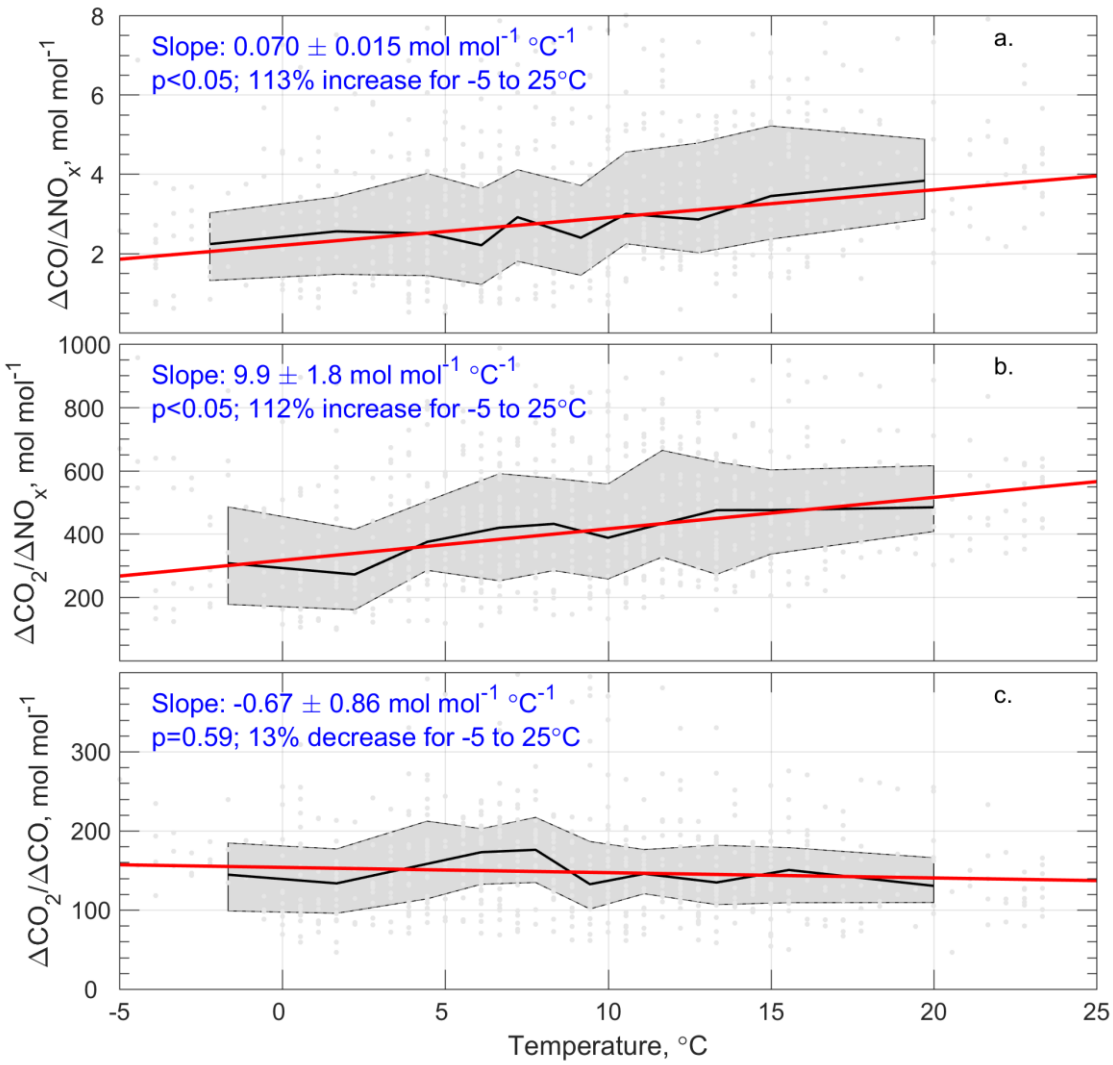

Figure 2.3. Hourly $\Delta CO/\Delta NO_x$ (a), $\Delta CO_2/\Delta NO_x$ (b), and $\Delta CO_2/\Delta CO$ (c) for all hours of the day and all values of specific humidity as a function of ambient temperature at the I-95 NR site in Howard County, MD. Emission ratios were estimated from one-minute data collected in November 2016 and February, November, and December 2017. Individual one-minute observations are shown by the light gray dots, which were placed into 10 bins, each containing an equal number of points. The black lines correspond to the median emission ratios in each bin, bounded by the 25th and 75th percentiles of the bins represented by the light gray lines. The solid red lines represent ordinary, linear least-squares regression fits of the binned median emission ratios. The uncertainty of the slope parameter of each trend was estimated using a Method of Maximum Likelihood, following Bevington and Robinson (2002).

The temperature dependence of emissions was further investigated by analyzing the behavior of $\Delta CO_2/\Delta NO_x$ and $\Delta CO_2/\Delta CO$ as a function of temperature. In our analysis, $\Delta CO_2/\Delta NO_x$ increased by 112% ($p<0.05$) while $\Delta CO_2/\Delta CO$ showed no statistically significant trend ($p=0.59$) as temperature increased from −5°C to 25°C (Figure 2.3 b–c). Since over 99% of vehicle emissions of carbon-containing compounds are in the form of CO_2, the emission of CO_2 is unlikely to have changed by a factor of two in the –5°C to 25°C range of temperature. Therefore, our roadside measurements indicate that vehicular emissions of NO_x decrease with increasing ambient temperature, while no significant trend was observed for $\Delta CO_2/\Delta CO$.

By estimating hourly emission ratios from the regression slopes of one-minute observations as done in Figure 2.3, there is no need to assume a background to subtract from hourly averaged concentrations of each pollutant. To verify, we tested the results of the temperature sensitivity of $\Delta CO/\Delta NO_x$ using several methods of estimating a constant background to calculate the hourly emission ratios that gave nearly identical results to those shown in Figure 2.3 (see Section A12 and Figure A10 and Figure **A11** in Appendix A for more information). These constant background values of [CO] and [NO_x] were estimated from the 5^{th} percentile of the dataset, the mean concentration from a cleaner wind corridor, a scatterplot method, and a suburban AQS site located ~10 km South/Southwest of the I-95 NR site (Section A12 in Appendix A). The average slope of $\Delta CO/\Delta NO_x$ as a function of temperature for these four background methods was 0.098 ± 0.017 (1σ; mol mol^{-1}) $°C^{-1}$ – the choice of background does not alter the general conclusions. In addition to one-minute and hourly observations

collected at the I-95 NR site, hourly data are also available at a NR site along highway DC-295 within the District of Columbia that will be examined in future work.

The temperature dependence of $\Delta CO/\Delta NO_x$ shown in Figure 2.3a was lower than the slope observed during DISCOVER-AQ (1.14 mol mol^{-1} $°C^{-1}$) possibly because the DISCOVER-AQ campaign took place 4 years prior to the NR observations and temperatures were higher in July 2011. The aircraft campaign may have captured the temperature dependence of vehicles under many types of conditions, whereas the emissions inferred at the NR site were mostly of vehicles traveling above 81 km hr^{-1}. During the summer an important source of CO is isoprene oxidation (Miyoshi and Washida, 1994). Production of CO from this source would increase the ratio at high temperatures when isoprene emissions are large. Aircraft measurements integrated emissions from a variety of sources (i.e., vehicles, vegetation, power plants). Since the emission of isoprene is temperature sensitive, more CO would have been produced from biogenic sources at higher temperatures, complicating the observed trend (see Section A13 in Appendix A for more information). This effect was likely captured by the aircraft measurements, but would have been overwhelmed by vehicular emissions at the NR site, especially during winter.

The rise in $\Delta CO/\Delta NO_x$ with increasing ambient temperature during the summer DISCOVER-AQ campaign was most likely caused at least in part by a temperature dependence of vehicular emissions since the dominant source of CO and NO_x in Maryland is vehicles; those results motivated this research. The mechanism controlling the observed temperature sensitivity of NO_x emissions during DISCOVER-AQ at the high temperatures may differ from the mechanism controlling

the sensitivity of NO_x emissions along I-95 at the low temperatures, however this is a subject for further investigation and out of the scope of this study. We have not studied the impact of temperature on emissions at the I-95 NR site in the summer, however an increase in $\Delta CO/\Delta NO_x$ with rising temperature observed in the winter at the NR site shows that vehicular emissions of NO_x, with current technology, are strongly sensitive to ambient temperature.

The impact of specific humidity ($gH_2O\ kg^{-1}$) on emission ratios is also examined. As noted above, temperature and humidity are positively correlated in the atmosphere (see Figure A2 in Appendix A). Figure 2.4 (a–b) shows that $\Delta CO/\Delta NO_x$ and $\Delta CO_2/\Delta NO_x$ both increased with higher specific humidity. However, the magnitudes of the trends are much smaller than those observed with temperature. The humidity dependence of these two emission ratios is not statistically significant ($p=1$ and $p=0.37$, respectively). Whereas values of $\Delta CO/\Delta NO_x$ and $\Delta CO_2/\Delta NO_x$ increased by ~110% over a −5 to 25°C range of temperature, emission ratios increased by only 34 and 23%, respectively, for a change of specific humidity from ~1 to 10 $gH_2O\ kg^{-1}$. Similar to what was found for temperature (Figure 2.3c), $\Delta CO_2/\Delta CO$ does not exhibit a statistically significant trend with humidity ($p=0.72$; Figure 2.4c).

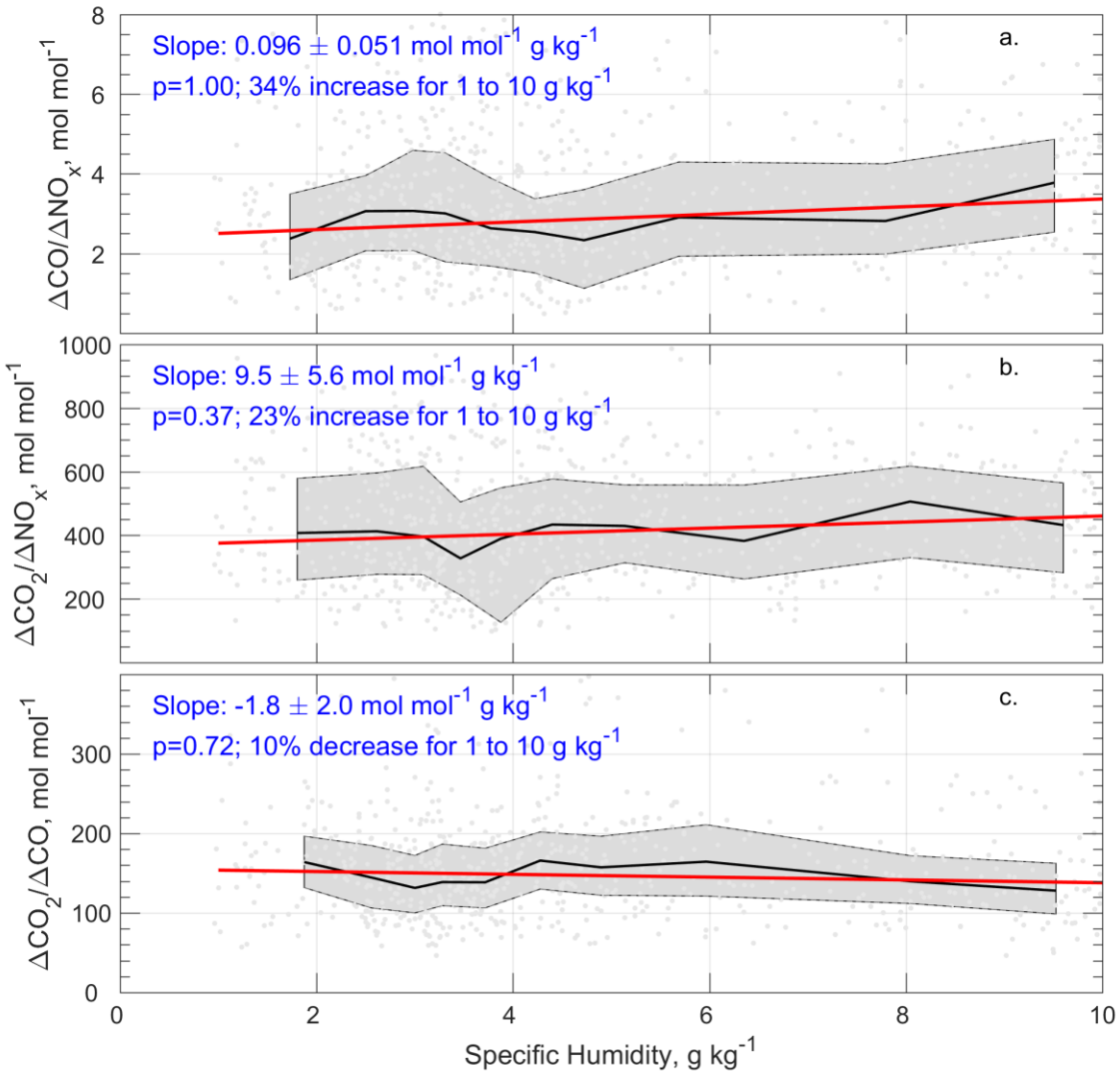

Figure 2.4. Hourly $\Delta CO/\Delta NO_x$ (a), $\Delta CO_2/\Delta NO_x$ (b), and $\Delta CO_2/\Delta CO$ (c) for all hours of the day and all values of temperature as a function of ambient specific humidity. Emission ratios were estimated from one-minute data collected at the I-95 NR site in Howard County, MD. Individual one-minute observations are shown by the light gray dots, which were placed into 10 bins, each containing an equal number of points. The black lines correspond to the median emission ratios in each of 10 bins, bounded by the 25th and 75th percentiles of the bins represented by the light gray lines. The solid red lines represent the ordinary least-squares regression fits of the binned median emission ratios.

To account for the variability of fleet composition with local time of day (Figure 2.1), we investigated three designated time windows (Table 2.2): 0:00 to 4:59,

5:00 to 10:59, and 15:00 to 20:59 Eastern Local Time (ET). Table 2.2 summarizes the ordinary least-squares regression slope values of unbinned scatterplots of $\Delta CO/\Delta NO_x$, $\Delta CO_2/\Delta NO_x$, and $\Delta CO_2/\Delta CO$, as function of temperature and specific humidity, in three time windows. Values of $\Delta CO_2/\Delta NO_x$ and $\Delta CO_2/\Delta CO$ showed a statistically significant increase with temperature from 0:00 to 4:59 ET, which may indicate a decrease in both NO_x and CO emissions with rising temperatures during these hours. Over the entire day, the bulk of the NO_x arises from diesel combustion while the bulk of CO is from gasoline combustion. In the morning hours from 0:00 to 4:59 ET, when truck traffic is highest relative to cars, diesel emissions of CO are at the highest fraction of the total and improved functioning of control devices on diesel vehicles appears to become detectable. The simultaneous decreases in both NO_x and CO emissions likely cancel each other out, which explains why there is no significant trend in $\Delta CO/\Delta NO_x$ with temperature from 0:00 to 4:59 ET. Both $\Delta CO/\Delta NO_x$ and $\Delta CO_2/\Delta NO_x$ exhibited a positive slope from 5:00 to 10:59 ET (0.073 mol mol^{-1} °C^{-1}, $p<0.05$; 8.5 mol mol^{-1} °C^{-1}, $p<0.05$), but statistically insignificant slope values in the afternoon rush hours (15:00 to 20:59 ET). Note that the ratio of CIV-to-total vehicles changed by a factor of approximately four (from 26% to 6%) from the 0:00 to 4:59 ET time period to the afternoon rush hours. The change in fleet makeup over the course of the day may impact our analysis when all hours of the day are considered (Figure 2.3 and Figure 2.4). Temperature impacts are still observed even when the analysis is divided into time windows.

Table 2.2. Slope values of unbinned $\Delta CO/\Delta NO_x$, $\Delta CO_2/\Delta NO_x$, and $\Delta CO_2/\Delta CO$ as a function of temperature (mol mol^{-1} $°C^{-1}$) and specific humidity (mol mol^{-1} (g_{H2O} $kg^{-1})^{-1}$) at the I-95 NR site in Howard County, MD. The data have been divided into three Eastern Local Time windows. Values of statistical significance are shown in bold. The percentages of SIV and CIV are indicated in each time window.

Slope as a function of temperature, mol mol^{-1} $°C^{-1}$	All day 0:00–23:59 ET 87% SIV 13% CIV	0:00–4:59 ET 74% SIV 26% CIV	5:00–10:59 ET 88% SIV 12% CIV	15:00–20:59 ET 94% SIV 6% CIV
$\Delta CO/\Delta NO_x$	**0.070±0.015 (p<0.05)**	−0.023±0.036 (p=0.62)	**0.049±0.025 (p<0.05)**	0.020±0.036 (p=0.40)
$\Delta CO_2/\Delta NO_x$	**9.9±1.8 (p<0.05)**	**5.4±4.7 (p<0.05)**	**8.8±3.5 (p<0.05)**	4.8±4.8 (p=0.21)
$\Delta CO_2/\Delta CO$	−0.67±0.86 (p=0.59)	**3.0±1.3 (p<0.05)**	0.098±0.75 (p=0.60)	−0.48±0.64 (p=0.53)
Slope as a function of specific humidity, mol mol^{-1} (g $kg^{-1})^{-1}$	**All day 0:00–23:59 ET 87% SIV 13% CIV**	**0:00–4:59 ET 74% SIV 26% CIV**	**5:00–10:59 ET 88% SIV 12% CIV**	**15:00–20:59 ET 94% SIV 6% CIV**
$\Delta CO/\Delta NO_x$	0.096±0.051 (p=1)	0.021±0.091 (p=0.78)	0.11±0.066 (p=0.074)	0.047±0.086 (p=0.78)
$\Delta CO_2/\Delta NO_x$	9.5±5.6 (p=0.37)	−6.4±12 (p=0.60)	13±9.2 (p=0.089)	−10±11 (p=0.46)
$\Delta CO_2/\Delta CO$	−1.8±2.0 (p=0.72)	4.8±3.4 (p=0.092)	−1.1±2.0 (p=0.81)	−0.68±1.5 (p=0.38)

A possible explanation for the increase in both $\Delta CO_2/\Delta NO_x$ and $\Delta CO_2/\Delta CO$ at the I-95 site from 0:00 to 4:59 ET, when the ratio of CIV/total vehicles was at its highest of the day at 26%, is that running emissions of CO and NO_x from CIVs may be more sensitive to temperature than emissions from SIVs. Recent studies by Grange et al. (2019) and Weber et al. (2019) reported a decrease in running emissions of NO_x with rising temperatures from European light-duty CIVs, most of which use similar combustion after-treatment devices found in the US fleet. In addition, the selective

catalytic reduction technology found in most trucks must reach ~200°C before the system begins to reduce NO_x emissions (Preble et al., 2019). These findings, coupled with the much higher ambient levels of [CO], [NO_x], and [CO_2] when wind at the NR site blew from the highway as opposed to the adjacent rest area (Figure A5), suggest that the ambient temperature sensitivity of emissions of NO_x observed in the 0:00 to 4:59 ET timeframe at the I-95 NR site is dominated by a sensitivity in running emissions from CIVs, rather than cold-starts or idling.

The increase in $\Delta CO/\Delta NO_x$ and $\Delta CO_2/\Delta NO_x$ with rising temperatures during the morning rush hours (5:00 to 10:59 ET) at the I-95 site, accompanied by no statistically significant trend in $\Delta CO_2/\Delta CO$, is likely due to a decrease in emissions of NO_x with increasing temperature. The ratio of CIV/total vehicles was 12% during the morning rush hours, thus we attribute the decrease in NO_x to both CIV and SIV. However, even though the fraction of CIV to total vehicles is on average less than 10% for the morning and afternoon rush hours (15:00 to 20:59 ET), vehicular NO_x emissions are likely dominated by truck emissions during these times due to their higher NO_x emission factors ($g_{NOx}\ kg_{fuel}^{-1}$) and greater consumption of fuel per mile traveled.

The same mechanism that drives the decrease in NO_x emissions with rising temperatures during the morning rush hours (5:00 to 10:59 ET) may be responsible for the majority of the trend in NO_x observed from 0:00 to 4:59 ET; simultaneous changes in CO and NO_x cancel out and lead to no significant change in $\Delta CO/\Delta NO_x$ with temperature in the latter time window. Slow wind speeds at the monitoring site from 0:00 to 4:59 ET may cause a portion of the vehicular cold-start effect (i.e.,

increasing CO and NO_x emissions with falling temperatures) from the adjacent rest area, especially from gasoline-fueled cars, to be sampled and included in the analysis. When low wind speeds of less than 0.5 m s^{-1} (about 30% of the hourly data in this time period) are excluded from the analysis in Table 2.2, the slope of $\Delta CO_2/\Delta NO_x$ with temperature changes by only ~10% and remains positive and statistically significant; the trend in $\Delta CO_2/\Delta CO$ with temperature remains positive but loses its statistical significance (Table A2 in Appendix A).

Sensitivity of emission ratios to humidity are more difficult to quantify. The analysis in Table 2.2 shows that for all hours of the day, both $\Delta CO/\Delta NO_x$ and $\Delta CO_2/\Delta NO_x$ increase slightly with rising specific humidity, however these trends are not statistically significant (p=1 and p=0.37, respectively). The greatest sensitivity in $\Delta CO/\Delta NO_x$ and $\Delta CO_2/\Delta NO_x$ to specific humidity occurs during the morning rush hours, from 5:00–10:59AM, with slope values of 0.11 mol mol^{-1} (g $kg^{-1})^{-1}$ (p=0.074) and 13 mol mol^{-1} (g $kg^{-1})^{-1}$ (p=0.089). The significance and sensitivity of these trends are weaker than for temperature.

2.3.2.2 Uncertainty Analysis for Temperature and Humidity Trends at I-95 NR Site

The known sources of uncertainty in the trends shown in Figure 2.3 and Figure **2.4** originate from uncertainty in the measurements of CO, NO_x, CO_2, temperature, and relative humidity, estimates of the hourly emission ratios, and the regression with temperature or specific humidity in those figures. Using Figure 2.3a as an example, the relative uncertainty (summation in quadrature of the accuracy, defined as the difference between concentration indicated in the standard and that indicated by the

instrument, uncertainty in the calibration standard gas, and the manufacturer's specified precision, zero drift and noise at the zero) was 8.0% for CO measurements, 4.9% for NO_x, and 0.15% for CO_2 (replacing the drift and noise at the zero reading with the maximum drift in the uncertainty calculation). The accuracy in temperature measurements is about ±0.2°C. We estimate 12% uncertainty in the hourly emission ratios shown by the light gray dots in Figure 2.3 (the average of the relative uncertainties in the hourly emission ratios, calculated by the absolute uncertainty in each hourly emission ratio, not shown in Figure 2.3, divided by the emission ratio in that hour), and 21% relative uncertainty in the slope of $\Delta CO/\Delta NO_x$ as a function of temperature from Figure 2.3a. The final uncertainty estimate for the trend in $\Delta CO/\Delta NO_x$ with temperature at the I-95 NR site (Figure 2.3**Error! Reference source not found.**a) is 26%, calculated by adding the squares of the relative uncertainties in quadrature. Repeating the same method for $\Delta CO_2/\Delta NO_x$ as a function of temperature yields a similar number, but for $\Delta CO_2/\Delta CO$ this correlation is weak with an uncertainty of 129%. The relative uncertainty in the trend with specific humidity is higher (Figure 2.4), 55% for $\Delta CO/\Delta NO_x$, 62% for $\Delta CO_2/\Delta NO_x$, and 112% for $\Delta CO_2/\Delta CO$.

2.3.3 Comparison of Observations with MOVES model

The temperature dependence of the inferred hourly emission ratios at the I-95 site was compared to MOVES2014a model output for Howard County, MD, where the I-95 site is located. Figure 2.5 shows the temperature dependence of $\Delta CO/\Delta NO_x$, $\Delta CO_2/\Delta NO_x$, and $\Delta CO_2/\Delta CO$ from MOVES output. The color of each line represents

the vehicle class. Motorcycles, passenger cars, passenger trucks, and light-commercial vehicles were assumed to run on gasoline, while buses, refuse trucks, and single- and combination-unit trucks were assumed to use diesel fuel. The most likely fuel used by each vehicle type shown in Figure 2.5 was determined from county model input data. The turquoise diamonds represent averaged emission ratios of $\Delta CO/\Delta NO_x$, $\Delta CO_2/\Delta NO_x$ and $\Delta CO_2/\Delta CO$, weighted to reflect actual contributions of NO_x and CO, respectively, by each vehicle class using traffic counts along I-95 (see section A15 in Appendix A for more information). Although the majority of vehicles passing the I-95 site were passenger cars, passenger trucks, light commercial trucks, and single- and combination-unit trucks, the impact of temperature on the weighted average emission ratios in the model output showed very little sensitivity to fleet makeup. That is, the average trend in emission ratios with temperature is similar among gasoline-fueled passenger cars, passenger trucks, and light commercial trucks, and between diesel-fueled single-and combination-unit trucks. Therefore, normal temporal variations in the fleet makeup do not impact our conclusions.

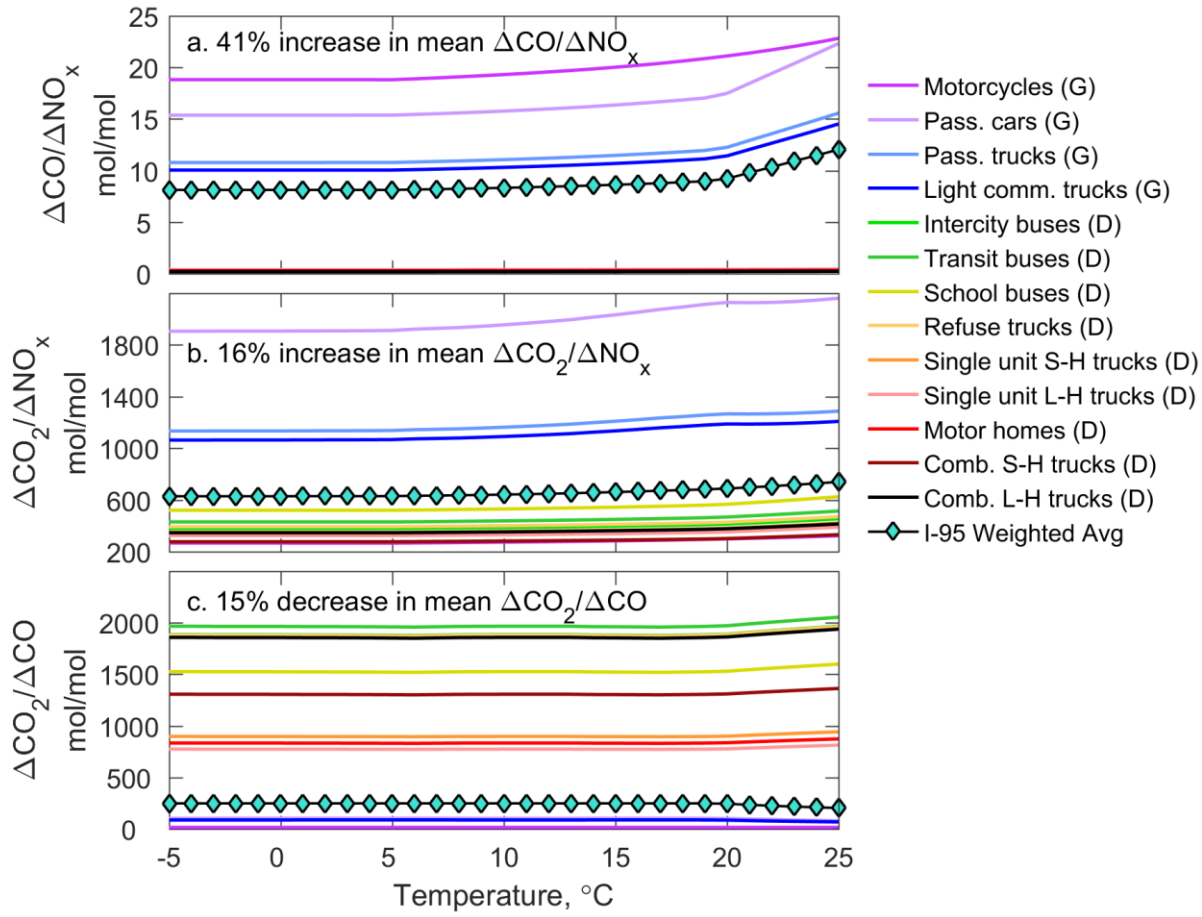

Figure 2.5. $\Delta CO/\Delta NO_x$, $\Delta CO_2/\Delta NO_x$, and $\Delta CO_2/\Delta CO$ calculated from average emission ratios weighted by vehicle speed and model year on rural restricted roads from MOVES output for Howard County, MD, using December 2014 input data. Plotted are the emission ratios as a function of temperature sorted by vehicle type for weekdays on rural restricted roads (such as I-95 in Howard County, MD). Each point represents an emission ratio at the indicated temperature and a specific humidity calculated from Figure A2 in Appendix A, an exponential best-fit of the temperature and specific humidity observations at the I-95 site. Passenger cars, passenger trucks, motorcycles, and light commercial trucks are assumed to run on gasoline, whereas buses, refuse trucks, and single- and combination-unit trucks were assumed to use diesel (based on county vehicle fuel data). Comb. S-H trucks denotes combination short-haul trucks while Comb. L-H trucks represents combination long-haul trucks.

The sensitivity of MOVES emissions output to model temperature appears to be due to an indirect effect in the model that adjusts the emission rates to the use of

air conditioners (AC). Below 20°C (68°F), MOVES emissions do not show any temperature dependence. Between 20°C and 25.6°C (78°F) the output of MOVES depends on temperature alone, and above 25.6°C emissions of CO, NO_x, and CO_2 from MOVES are adjusted for heat index which includes both temperature and relative humidity (Figure 2.5; Equation A2 in Appendix A).

Over the temperature range from −5°C to 25°C (Figure 2.5), MOVES showed increases of 41% in $\Delta CO/\Delta NO_x$, 16% in $\Delta CO_2/\Delta NO_x$, and 15% in $\Delta CO_2/\Delta CO$. Figure A12 in Appendix A shows the change with temperature of CO, NO_x, and CO_2 emission rates (mol mile^{-1}) from MOVES output. The cause for the increase in $\Delta CO/\Delta NO_x$ and $\Delta CO_2/\Delta NO_x$ in MOVES is a rise in emissions of CO and CO_2 combined with a decrease in NO_x emissions as temperature rises. A test for the effects of specific humidity on emission ratios showed that $\Delta CO/\Delta NO_x$ and $\Delta CO_2/\Delta NO_x$ increased by 16% and 14%, respectively, from 1 to 10 gH_2O kg^{-1} (Figure A13 in Appendix A). MOVES does not adjust CO and CO_2 emissions in response to specific humidity, thus there is no change in $\Delta CO_2/\Delta CO$ with specific humidity. The increase in $\Delta CO/\Delta NO_x$ and $\Delta CO_2/\Delta NO_x$ is due to a direct decrease of NO_x emissions with increasing specific humidity unrelated to the AC factor. Thus, specific humidity effects in MOVES can account for a change of only 16% in $\Delta CO/\Delta NO_x$ from 1 to 10 gH_2O kg^{-1}.

Model guidance suggests that the direct AC effects are only applied to passenger vehicles and light commercial trucks, which does not explain the increase in the CO_2 emission rate for all other vehicle types evident in Figure 2.5 and Figure A12 in Appendix A. While only CO, NO_x, and HC are affected by the AC adjustment term in the model, the energy consumption increases as AC usage increases. The

calculated CO_2 emission rates use the energy consumption in their calculation, which in turn causes $\Delta CO_2/\Delta CO$ and $\Delta CO_2/\Delta NO_x$ from all other vehicle types to increase slightly due to a rise in CO_2 when the AC in the model is turned on at temperatures of 20°C and above.

In the temperature range of –5°C to 25°C, MOVES exhibits a much smaller increase in $\Delta CO/\Delta NO_x$ and $\Delta CO_2/\Delta NO_x$ than was observed during DISCOVER-AQ and at the two NR sites (Table 2.3). The 113% increase in $\Delta CO/\Delta NO_x$ and the 112% increase in $\Delta CO_2/\Delta NO_x$ at the I-95 site cannot be explained by a temperature dependence of CO and CO_2 emissions from air conditioner use, as in MOVES. Rather, these increases are likely due to a decrease in mobile emissions of NO_x with rising ambient temperatures. As shown in Figure A12 in Appendix A, over the same temperature range as the observations, MOVES estimates that CO_2 emissions increase by only 3.5%. Assuming this increase in vehicular CO_2 emissions with temperature is similar to that at the I-95 site, the primary factor governing the increase in $\Delta CO_2/\Delta NO_x$ and $\Delta CO/\Delta NO_x$ with temperature observed at I-95 must be a decrease in the emission of NO_x as temperature rises.

Table 2.3. Comparison of the change in $\Delta CO/\Delta NO_x$, $\Delta CO_2/\Delta NO_x$, and $\Delta CO_2/\Delta CO$ with ambient temperature from aircraft and NR observations and MOVES output.

Percent change with temperature	Temperature range	$\Delta CO/\Delta NO_x$	$\Delta CO_2/\Delta NO_x$	$\Delta CO_2/\Delta CO$
DISCOVER-AQ	26°C to 32°C	114%		
I-95 NR Observations	−5°C to 25°C	113%	112%	-13%
MOVES	−5°C to 25°C	41%	16%	15%

[1]MOVES run for Howard County, MD only, where I-95 NR site is located.

2.4 Conclusions

Observations collected in the Baltimore Washington region at a surface NR monitoring site along I-95 (a major eight-lane interstate highway) in the cold season, and aboard an aircraft in the summer indicate a significant decrease in vehicular NO_x emissions with increasing temperature. Tailpipe emissions of CO appear relatively insensitive to temperature or humidity, but between −5°C and 25°C highway emissions of NO_x decrease by a factor of approximately two. This result is robust to changes in sampling time, time of day, wind direction, and methods for determining background. NR observations also indicate a modest (~23%) increase in $\Delta CO_2/\Delta NO_x$, marked by a decrease in NO_x emissions, with increasing specific humidity between 1 and 10 g kg^{-1}.

We cannot presently quantify the impact of cold-starts, but the close proximity of the NR analyzer to the highway (~12 m) and high hourly counts of passing traffic (8430 vehicles hr^{-1}) suggest that running vehicular emissions are primarily responsible for the sensitivity of NO_x emissions to temperature and humidity.

The higher fuel-specific NO_x emission factors, combined with the greater amount of fuel used per vehicle mile traveled, suggest that trucks dominate vehicular emissions of NO_x throughout the day. The greater sensitivity at the I-95 NR site of $\Delta CO_2/\Delta NO_x$ and $\Delta CO_2/\Delta CO$ to temperature in the early morning hours (0:00 to 4:59 ET), when the ratio of diesel trucks to total vehicles is highest of the day and NO_x emissions from diesel-fueled vehicles outweigh those from light-duty gasoline vehicles the most, suggests that truck emissions exhibit a strong dependence on temperature.

Analysis of CO and NO_x altitude profiles from DISCOVER-AQ in July 2011 indicate an increase in $\Delta CO/\Delta NO_x$ of ~110% between 25 and 34°C surface temperature – consistent with a decrease in NO_x emissions. These aircraft data reflect integrated biogenic and anthropogenic sources from across the entire urban areas including vehicles and power plants. This ratio also decreased by ~85% as specific humidity increased from ~8 to 18 g kg^{-1}.

MOVES, the official model used by the US EPA to calculate mobile emissions, includes an increase in $\Delta CO/\Delta NO_x$ with rising temperature of 41% and in $\Delta CO_2/\Delta NO_x$ of 16% over the range −5 to 25°C, and an increase of 16% in $\Delta CO/\Delta NO_x$ and 14% in $\Delta CO_2/\Delta NO_x$ as specific humidity increased from 1 to 10 g kg^{-1}. The model underpredicts both the temperature and specific humidity impacts compared to the NR site, indicating that the default setting of unity in the multiplicative temperature adjustment factor of running emissions within MOVES may need to be reexamined.

The sensitivity of NO_x emissions to temperature may help explain why studies conducted during the summer find overestimates of NO_x emissions in the NEI (Anderson et al., 2014; Mao et al., 2018; McDonald et al., 2018; Souri et al., 2016; Travis et al., 2016), but a study conducted in the winter suggests good agreement (Salmon et al., 2018). According to our analysis, higher NO_x emissions occur at lower temperatures; observations should better match the higher NEI estimate during the winter.

Air quality models provide the means to forecast hazardous air pollution. The discrepancy between modeled NO_x and the emission of NO_x from inventories is especially important to investigate (Canty et al., 2015; Duncan et al., 2010; Goldberg

et al., 2016). Our next steps will be to investigate the MOVES2014a code to improve agreement with the NR observations, repeat this analysis at a different NR site located in the District of Columbia, where trucks are fewer, and assess the implications of these changes to future surface ozone attainment strategies. Incorporating the impact of temperature on emissions of NO_x within MOVES will allow air quality models to better represent mobile emissions inferred from real-world measurements.

Chapter 3: Investigation of a Temperature Sensitivity of Mobile Emissions of BC and Comparison to Emissions From MOVES

The work in this chapter and Chapter 4 is currently in preparation for a paper to be submitted to the journal *Atmospheric Environment* under the title "Near-Road Observations of BC, CO, NO_x, and CO_2: Impacts of COVID-19 Restrictions, Traffic Patterns, and Temperature". I am the first author of this paper and collaborated with five co-authors from the University of Maryland. Numbered references within this chapter have been adjusted to reflect the numbering system of the dissertation.

3.1 Introduction

The temperature sensitivity observed in mobile NO_x running emissions (Chapter 2) warrants further investigation into similar air pollutants commonly found in vehicular exhaust, including BC. Black carbon, a carbonaceous component of fine particulate matter, is a public health hazard because of its negative impact on the respiratory system and possible cancer risk. Diesel-powered trucks, which we found to exhibit a temperature dependence in NO_x emissions in Chapter 2, are the dominant emitter of highway BC emissions, contributing approximately 77% of on-road BC emissions (2017 NEI; data available at https://www.epa.gov/air-emissions-inventories/2017-national-emissions-inventory-nei-data). With on- and off-road vehicles accounting for 42% of total BC emissions (2017 NEI), populations living near highways may experience the largest health impacts due to elevated ambient

BC levels from the nearby roadway. In this Chapter I will examine the temperature sensitivity of inferred BC emissions at the I-95 NR site across the different seasons as well as within the cold season only, similar to Chapter 2.

Ambient temperature has been found to impact on-road vehicular emissions (Grange et al., 2019; Hall et al., 2020; Li and Lü, 2021; Saha et al., 2018; Weber et al., 2019). Inferred mobile NO_x emissions at the I-95 NR site in Maryland were lower at higher outdoor temperatures while CO and CO_2 emissions remained relatively constant (Hall et al., 2020 and Chapter 2). A similar temperature sensitivity was reported at a NR site in North Carolina (US), with higher NO_x emission factors in winter than in summer (Saha et al., 2018). Further studies examining the European vehicle fleet found declining mobile NO_x emissions with rising ambient temperatures in light-duty diesel vehicles (Grange et al., 2019; Weber et al., 2019). In addition to mobile NO_x emissions, BC emissions also appear temperature sensitive. Some evidence suggests that mobile BC emissions from diesel-fueled vehicles peak at the highest ambient temperatures (Book et al., 2015; Chen et al., 2001; Kondo et al., 2006). Other studies found little seasonal difference in the contribution of $PM_{2.5}$ mass concentration from diesel vehicles (Kim and Hopke, 2012); gasoline-powered vehicles may even emit higher BC emissions at colder temperatures, such as during cold-starts (Schauer et al., 2008).

Mobile emissions reported in the NEI are estimated using output from the MOVES model developed by the US EPA (US EPA, 2015a). MOVES incorporates multiplicative factors to adjust mobile hot-running emissions of CO, NO_x, and BC for ambient temperature. In both the previous version (MOVES2014b) and the latest

version (MOVES3), the adjustment factors for CO and NO_x are set to unity and running emissions from any gasoline- or diesel-powered vehicle are not adjusted for temperature (US EPA, 2020b, 2015b). MOVES2014b includes an adjustment for hot-running BC emissions for gasoline vehicles of model year (MY) 2004 and earlier but does not modify running BC emissions from diesel-fueled vehicles (US EPA, 2015b). The temperature sensitivity in running BC emissions from MY 2004 and older gasoline vehicles was removed in MOVES3 (US EPA, 2020b). More details on the temperature impact on running NO_x, CO, and CO_2 emissions in MOVES2014b are provided in Hall et al. (2020). The absence of a temperature sensitivity in mobile BC emissions simulated by MOVES may also help to explain a previous study showing that the CMAQ model, which indirectly uses mobile emissions simulated by MOVES, underestimates ambient BC concentrations in the summer but is consistent with observations in the winter (Appel et al., 2008).

In this study we use ambient measurements of BC, CO, and CO_2 collected at a fixed NR monitor located along I-95 in Maryland to infer mobile emissions using ratios. We present evidence for a temperature dependence in mobile BC emissions and compare the results to the temperature sensitivity of BC emissions from MOVES3.

3.2 Methodology

3.2.1 Interstate-95 Near-Road Observations

Ambient pollutant concentrations and meteorological data were collected at a NR site located ~12 m from the southbound leg of I-95, an eight-lane interstate

highway in Maryland (Figure 3.1; 39° 8’ 35.38” N, 76° 50’ 45.53” W). The site is managed by the MD Department of the Environment as part of the US EPA Air Quality System (AQS), and the monitoring site follows standard measurement collection and quality control protocol outlined in the Code of Federal Regulations (CFR) 40 part 58 (available at http://www.ecfr.gov/cgi-bin/ECFR?page=browse). Hourly-averaged data were calculated from 10-second averaged NO_x and CO mixing ratios, 1-min averaged BC concentrations ([BC]), and 2-s averaged CO_2 abundances. To isolate highway emissions, only hours when winds were blowing from the adjacent highway (25° to 225° clockwise from North) were used in these analyses. Allowing wind from all direction had little impact on the results.

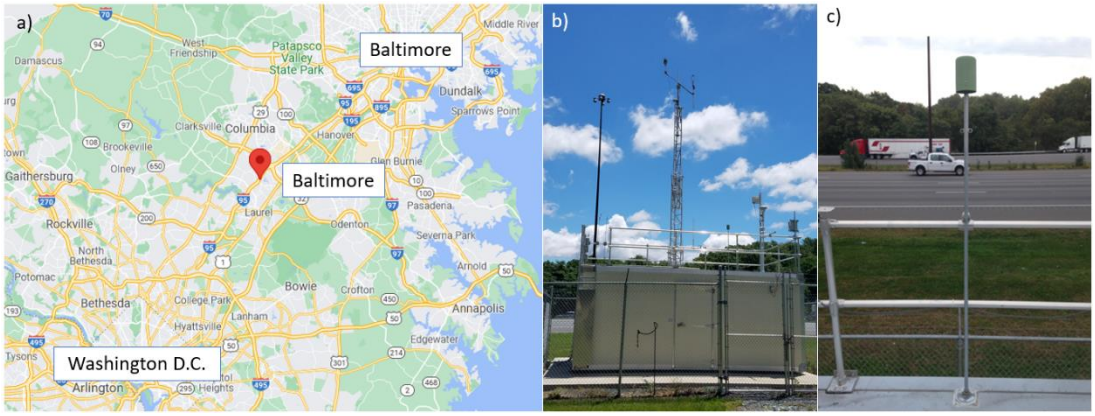

Figure 3.1. Location of the I-95 near-road (NR) monitoring site in the Baltimore-Washington region (a). The trailer housing the ambient measurement analyzers is shown in (b). A rooftop view of the proximity of the trailer to the adjacent major highway is presented in (c).

The observations used in this chapter were collected between January 2017 and December 2018. Meteorological variables including temperature, pressure, relative humidity, and wind direction were sampled using a Vaisala WXT 520 instrument. Carbon monoxide levels were sampled by infrared radiation absorption

using a Teledyne API 300 U analyzer and exhibited a mean relative calibration accuracy of 2.3% at 500 ppbv. Ambient measurements of CO_2 concentrations were collected using a Los Gatos Research (LGR) Fast Greenhouse Gas Analyzer (FGGA) with the Enhanced Performance Option (Los Gatos Research, 2013). The relative accuracy of CO_2 levels collected with the LGR analyzer is 0.089% at 516 parts per million by volume (ppmv) by comparison to known concentrations from the National Institute of Standards and Technology. More details about the analyzers used to measure CO, and CO_2 mixing ratios can be found elsewhere (Hall et al., 2020; Martin et al., 2017). While the accuracy of the analyzers is important, the conclusions of this study depend more on precision and repeatability because we compare differences in emission ratios by temperature. The overall uncertainty of the BC and CO analyzers, as employed, is better than 10% (API, 2017; Grimes and Dickerson, 2021). For CO_2, the relative uncertainty is less than 1% (Los Gatos Research, 2018; Martin et al., 2017).

Black carbon concentrations were collected with a Magee Scientific TAPI M633 (AE33) Aethalometer following standard EPA AQS operating and quality control procedures outlined in the CFR. The Aethalometer measures light attenuation at seven wavelengths, but 880 nm is typically chosen to represent BC concentrations ([BC]). The AE33 analyzer uses the dual-spot technique, in which aerosols are simultaneously collected on two spots of filter paper at different flow rates, to minimize the filter loading effect (Magee Scientific, 2018). While Aethalometers are widely used to measure [BC] within the AQS network, assessing the uncertainty of [BC] can be challenging due to a number of factors including the

lack of calibration standards. Grimes & Dickerson (2021) used BC surrogate particles to show that [BC] measured by a Magee AE 31 Aethalometer was within 5% of concentrations derived from an in-situ technique at 880 nm and for mass concentrations less than 2.5 μg m^{-3} (for reference, the 75th percentile [BC] at the I-95 NR site in all of 2017 and 2018 was 1.8 μg m^{-3}).

3.2.2 Inferred Emission Ratios and Temperature Sensitivity Analysis

The proximity of the NR monitor to the highway provides an ideal setting to analyze mobile emissions. Black carbon, CO, and CO_2 share vehicles as a common source, resulting in similar patterns for ambient measurements of BC, CO, and CO_2 in the NR environment. Covariations in pollutants are useful to study trends in vehicular emissions through inferred emission ratios often applied to trace specific sources in plume analysis. Here we calculate hourly emission ratios ($\Delta BC/\Delta CO$, $\Delta BC/\Delta CO_2$) from the slope parameter of linear geometric mean regression fits performed on five-minute average mixing ratios of two pollutants sampled within that hour. For example, the regression slope of five-minute averaged [BC] and CO mixing ratios represents the hourly $\Delta BC/\Delta CO$. Only hours with more than six observations are used in the analysis.

The types of vehicles passing the I-95 site impact the emissions – diesel-powered trucks emit much higher BC emissions relative to CO and CO_2 emissions; the exhaust from trucks often contains much higher $\Delta BC/\Delta CO$ and $\Delta BC/\Delta CO_2$ ratios than gasoline-powered light-duty vehicles. For instance, $\Delta BC/\Delta CO$ simulated by

MOVES3 for Howard County is two to three orders of magnitude higher in CIVs than in SIVs (Figure 3.2).

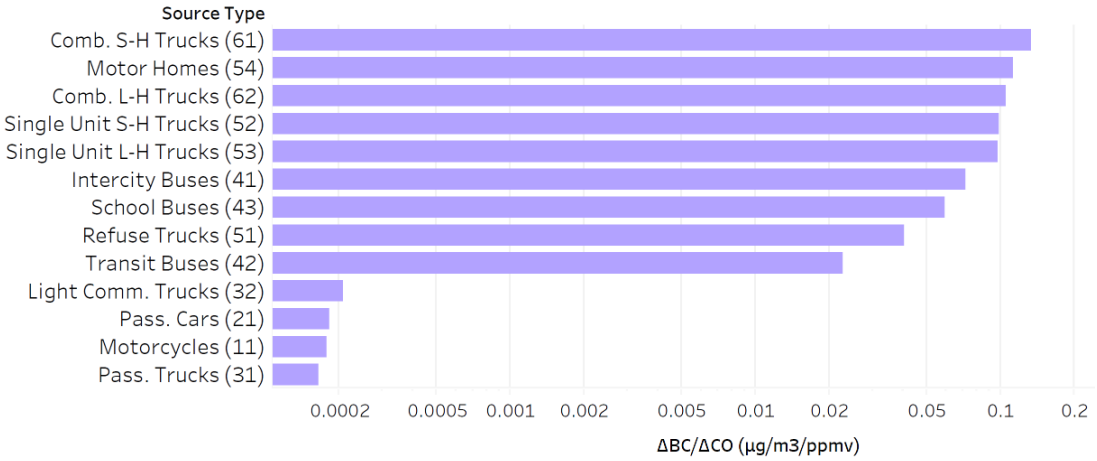

Figure 3.2. MOVES3 simulated ΔBC/ΔCO for Howard County, MD using 2017 input data, the latest year with available data. Emission ratios represent an average from −5 to 20°C.

Compression-ignited vehicles (CIVs) may represent the minority of vehicles passing the NR site, however their contribution to highway emissions of BC and NO_x can be substantial. The fraction of CIVs exhibits both a weekday and a time-of-day dependence, with higher fractions occurring on weekdays and in the overnight period (Table 3.1). We use Eastern Local Time (ET) for the analysis by hour of day, which is equivalent to Eastern Standard Time from early-November to mid-March and includes daylight savings for the remainder of the year. To investigate the type of vehicles responsible for the temperature sensitivity, I will perform the analysis for all days and hours, as well as by weekday and time frame (overnight, morning rush hours, and afternoon rush hours).

Table 3.1. The fraction of vehicles that were CIVs for April 2017 and 2018 at the I-95 NR site. The fraction is calculated based on all days and hours, as well as separated by weekday and local time window.

April 2017 & 2018	Fraction CIV
All Days and Hours	12%
Weekdays Only (M-F)	14%
Weekends Only (S-S)	7.4%
Overnight Hours (23:00 – 4:59 AM Local)	22%
Morning Rush Hours (5:00 – 9:59 AM Local)	11%
Afternoon Rush Hours (14:00 – 20:59 Local)	7.3%

3.2.3 MOVES3 Temperature Sensitivity Simulations

The latest version of the US EPA MOVES model, MOVES3, was used to simulate mobile emissions for Howard County, MD, in the winter using 2017 input data, the latest year with available data. The primary difference between summer and winter months in the model and in the real-world is the volatility of the fuel, with winter fuel used from September through April and summer fuel used from May through August (US EPA, 2021d). In this study, MOVES3 simulations were performed for the month of December when winter fuels are used. Repeating the analysis for summer yields little difference in our results.

MOVES3 requires county-specific input data including vehicle speed, road type, and age distributions; vehicle miles traveled (VMT) by vehicle group, hour,

day, and month; an average 24-hour profile of temperature and relative humidity; vehicle population; inspection and maintenance; and fuel information (Table 3.2). MOVES3 was run in emission rates mode and at the county-level scale. All input, except for fuel information, was supplied by the Maryland Department of the Environment (MDE). For input on fuel specifics, MOVES3 default data for Howard County, MD, was used as this information has not yet been finalized by MDE. Emission rates generated by MOVES are a function of temperature, relative humidity, vehicle type, fuel, speed, road type, model year, and weekday/weekend. A detailed explanation of how weighted-average emission ratios are calculated using the average fleet composition along I-95 is provided in Hall et al. (2020).

Table 3.2. Input data required for MOVES3 county-level simulations used in this study. Data for Howard County, MD, are compiled by the Maryland Department of the Environment.

Input Group	MOVES3 Input
VMT by:	Road Type
	Hour
	Day
	Month
	Source Type
Fuel Information	Fuel Supply
	Fuel Formulation
	Alternative Vehicle Fuel Technologies (AVFT)
	Fuel Usage Fraction
	Average Speed Distribution
	Source Type Population
	Vehicle Age Distribution
	I/M Coverage
	Meteorology Data

MOVES3, does not incorporate a temperature adjustment for hot-running BC emissions from either CIVs or SIVs. While neither MOVES3 nor the previous version, MOVES2014, adjusts hot-running BC emissions from CIVs, the default setting of MOVES2014 incorporates an adjustment for running BC emissions from pre-2004 model year SIVs for temperature using a multiplicative factor (US EPA, 2020b, 2015b). To verify the documented absence of a temperature sensitivity in MOVES3 output, weighted average emission ratios are calculated in 1°C increments from −5°C to 25°C and the results presented in Section 3.3.2.

3.3 Results and Discussion

3.3.1 Temperature Sensitivity in Near-Road Ambient Observations

This section discusses vehicular BC emissions, especially those from diesel trucks, and their sensitivity to ambient temperature using observations collected at the I-95 NR site. As demonstrated in Hall et al. (2020), vehicular NO_x emissions from diesel trucks are dependent on ambient temperature, with emissions decreasing as temperatures rise. Here we examine trends in $\Delta BC/\Delta CO$ and $\Delta BC/\Delta CO_2$ with ambient temperature during the cold season (November – February) from 2017 to 2018. We then compare the trends in $\Delta BC/\Delta CO$ and $\Delta BC/\Delta CO_2$ with temperature to those from MOVES3 output in these cold months.

Previous studies report a seasonal cycle in observed $\Delta BC/\Delta CO$ at suburban and urban sites. For example, both Chen et al. (2001) and Kondo et al. (2006) examined ambient BC and CO observations and found higher $\Delta BC/\Delta CO$ emission

ratios in the summer than in the winter. Although these sites were not classified as near-road, measurements of BC and CO exhibited strong correlation indicative of a shared source: vehicles.

Chen et al. (2001) also examined the seasonality of absolute ambient levels of BC and CO at Fort Meade, MD, and found no discernible seasonal trend in BC concentrations while CO mixing ratios were highest in the winter and lowest in the summer. With vehicles being an important source of both BC and CO, the authors speculated that greater BC source strength during the summer, such as from vehicles, may contribute to summertime concentrations and partially explain the difference in seasonal cycles between BC and CO (Chen et al., 2001). An analysis of ambient abundances at the I-95 NR site supports the findings of Chen et al. (2001), with ambient BC and CO abundances following opposite seasonal cycles (Figure B1).

I find a seasonal cycle in ΔBC/ΔCO emission ratios similar to prior studies (Chen et al., 2001; Kondo et al., 2006) is evident at the I-95 NR site. Figure 3.3 shows the seasonal variability in ΔBC/ΔCO at the I-95 NR site, with highest ΔBC/ΔCO occurring in the summer and lowest ΔBC/ΔCO during winter. Seasonal averages of ΔBC/ΔCO, calculated from the hourly emission ratios, were strongly correlated with ambient temperature (r^2=0.96) and increased by 81% from winter (~5°C) to summer (~25°C). The seasonal changes in ΔBC/ΔCO and proximity of the NR site to a major highway suggests a temperature sensitivity in vehicular emissions, particularly those from diesel trucks.

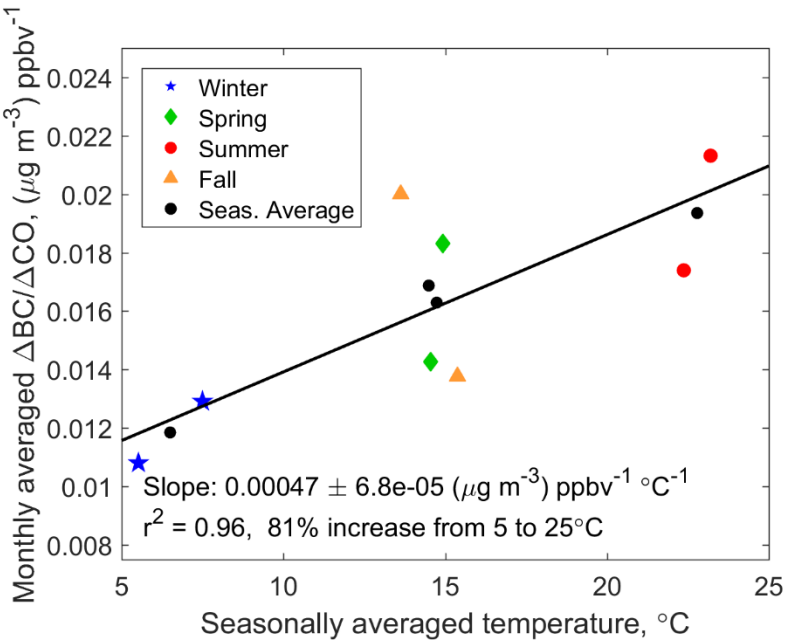

Figure 3.3. Seasonal variability in ΔBC/ΔCO [(μg m^{-3}) $ppbv^{-1}$] inferred from observations collected at the I-95 NR site from January 2017 thru December 2018. Blue stars represent winter (December – February), green diamonds represent spring (March – May), red circles represent summer (June – August), and orange triangles represent fall (September – November). The average emission ratio in each season is represented by the filled black circles, fitted using a linear geometric mean regression (solid black line) with regression statistics provided on the bottom of the plot.

To avoid potential impacts of seasonal fuel switching on emissions, we focus on the temperature dependence of ΔBC/ΔCO during the cold season. ΔBC/ΔCO and $\Delta BC/\Delta CO_2$ inferred from ambient observations at the I-95 NR site exhibit a positive correlation with ambient temperature considering all hours and days of the week during the cold months, defined as November, December, January, and February, in 2017 and 2018. Hourly ΔBC/ΔCO and $\Delta BC/\Delta CO_2$ were placed into ten equal-numbered bins, sorted by ascending temperature. Figure 3.4 shows the median (black diamonds), and 25th and 75th percentile (black dashed lines) values for each of these bins, along with an ordinary linear least-squares regression fit to the median

values (red line). Considering all data, both emission ratios exhibited a statistically significant increasing trend with temperature: [1.6 ±0.42×10^{-4} (μg m^{-3}) $ppbv^{-1}$ $°C^{-1}$] in ΔBC/ΔCO and [1.8 ±0.44×10^{-3} (μg m^{-3}) $ppbv^{-1}$ $°C^{-1}$] in ΔBC/ΔCO_2, equivalent to an increase of 54% in ΔBC/ΔCO and 83% in ΔBC/ΔCO_2 from −5°C to 20°C (Figure 3.4). Similar temperature sensitivities were obtained when hourly emission ratios were calculated with an orthogonal linear regression instead of geometric mean regression.

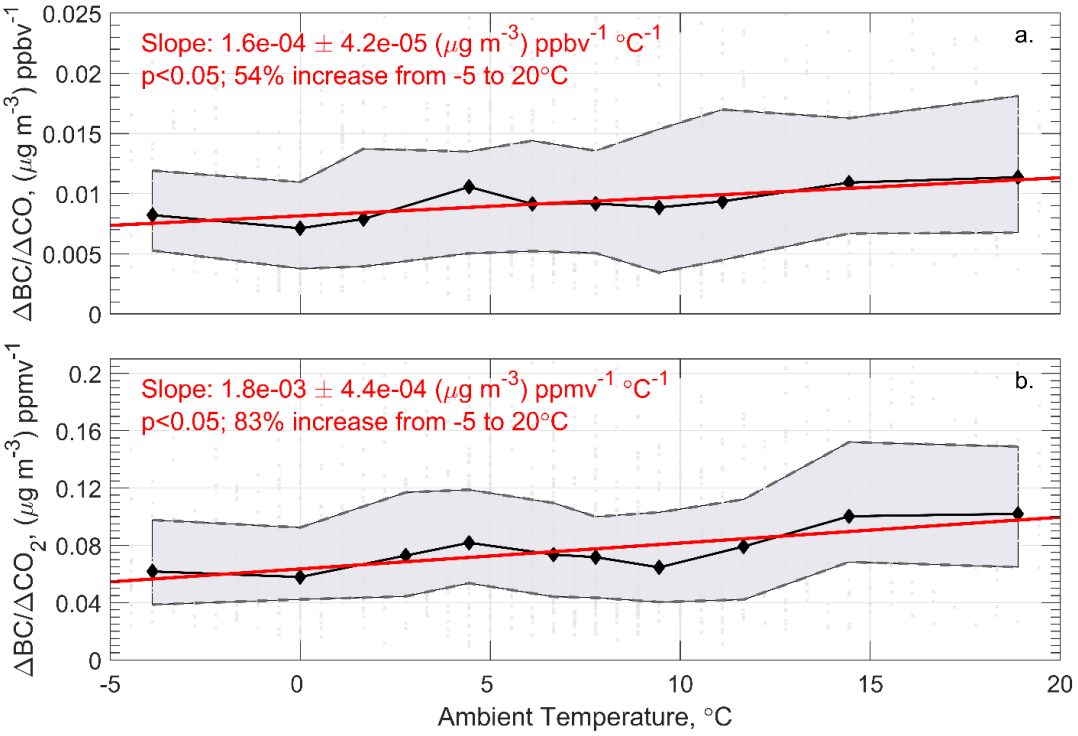

Figure 3.4. Hourly ΔBC/ΔCO (a) and ΔBC/ΔCO_2 (b) inferred from I-95 NR observations as a function of ambient temperature for the months of November, December, January, and February in 2017 and 2018. Hourly ratios (light gray points) were estimated from the slope values of linear geometric mean regressions (±standard error) performed on 5-minute averaged data within each hour. Only hours with winds originating from the highway were included in the analysis. Hourly data were compiled into ten equal-sized bins, with the median value of each bin represented by the black diamonds, and the 25th and 75th percentile values by the dashed black line. An ordinary least-squares regression was fit to the binned median values (red line) and the details of the regression provided in the top left of each plot.

The statistical significance of each trend was determined by the non-parametric Mann-Kendall test (Gilbert, 1987; Kendall, 1975; Mann, 1945).

As shown previously, vehicular emissions of CO and CO_2 do not appear sensitive to temperature during the cold season (Hall et al., 2020). Thus, the increase in $\Delta BC/\Delta CO$ and $\Delta BC/\Delta CO_2$ is likely due to an increase in BC emissions from mobile sources at higher temperatures. Some evidence suggests that gasoline vehicles utilizing direct injection and particulate filters appear to remove BC more efficiently at lower intake temperatures (Chan et al., 2013). Direct injection, the mechanism in diesel engines, may also be employed with gasoline engines and has been on the rise in recent years (US EPA, 2020a) to provide more power and increase fuel efficiency. Like in diesel engines, this mechanism of injecting fuel directly into the cylinder produces more BC emissions. However, diesel engines emit the vast majority of BC at the NR site and thus a more plausible explanation for the temperature sensitivity lies within diesel vehicles. In diesel engines with turbochargers, the process of compressing intake air in the turbocharger leads to hotter air with lower density entering the engine cylinders. Lower air density of the air entering the cylinders may favor elevated BC production in diesel engines as the air-to-fuel ratio is reduced (Chen et al., 2001; Ghazikhani et al., 2013). Diesel trucks equipped with turbochargers typically also utilize charge-air coolers, or turbo coolers. In an air-to-air turbo cooler, the hot and compressed air is passed through the device on its way to the cylinders and cooled via heat exchange with cooler outside air (Joshi et al., 2009; Sher, 1998). The purpose of the coolers is to reduce the temperature, and raise the density, of the intake air, resulting in lower NO_x and

BC emissions (Cipollone et al., 2017). Because compressed air is cooled by heat exchange with ambient air, and also because the coolers degrade over time (Joshi et al., 2009), warmer ambient temperatures may lead to less cooling of the intake air and, in turn, higher BC emissions at warmer temperatures. This process can lead to increasing BC emissions, and therefore $\Delta BC/\Delta CO$ and $\Delta BC/\Delta CO_2$, with rising temperatures, as observed in Figure 3.4.

To further explore the contribution of the vehicle fleet composition on the temperature sensitivity, we repeat the analysis by day of week and at different times of the day. Both $\Delta BC/\Delta CO$ and $\Delta BC/\Delta CO_2$ exhibit an increase with rising temperature on weekdays ($p<0.05$), however a statistically significant trend was absent on weekends (Table 3.3). Both the total truck traffic (1,022 vehicles/hour on weekdays and 433 vehicles/hour on weekends) and the fraction of CIVs (14% on weekdays and 7.4% on weekends) drop by a factor of ~ two from weekdays to weekends. Additionally, traffic jams are typically more frequent on weekdays than on weekends, resulting in higher weekday BC emissions from diesel trucks due to the stop-and-go effect that will be discussed in Chapter 4. With diesel trucks emitting the bulk of on-road BC emissions, the increase in $\Delta BC/\Delta CO$ and $\Delta BC/\Delta CO_2$ with rising temperatures on weekdays suggests that diesel vehicles are sensitive to temperature.

Table 3.3. Measured ΔBC/ΔCO and $\Delta BC/\Delta CO_2$ as a function of ambient temperature during the months of November, December, January, and February in 2017 and 2018 at the I-95 NR site. Hourly emission ratios were placed into ten equal-sized bins and an ordinary linear regression fit to the median emission ratios of each bin, the same as in Figure 3.4. The analysis was conducted for all hours and days and then separated by weekday, weekend, overnight, morning rush hours, and afternoon rush hours.

	I−95 Fleet CIV / SIV	(ΔBC/ΔCO) / T ($\mu g\ m^{-3}$) $ppbv^{-1}\ °C^{-1}$	($\Delta BC/\Delta CO_2$) / T ($\mu g\ m^{-3}$) $ppmv^{-1}\ °C^{-1}$
All Days and Hours	12% / 88%	**$1.63\ (\pm 0.45) \times 10^{-4}$ (p<0.05)**	**$1.82\ (\pm 0.49) \times 10^{-3}$ (p<0.05)**
Weekdays Only	14% / 86%	**$1.88\ (\pm 0.78) \times 10^{-4}$ (p<0.05)**	**$1.91\ (\pm 0.33) \times 10^{-3}$ (p<0.05)**
Weekends Only	7.4% / 92.6%	$-0.098\ (\pm 0.069) \times 10^{-4}$ (p=0.72)	$0.13\ (\pm 0.44) \times 10^{-3}$ (p=1)
Overnight (23 – 4:59 ET)	22% / 78%	**$3.25\ (\pm 0.96) \times 10^{-4}$ (p<0.05)**	**$1.73\ (\pm 1.0) \times 10^{-3}$ (p<0.05)**
Morning Rush Hours (5 – 9:59 ET)	11% / 89%	**$4.15\ (\pm 0.95) \times 10^{-4}$ (p<0.05)**	**$2.67\ (\pm 0.57) \times 10^{-3}$ (p<0.05)**
Afternoon Rush Hours (14 – 20:59 ET)	7.3% / 92.7%	**$1.82\ (\pm 0.49) \times 10^{-4}$ (p<0.05)**	$1.80\ (\pm 2.67) \times 10^{-3}$ (p=0.074)

A positive trend in ΔBC/ΔCO with temperature is evident in all three local time windows. The slope [($\mu g\ m^{-3}$) $ppbv^{-1}\ °C^{-1}$] is highest during the morning rush hours [$4.15\ (\pm 0.947) \times 10^{-4}$, $p<0.05$], followed by the overnight period [$3.25\ (\pm 0.963) \times 10^{-4}$, $p<0.05$], and is lowest in the afternoon rush hours [$1.82\ (\pm 0.493) \times 10^{-4}$, $p<0.05$] (Table 3.3) indicating that both fleet make-up and driving conditions contribute to BC emissions.

Patterns in the temperature dependence of ΔBC/ΔCO by local time follow diel trends in the fraction of CIVs and vehicular traffic. The overnight period experiences the highest fraction of CIVs to total vehicles even though the total

number of trucks on the road is lower than during the rest of the day. The temperature dependence in BC emissions observed in the overnight period is likely driven by the high fraction (22%) of diesel vehicles (Table 3.3).

The morning rush hour exhibits the largest slopes of $\Delta BC/\Delta CO$ and $\Delta BC/\Delta CO_2$ with temperature. While the fraction of CIVs to total vehicles in the morning (11%) is lower than overnight (22%), stop-and-go traffic is more common during the morning rush hour than during the overnight period (Table 3.4). A plausible explanation for the observed temperature sensitivity in the morning is that elevated BC emissions from CIVs due to frequent acceleration, a topic of discussion in Chapter 4, during the morning rush hour enhance the temperature effect from diesel engines.

Table 3.4. Weighted average vehicle speeds (μ in m s^{-1}) and the fraction of vehicles driving under 22 m s^{-1} ($frac_{<22mps}$) at the I-95 traffic counter site for the months of November, December, January, and February in 2017 and 2018. Values are reported for all hours and days and then separated by weekday, weekend, overnight, morning rush hours, and afternoon rush hours.

Time Period	Speed and Traffic Congestion
All days and hours	μ=26.7 m s^{-1} $frac_{<22mps}$ = 21.0%
Weekdays (Mo − Fr)	μ=26.1 m s^{-1} $frac_{<22mps}$ = 24.6%
Weekends (Sa and Su)	μ=28.5 m s^{-1} $frac_{<22mps}$ = 10.0%
23:00 – 04:59 (early morning)	μ=30.1 m s^{-1} $frac_{<22mps}$ = 1.2%
05:00 – 09:59 (morning rush)	μ=26.8 m s^{-1} $frac_{<22mps}$ = 20.8%
14:00 – 20:59 (afternoon rush)	μ=24.8 m s^{-1} $frac_{<22mps}$ = 32.5%

The trend in $\Delta BC/\Delta CO$ with temperature in the afternoon rush hours has the lowest slope considering all times of day [1.82 (± 0.49) $\times 10^{-4}$, $p<0.05$] (Table 3.3). The slope of $\Delta BC/\Delta CO_2$ was also at a minimum in the afternoon rush hours, but the trend was statistically only significant at the ~90% confidence level ($p=0.074$). Given that CIVs make up only 7.3% of the vehicles passing the NR site in the afternoon, the sensitivity in $\Delta BC/\Delta CO$ likely originates from high BC emissions by CIVs due to a peak in stop-and-go traffic during the afternoon rush hour or a combination of CIV and SIV.

3.3.2 Temperature Impact on MOVES Estimated BC Emissions

Here we compare the $\Delta BC/\Delta CO$ and $\Delta BC/\Delta CO_2$ temperature sensitivity in mobile emissions inferred at the I-95 NR site to MOVES3 output. MOVES3 was run using 2017 input data, the latest year with available data, supplied by the Maryland Department of the Environment for Howard County, MD. Mobile emissions were simulated for Howard County, MD, the county in which the NR site resides. Data used as input for the model include average speed distribution, meteorology, road type distribution, fuel information, and vehicle age, populations, and miles traveled by hour, weekday, and month for Howard County, MD.

Unlike prior versions, MOVES3 does not adjust hot-running exhaust of $PM_{2.5}$ from any gasoline or diesel vehicle for ambient temperature; The temperature adjustment for gasoline vehicles of MY 2004 and earlier was removed in the development of MOVES3 (US EPA, 2020a; Table 3.5). Figure 3.5 documents the lack of sensitivity in BC emissions to temperature in MOVES3. The temperature

dependence simulated by MOVES in the I-95 weighted average from −5°C to 20°C is negligible for both ΔBC/ΔCO (0.04%) and ΔBC/ΔCO_2 (0.02%) and arises because of a small indirect adjustment to CO and CO_2 emissions due to increased air conditioner use at higher temperatures that exists in both MOVES3 and MOVES2014 (Hall et al., 2020; US EPA, 2020b). The absence of a trend is robust regardless of vehicle type and fuel use. Temperature adjustment factors for hot-running emissions in MOVES3 do not appear to represent conditions along I-95 well: The observed increase in emission ratios from −5 to 20°C at the I-95 NR site, considering all weekdays and hours of the day, was 56% in ΔBC/ΔCO and 83% in ΔBC/ΔCO_2 (Figure 3.4). With the air conditioning effect at a minimum in the observed temperature range and inferred mobile emissions of CO and CO_2 at the NR site exhibiting an insignificant temperature impact (Hall et al., 2020), the trends in ΔBC/ΔCO and ΔBC/ΔCO_2 are likely caused by an increase in BC emissions with rising temperatures.

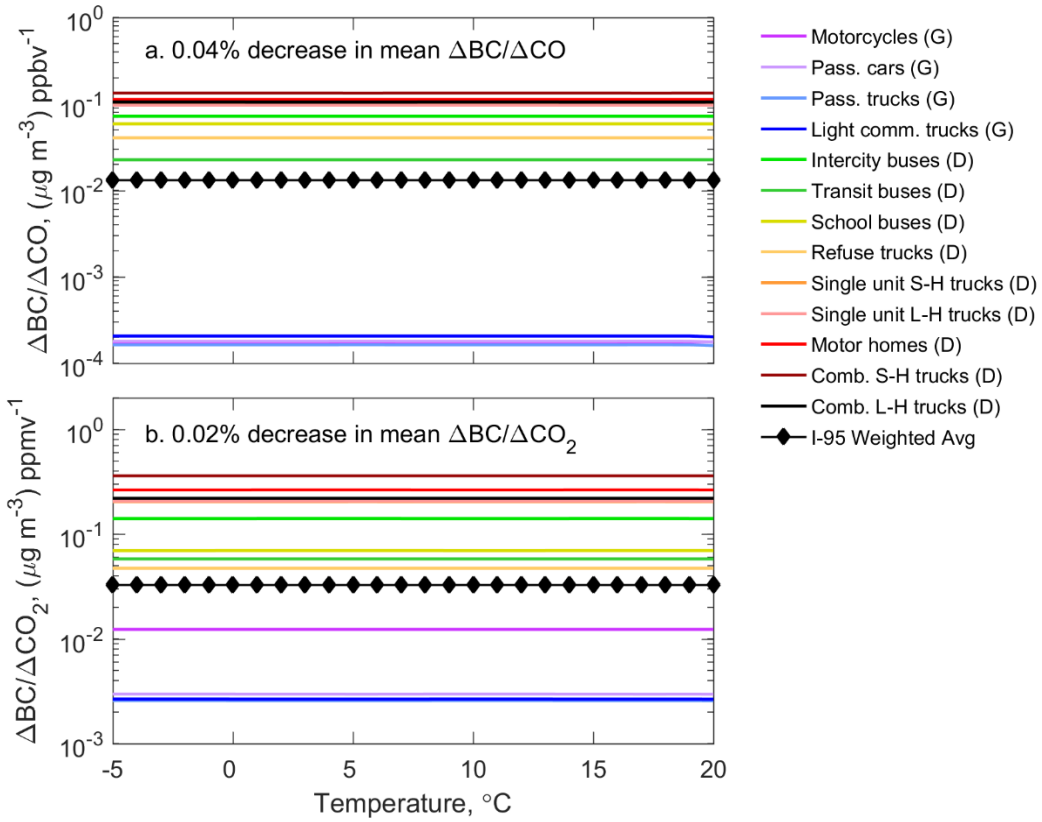

Figure 3.5. MOVES3 simulated ΔBC/ΔCO and ΔBC/ΔCO_2 as a function of temperature for the thirteen different vehicle types modeled in MOVES. The dominant type of fuel (G for gasoline and D for diesel) is provided next to each vehicle type and is based on county-level data compiled by the Maryland Department of the Environment mobile emissions team. The weighted average emission ratios were calculated using the fractions of various vehicle types derived from traffic counts collected at the traffic counter site along I-95. S-H indicates short-haul while L-H represents long-haul combination unit trucks.

Table 3.5. Temperature adjustments in MOVES2014b and MOVES3 for hot-running emissions of BC, CO, and NO_x from gasoline and diesel vehicles. (See https://nepis.epa.gov/Exe/ZyPDF.cgi?Dockey=P1010M29.pdf for more information)

	MOVES2014b	MOVES3
Gasoline		
BC	Model Year 2004 and earlier	None
CO	None	None
NO_x	None	None
Diesel		
BC	None	None
CO	None	None
NO_x	None	None

3.4 Conclusions

Inferred vehicular BC emissions (like NOx) exhibit a sensitivity to ambient temperature. For two years prior to COVID restrictions, $\Delta BC/\Delta CO$ increased by 80% from winter to summer, as has been reported previously (Chen et al., 2001; Kondo et al., 2006). We confirmed this conclusion by confining the analysis to the cold seasons of 2017 and 2018 to minimize seasonal differences in fuel and fleet composition and find a 50% increase in inferred BC emissions as temperature increases from −5 to 20°C when all hours and days within a season are considered. The overnight period, when the fraction of CIVs is at a maximum, has a strong increase in $\Delta BC/\Delta CO$ and $\Delta BC/\Delta CO_2$ with temperature, suggesting BC emissions from diesel trucks are sensitive to temperature. The sensitivity could result from lower air density at higher temperatures producing elevated BC emissions from diesel engines (Chen et al., 2001; Ghazikhani et al., 2013).

A comparison of the observed temperature impact to that from MOVES3 suggests that hot-running emissions of BC are not adjusted for ambient temperature in MOVES3 as generally used for any vehicle type. The lack of a temperature sensitivity in the documentation (US EPA, 2020b) is supported by our MOVES3 simulations that show an increase of only 0.04% in $\Delta BC/\Delta CO$ and 0.02% in $\Delta BC/\Delta CO_2$ from −5 to 20°C. MOVES3 does include a cold-start effect, however considering the proximity of the I-95 NR site to the adjacent eight-lane highway (200,000 passing vehicles a day) and focusing the analysis on wind directions coming only from the highway, fresh emissions from passing vehicles overwhelm potential cold-start emissions from the nearby rest area. The lack of a trend in BC emissions with temperature may also help to explain a previous study that found CMAQ modeled BC concentrations consistent with observed summer but not winter concentrations (Appel et al., 2008).

Mobile emissions for the NEI and air quality models are estimated with the SMOKE-MOVES tool that uses MOVES. Emission inventories such as the NEI provide the means to assess the total emissions of a pollutant and also to determine the most important sources of each air pollutant. According to the 2017 NEI, on- and off-road vehicles are the dominant source of BC emissions both nationally and within Maryland. Poor agreement in the observed and simulated temperature sensitivity of vehicular BC emissions discussed in this chapter may be partially remedied by incorporating an appropriate temperature effect within MOVES3. Such an adjustment would enhance the overall accuracy of mobile emissions estimates.

By identifying ambient temperature as an important factor influencing vehicular BC emissions, the results of this study provide policy-relevant insight into how to further reduce BC emissions from vehicles. Modifying engine and exhaust-aftertreatment devices may help lower BC emissions at higher temperatures and lower the contribution of vehicles on overall ambient BC concentrations. Further reductions in mobile BC emissions would benefit the health of populations living near roadways and other areas strongly influenced by vehicular exhaust.

Chapter 4: Response of Near-Road Inferred Vehicular Emissions to Changes in Traffic Patterns due to Travel Restrictions in the COVID-19 Pandemic

The work in this chapter and Chapter 3 is currently in preparation for a paper to be submitted to the journal *Atmospheric Environment* under the title "Near-Road Observations of BC, CO, NO_x, and CO_2: Impacts of COVID-19 Restrictions, Traffic Patterns, and Temperature". I am the first author of this paper and collaborated with five co-authors from the University of Maryland. Numbered references within this chapter have been adjusted to reflect the numbering system of the dissertation.

4.1 Introduction

Vehicles emit substantial amounts of CO, NO_x ($NO + NO_2 = NO_x$), BC, and CO_2. Both CO and NO_2 are criteria pollutants regulated by the US EPA due to their hazards to human health and role as precursors to the formation of O_3 (P. Crutzen, 1973; Pusede and Cohen, 2012; Sather and Cavender, 2016). PM2.5, including BC, is regulated by the US EPA due to the adverse health and visibility impacts (US EPA, 2021e). Both BC and CO_2 absorb radiation and can have adverse radiative forcing (US EPA, 2021f).

According to the 2017 NEI, the mobile sector is the dominant emitter of CO and NO_x both nationally and within Maryland, contributing to 54% of total CO (including wildfires) and 59% of total NO_x emissions nationally and 86% of total CO and 76% of total NO_x emissions within Maryland. The mobile sector is also the largest contributor to BC emissions, representing 42% of total emissions nationally

and 58% in Maryland. Within the on-road mobile sector in Maryland, diesel engines emit 75% of BC, 41% of NO_x, and only 3.8% of CO, with similar percentage on the national scale. (2017 NEI data is available at https://www.epa.gov/air-emissions-inventories/2017-national-emissions-inventory-nei-data).

Lockdown mandates imposed in response to the COVID-19 public health emergency in early 2020 resulted in a sharp decline in the number of on-road vehicles, a decrease in traffic congestion, and lower vehicular emissions (Du et al., 2021; Harkins et al., 2021; Hudda et al., 2020; Yang et al., 2021; Zeng et al., 2021). In Maryland, the largest decrease in commuter vehicles and diesel trucks occurred in April 2020.

Differences in on-road vehicle fleet composition, such as the split between diesel trucks and gasoline cars, can affect the concentrations of various mobile air pollutants disproportionally (Grieshop et al., 2006; Hudda et al., 2020). Diesel engines inject the fuel directly into the engine cylinders (known as direct injection) and tend to operate fuel-lean, while gasoline engines typically premix the air and fuel upstream of the engine cylinders and operate at lower air-to-fuel ratios and lower maximum temperature. The latter process results in higher CO emissions and lower BC and NO_x emissions in gasoline compared to diesel-fueled vehicles (Ban-Weiss et al., 2008; Park et al., 2011). For example, tailpipe emissions from diesel trucks contain higher $\Delta NO_x/\Delta CO_2$ emission ratios relative to gasoline vehicles because CIVs produce more NO_x than SIVs and diesel engines typically run more efficient, resulting in lower CO_2 than from a gasoline engine of comparable size (O'Driscoll et al., 2017). Turbocharger lag, resulting from acceleration in diesel

trucks, produces soot – a mix of BC, metals, unburnt fuel and oil, and sulfates (Rakopoulos and Giakoumis, 2009). Therefore fewer instances of acceleration result in lower BC emissions (Giakoumis and Zachiotis, 2021).

In this study we use ambient measurements of BC, CO, NO_x, and CO_2 mixing ratios collected at a fixed, NR monitor located along Interstate-95 (I-95) in Maryland to infer mobile emissions using emission ratios. Our goal is to quantify the impact of changes in on-road vehicle fleet composition and the near-elimination in traffic jams on highway emissions.

4.2 Methodology

4.2.1 Interstate-95 Near-Road and Traffic Observations

The ambient observations used to infer emission ratios were collected at the I-95 NR monitoring site in Maryland. The site is managed by the MDE and follows all US EPA AQS collection and quality control procedures (Hall et al., 2020).

Hourly-averaged data were derived from 10-second averaged NO_x and CO mixing ratios, 1-minute averaged BC concentrations ([BC]), and 2- or 5-second averaged CO_2 levels. Only hours with winds blowing from the highway (25° to 225° Compass) were used in results presented in this chapter, however conducting the analysis for all wind directions yields similar results.

Observations at the NR site used in this study were collected between January 2017 and December 2018, then again from March 2020 thru December 2020. Temperature, pressure, relative humidity, and wind information were collected using a Vaisala WXT 520 instrument. NO_x mixing ratios were measured

by chemiluminescence using a Teledyne Advanced Pollution Instrumentation (API) Model 200 U analyzer (API, 2013). The analyzer is equipped with a hot molybdenum converter that reduces reactive nitrogen species other than NO_x (Dickerson et al., 2019; Fehsenfeld et al., 1987), however fresh NO_x emissions from the adjacent highway dominate the NO_x measurements. The mean relative calibration accuracy of the NO_x analyzer, defined here as the average relative difference between analyzer measurements and a calibration standard at set concentrations, was 4.7% for abundances between 9 and 12 parts per billion by volume (ppbv) following routine quality control checks performed twice a month as outlined in the Code of Federal Regulations (CFR) for AQS sites.

Carbon monoxide was measured using a Teledyne API 300 U analyzer, BC using the 880 nm channel of a Magee Scientific TAPI M633 (AE33) Aethalometer, and CO_2 using a LGR FGGA analyzer (2017 – 2018) and a Picarro Greenhouse Gas Analyzer (2020). The API 300 U, Aethalometer, and LGR instrument specifications, including parameters contributing to instrument uncertainty, have been described in detail in Chapters 2 and 3. Ambient measurements of CO_2 concentrations prior to March 22, 2020 were collected using the LGR FGGA. Starting March 23, 2020, CO_2 mixing ratios were measured by cavity ringdown spectroscopy using a Picarro Greenhouse Gas Analyzer with a manufacturer's stated relative accuracy of better than 0.025% between 300 and 500 ppmv (Picarro, 2019). An intercomparison of CO_2 abundances measured by the LGR and Picarro analyzers is presented in Figure 4.1 and shows excellent correlation between 400 and 580

ppmv (r^2 =0.99994) and nearly identical mixing ratios with relative differences of less than 0.06%.

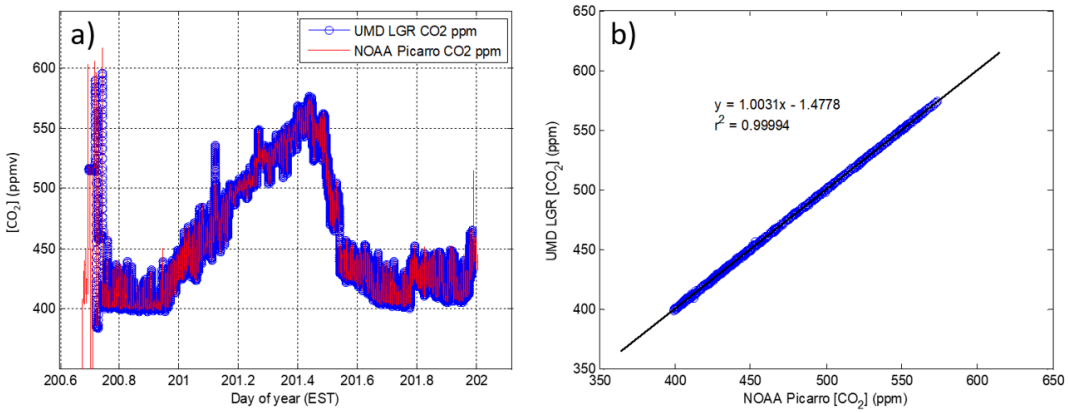

Figure 4.1. Comparison of ambient CO_2 mixing ratios (ppmv) measured with a Los Gatos Research (LGR) FGGA analyzer and a Picarro Greenhouse Gas Analyzer, shown in a time series of one-second data (a) and a scatterplot of one-minute observations (b). The intercomparison data were collected on July 18−19, 2020. Figures courtesy of Dr. Xinrong Ren.

Hourly traffic observations along I-95 were collected by an in-road traffic sensor, operated by the Maryland State Highway Administration. The sensor is located 8 km north of the ambient NR trailer and had a daily average of ~200,000 passing vehicles prior to March 2020. Vehicle information is measured using a combination of piezo pressure sensors and inductive loops that count the number of axles and spacing between axles. This technique allows the site to count the hourly total number of passing vehicles, as well as types of vehicles passing over the sensors and vehicle speed using the number of and distance between the axles (US Department of Transportation Federal Highway Administration, 2014).

4.2.2 Inferred Emission Ratios and Traffic Pattern Analysis

Due to vehicles emitting BC, CO, NO_x, and CO_2, ambient measurements of these gases often follow similar patterns. These covariations are used here to estimate hourly emission ratios of $\Delta BC/\Delta CO$, $\Delta BC/\Delta CO_2$, $\Delta NO_x/\Delta CO$, $\Delta NO_x/\Delta CO_2$, and $\Delta CO/\Delta CO_2$, similar to Chapters 2 and 3. The hourly emission ratios are calculated as the slope of a linear geometric mean regression performed every hour on five-minute averaged data of two pollutants sampled within that hour. Only hours with more than 30 minutes of observations are used to calculate an hourly ratio.

The vehicle fleet composition passing the NR site impacts the emission ratios as different types of vehicles emit varying amounts of BC, CO, and CO_2. Fuel-specific BC emission factors (g_{BC}/kg_{fuel}) from CIVs are up to 50 times higher than those from light-duty SIVs (Ban-Weiss et al., 2008; Dallmann et al., 2013), while CO emission factors are roughly half of those from SIVs (Dallmann et al., 2013). Combined, this leads to much higher $\Delta BC/\Delta CO$ ratios from CIVs.

While CIVs represent the minority of vehicles passing the NR site, the fraction of CIV varies drastically from weekday to weekend and over the course of the day. The fraction of CIVs on weekdays (14%) drops by almost a factor of two on weekends (7.4%). In contrast, the fraction and total number of SIVs changes relatively little, from 86% on weekdays to 92.6% on weekends. The overnight period (23:00 to 4:59 ET) has the highest fraction of CIVs and this fraction drops by 50% into the morning rush hours and by ~67% during the afternoon rush hours. To minimize the effects of a changing vehicle fleet on the speed and temperature

sensitivity, our analyses are presented by weekday/weekend and time-of-day, as well as all days and hours combined.

4.3 Results and Discussion

4.3.1 Vehicle Fleet and Speed Characteristics Before COVID-19 and in April 2020

Patterns and changes in vehicular traffic flow are useful to study trends in mobile emissions. Travel restrictions for the COVID-19 pandemic began in mid-March 2020 in the Baltimore-Washington Region (BWR) and led to a peak decrease in on-road vehicle counts in April 2020 (Figure 4.2 and Figure C.1). The average daily total number of vehicles passing the site was ~192,000 pre-COVID (April 2017 and 2018) and decreased to ~96,300 in April 2020. Light-duty passenger vehicle counts were 60% lower in April 2020 relative to pre-covid levels, while the number of buses was down by 85%, single-unit trucks by 21%, and trailer (combination-unit) trucks by 8.6% (Figure 4.2).

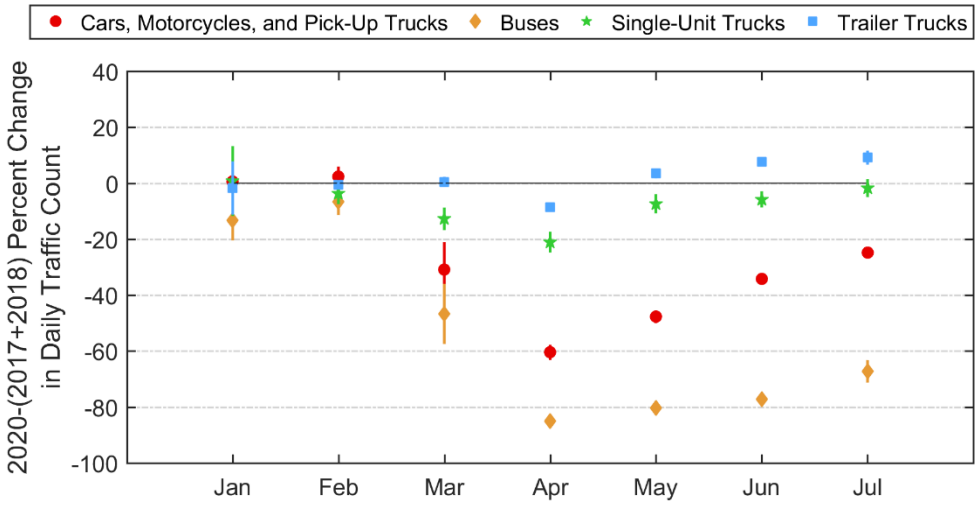

Figure 4.2. Relative difference (%) in monthly 2020 traffic counts compared to 2017 and 2018 for the months of January through July at the I-95 NR site. Vehicle

type is represented by the symbol and color shown in the legend and error bars represent the 95% confidence intervals (2σ).

Of the vehicles passing the traffic sensor, the typical pre-COVID fleet composition was 88% cars, motorcycles, and light-duty pick-up trucks; 1.3% buses; 3.0% single-unit trucks; and 7.7% tractor-trailer trucks. The highest fraction of CIVs (single-unit and tractor-trailer trucks) typically occurs overnight from 23:00 to 4:59 ET, with an average (±1σ) of 0.22 ±0.072 (Figure 4.3c). During this period there are few passenger cars on the road. The fraction of CIVs drops down to 0.11 ±0.027 during the morning rush hour (5:00 to 9:59 ET) and further declines to 0.073 ±0.024 during the afternoon rush hour (14:00 – 20:59 ET). In terms of day-of-week, the fraction of CIVs decreases by a factor of ~ 2 from 0.14 on weekdays to 0.074 on weekends (Figure 4.3f).

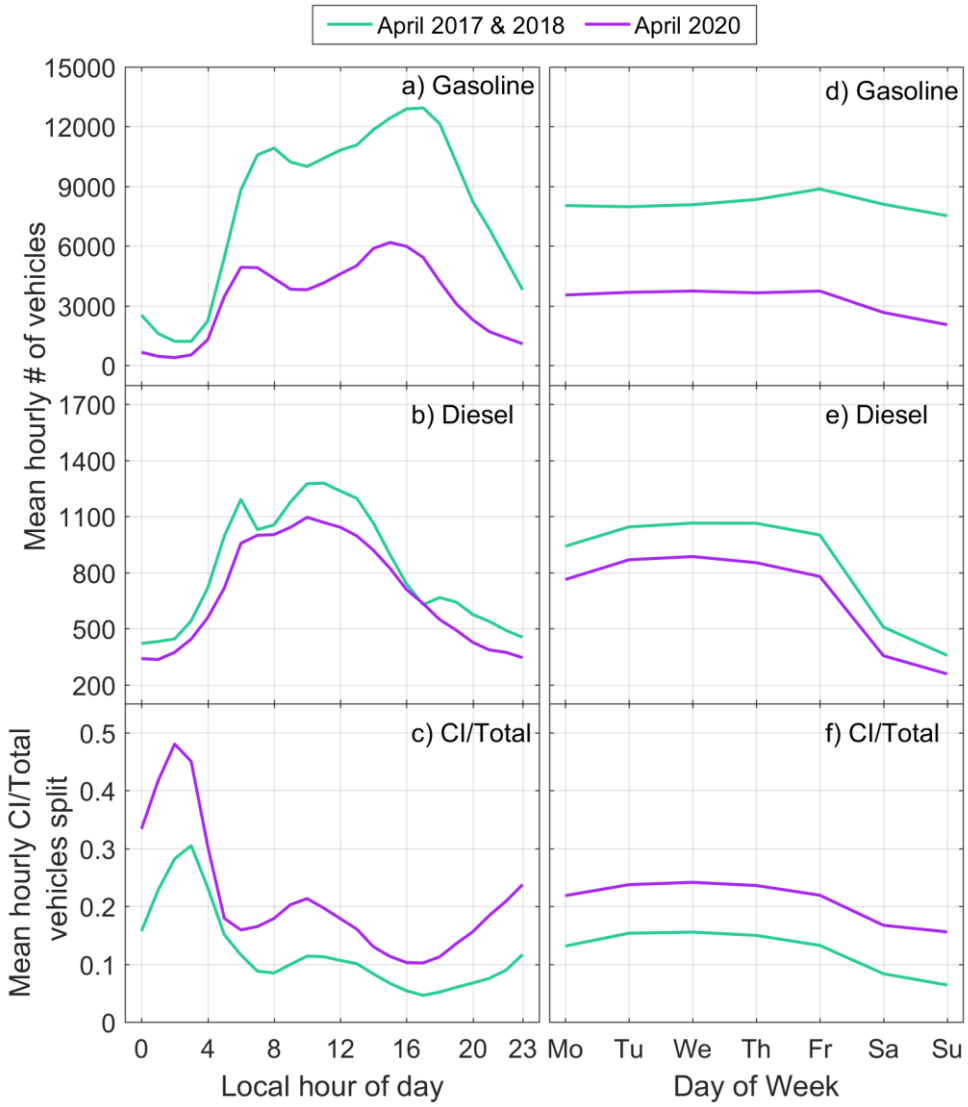

Figure 4.3. Traffic composition by local time (a-c) and weekday (d-f) of vehicles passing the I-95 NR site pre-COVID (April 2017 & 2018) and in April 2020. Changes in total gasoline (a, d) and diesel (b, e) vehicle counts are represented by the average hourly number of vehicles at each hour or day of the week. The CIV to total vehicle split is shown as a fraction by time of day (c) and day of the week (f).

The traffic composition in April 2020 was 79% cars, motorcycles, and pick-up trucks; 0.010% buses; 4.9% single-unit trucks; and 16% tractor-trailer trucks. The number of on-road passenger cars declined more than the number of trucks, resulting in a doubling of the fraction of trucks relative to SIVs on I-95 from 10.7%

pre-COVID to 20.9% in April 2020. Mobile emissions inferred from ambient observations in April 2020 thus had a greater contribution from diesel trucks than in prior years. A comparison of vehicle fleet composition in April 2020 and April 2017 and 2018 is provided in Table 4.1 and shows higher CIV fractions in April 2020 for all days and hours due to the greater decrease in passenger car volumes compared to truck counts. I examine all hours and days of the week, in addition to a detailed breakdown by weekday and local time window to account for the variability in the vehicle fleet.

Table 4.1. Traffic composition of vehicles passing the I-95 NR traffic counter pre-COVID (April 2017 and 2018) and in April 2020 by weekday and local time. SIV represents spark-ignited vehicles and CIV indicates compression ignited vehicles.

	April 2017 & 2018 SIV (CIV)	**April 2020 SIV (CIV)**
All Days and Hours	88% (12%)	79% (21%)
Weekdays Only (M-F)	86% (14%)	77% (23%)
Weekends Only (S-S)	93% (7%)	84% (16%)
Overnight Hours (23:00 – 4:59 AM Local)	78% (22%)	63% (37%)
Morning Rush Hours (5:00 – 9:59 AM Local)	89% (11%)	82% (18%)
Afternoon Rush Hours (14:00 – 20:59 Local)	93% (7%)	88% (12%)

4.3.2 Traffic Pattern Changes and the Impact on Mobile Emissions

Significant reductions in the number of on-road vehicles in April 2020 affected fleet composition, speed, and stop-and-go traffic trends. The weighted

average vehicle speed (μ) on I-95 was 14% higher in April 2020 (μ=30.3 m s^{-1}; for reference, 1 m s^{-1}=2.2 miles hr^{-1}=3.6 km hr^{-1}) compared to prior years (μ=26.6 m s^{-1}) and the fraction of vehicles driving slower than 22 m s^{-1} was nearly eliminated in April 2020 (Figure 4.4). The threshold of 22 m s^{-1} (~48 mph) was selected because the speed limit on this portion of the highway is 29 m s^{-1} (65 mph) and speeds slower than 22 m s^{-1} typically indicate traffic jams marked by more frequent braking and accelerating. Repeating this analysis by weekday and local time shows consistent results with higher speeds and virtually eradicated stop-and-go traffic in April 2020 relative to prior years (Table 4.2). The only hours with comparable average vehicle speed and lack of traffic congestion between April 2020 and prior years are 23:00 – 4:59 AM ET, when there are fewer vehicles on the road and little traffic congestion (Table 4.2).

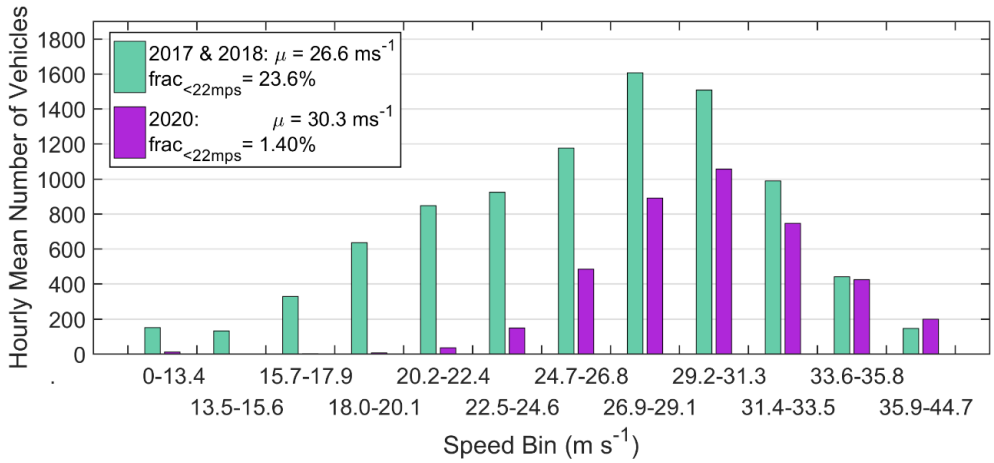

Figure 4.4. Hourly total number of vehicles averaged in each of 12 speed bins in April 2017 and 2018 (turquoise) compared to April 2020 (purple) at a traffic sensor located on I-95 in Howard County, MD. Provided in the top left-hand corner is the weighted average speed and the fraction of vehicles driving at less than 22 m s^{-1} ($frac_{<22mps}$) pre-COVID and in April 2020.

Table 4.2. Weighted average vehicle speeds (μ in m s^{-1}) and the fraction of vehicles driving under 22 m s^{-1} ($frac_{<22mps}$) at the I-95 traffic counter site for all data and also separated by weekday and local time, pre-COVID and in April of 2020.

	April 2017 and 2018	April 2020
All days and hours	μ=26.6 m s^{-1} $frac_{<22mps}$ = 23.6%	μ=30.3 m s^{-1} $frac_{<22mps}$ = 1.40%
Weekdays (Mo − Fr)	μ=26.4 m s^{-1} $frac_{<22mps}$ = 24.3%	μ=30.2 m s^{-1} $frac_{<22mps}$ = 1.28%
Weekends (Sa and Su)	μ=28.6 m s^{-1} $frac_{<22mps}$ = 11.0%	μ=31.0 m s^{-1} $frac_{<22mps}$ = 1.97%
23:00 – 04:59 (early morning)	μ=30.3 m s^{-1} $frac_{<22mps}$ = 0.80%	μ=30.3 m s^{-1} $frac_{<22mps}$ = 1.40%
05:00 – 09:59 (morning rush)	μ=26.6 m s^{-1} $frac_{<22mps}$ = 24.1%	μ=30.3 m s^{-1} $frac_{<22mps}$ = 1.23%
14:00 – 20:59 (afternoon rush)	μ=24.9 m s^{-1} $frac_{<22mps}$ = 35.4%	μ=30.5 m s^{-1} $frac_{<22mps}$ = 1.54%

Fewer vehicles on the road in April 2020 resulted in reduced mobile emissions as well as lower ambient levels of BC, CO, NO_x, and CO_2 compared to prior years at the I-95 NR site (Table 4.3). Rather than using absolute concentrations, affected by other processes including changing boundary layer height, we use concentration ratios to infer emissions and to better understand the impact of fewer vehicle miles traveled and changing traffic patterns.

Table 4.3. Summary of five-minute averaged ambient measurements of [BC], [CO], [NO_x], and [CO_2] at the I-95 NR site in Howard County, MD for pre-COVID (April 2017 and 2018) and April 2020.

I-95 Site five-min data	Number of valid data points	5th percentile	95th percentile	Median	Mean	Standard deviation
April 2017 and 2018						
[BC] ($\mu g\ m^{-3}$)	17,225	0.060	3.04	0.80	1.05	1.02
[CO] (ppbv)	15,554	150	433	238	259	94.1
[NO_x] (ppbv)	16,531	4.90	71.5	25.6	30.8	22.3
[CO_2] (ppmv)	13,075	417	491	439	444	25.4
April 2020						
[BC] ($\mu g\ m^{-3}$)	8,629	0.076	2.0	0.44	0.67	0.71
[CO] (ppbv)	7,844	131	351	205	218	78.1
[NO_x] (ppbv)	8,381	2.52	64.1	14.8	22.0	20.5
[CO_2] (ppmv)	8,455	420	488	434	442	21.9

A comparison of inferred emission ratios for April 2020 and pre-COVID by weekday and local time is presented in Table 4.4. April 2020 was slightly cooler than the reference years (Table 4.4) and BC emissions have previously been demonstrated to be temperature sensitive (Chapter 3). Using the temperature sensitivity discussed in Chapter 3 and presented in Figure 3.4, the difference in temperature between April 2020 relative to prior years is small (2.2°C) and can only account for a 3 - 4% decrease in the $\Delta BC/\Delta CO$ and $\Delta BC/\Delta CO_2$.

Table 4.4. Median inferred emission ratios for April 2017 & 2018 ("pre-COVID") and April 2020 ("2020") at the I-95 NR site. Also provided is the relative difference (%), with the statistical significance indicated by p-value, between each pair of median values for each emission ratio and time period. Percentages of CIVs and SIVs provided are for typical pre-COVID traffic composition. A comparison of the vehicle fleet pre-COVID and in April 2020 is shown in Table 4.1.

	T °C	$\Delta BC/\Delta CO$ ($\mu g\ m^{-3}$) $ppbv^{-1}$	$\Delta BC/\Delta CO_2$ ($\mu g\ m^{-3}$) $ppmv^{-1}$	$\Delta NO_x/\Delta CO$ $mol\ mol^{-1}$	$\Delta CO/\Delta CO_2$ $mol\ mol^{-1}$	$\Delta NO_x/\Delta CO_2$ $mol\ mol^{-1}$
All Days and Hours			**(Pre-COVID: 12% CIV, 88% SIV)**			
Pre−COVID	14.4	0.0119	0.0920	0.247	0.00802	0.00205
2020	12.2	0.0087	0.0675	0.276	0.00840	0.00237
Relative		**−26.9%**	**−26.6%**	11.7%	4.74%	**15.6%**
Change (%)		**(p<0.05)**	**(p<0.05)**	(p=0.074)	(p=0.41)	**(p<0.05)**
Weekdays Only			**(Pre-COVID: 14% CIV, 86% SIV)**			
Pre−COVID	13.9	0.0143	0.0997	0.282	0.00769	0.00221
2020	11.7	0.0110	0.0761	0.313	0.00719	0.00249
Relative		**−23.1%**	**−23.7%**	**11.0%**	−6.50%	**12.7%**
Change (%)		**(p<0.05)**	**(p<0.05)**	**(p<0.05)**	(p=0.26)	**(p<0.05)**
Weekends Only			**(Pre-COVID: 7.4% CIV, 92.6% SIV)**			
Pre−COVID	15.3	0.0064	0.0596	0.159	0.00909	0.00141
2020	12.2	0.0044	0.0496	0.169	0.0125	0.00205
Relative		**−31.3%**	−16.8%	6.29%	**37.5%**	**45.4%**
Change (%)		**(p<0.05)**	(p=0.27)	(p=0.68)	**(p<0.05)**	**(p<0.05)**
23:00 – 4:59 AM Local Time			**(Pre-COVID: 22% CIV, 78% SIV)**			
Pre−COVID	11.7	0.0173	0.1150	0.439	0.00662	0.00303
2020	10.0	0.0146	0.0813	0.549	0.00526	0.00294
Relative		−15.6%	**−29.3%**	**25.1%**	−20.5%	−2.97%
Change (%)		(p=0.12)	**(p<0.05)**	**(p<0.05)**	(p=0.21)	(p=0.76)
5:00 – 9:59 AM Local Time			**(Pre-COVID: 11% CIV, 89% SIV)**			
Pre−COVID	11.7	0.0141	0.0955	0.280	0.00763	0.00196
2020	10.0	0.0109	0.0708	0.296	0.00645	0.00208
Relative		**−22.7%**	**−25.9%**	5.71%	−15.5%	6.12%
Change (%)		**(p<0.05)**	**(p<0.05)**	(p=0.17)	(p=0.23)	(p=0.76)
14:00 – 20:59 Local Time			**(Pre-COVID: 7.3% CIV, 92.7% SIV)**			
Pre−COVID	18.3	0.0087	0.0764	0.189	0.00893	0.00163
2020	14.4	0.0043	0.0547	0.169	0.0128	0.00248
Relative		**−50.6**	**−28.4**	−10.6	**43.3%**	**52.1%**
Change (%)		**(p<0.05)**	**(p<0.05)**	(p=0.12)	**(p<0.05)**	**(p<0.05)**

Most notable from the results in Table 4.4 is that ΔBC/ΔCO in April 2020 was 26.9% ($p<0.05$) lower than in prior years, considering all days and hours. Likewise, $\Delta BC/\Delta CO_2$ was 26.6% ($p<0.05$) lower in April 2020. With SIVs exhibiting a much larger decline in numbers than CIVs in 2020, one initial hypothesis was that the reduction in mobile CO and CO_2 emissions would be greater than that for BC and thus lead to an increase in ΔBC/ΔCO and $\Delta BC/\Delta CO_2$ during April 2020. Instead, we observed consistently lower ΔBC/ΔCO in April 2020 for the whole time period. $\Delta BC/\Delta CO_2$ exhibited a statistically significant decrease in all considered time periods except for weekends, which had a statistically insignificant decrease in the emission ratio. These findings likely indicate that the influence of vehicle fleet changes on ΔBC/ΔCO $\Delta BC/\Delta CO_2$ was overshadowed by a drastic change in another highway characteristic: stop-and-go traffic.

While the differences in mean traffic speeds were generally minor (<6 m s^{-1}), the fraction of vehicles driving below 22 m s^{-1} ($frac_{<22mps}$) dropped down from ~28% in prior years to less than 2% in April 2020 (Figure 4.4 and Table 4.2). The afternoon rush hour (14:00 – 20:59 ET), when the $frac_{<22mps}$ is highest of the day at 35.4% (Table 4.2), exhibited the largest decrease in ΔBC/ΔCO (−50.6%, $p<0.05$) from April 2017 and 2018 to April 2020 (Table 4.4). The morning rush hour also saw a significant improvement in traffic flow, with the percentage of vehicles driving slower than 22 m s^{-1} decreasing from 24.1% pre-COVID to 1.23% in April 2020, and a concurrent decrease of 22.7% in ΔBC/ΔCO and 25.9% in $\Delta BC/\Delta CO_2$ (Table 4.4). The drop in ΔBC/ΔCO during the overnight period (23:00 – 4:59 ET),

when traffic flow did not differ much in April 2020 compared to previous years, was less remarkable and statistically insignificant (−15.6%, p=0.12).

The difference in $\Delta BC/\Delta CO$ and $\Delta BC/\Delta CO_2$ between weekdays and weekends suggests that CIVs are the primary contributor to mobile BC emissions at this site. The median pre-COVID $\Delta BC/\Delta CO$ ratio on weekdays was 0.0143 μg m^{-3} $ppbv^{-1}$ compared to the weekend ratio of 0.0064 μg m^{-3} $ppbv^{-1}$, a decrease of 55.3% (Table 4.4). Similarly, $\Delta BC/\Delta CO_2$ decreased by 40.4% from 0.100 μg m^{-3} $ppmv^{-1}$ on weekdays to 0.0596 μg m^{-3} $ppmv^{-1}$ on weekends. The decrease in both ratios from weekdays to weekends follows the change in the fraction of CIVs passing the NR site: the fraction of CIVs dropped from 14% on weekdays to 7.4% on weekends, resulting in a decrease of 47.1%. These observations provide strong evidence that CIVs dominate the BC emissions at the I-95 NR site.

Figure 4.4 shows that the typical traffic congestion, marked by frequent braking and accelerating, was nearly eradicated in April 2020. Two mechanisms may help to explain this finding: enhanced BC emissions from brake pads and acceleration in CIVs. Vehicular brake pads, composed of various metals and graphite, are known to emit BC and a variety of other species (Lyu and Olofsson, 2020). Significant reductions in stop-and-go traffic in April 2020 thus led to lower BC emissions from brake pads. Black carbon is also released from the exhaust of CIVs during acceleration (Giakoumis and Zachiotis, 2021; Rakopoulos and Giakoumis, 2009). With CIVs representing the dominant source of tailpipe BC emissions, the near-elimination of traffic jams in April 2020 produced a larger reduction in mobile BC emissions than the effect of fewer on-road SIVs on CO

emissions. With a decrease in SIVs of ~60% in April 2020 and assuming a comparable reduction in CO emissions, the decrease in ΔBC/ΔCO of 26.7% (considering all days and hours) indicates that BC emissions likely decreased by ~70%, a number compatible with the decrease in the median BC concentration of nearly a factor of two.

In addition to ΔBC/ΔCO, Table 4.4 presents the results for various other emission ratios. Comparison of CO and NO_x to CO_2 provides better understanding of the effectiveness of exhaust-aftertreatment devices, specifically catalytic converters, installed in vehicles passing the NR site. Trucks generally emit less CO relative to CO_2, resulting in lower $\Delta CO/\Delta CO_2$ than cars. With fewer SIVs on roads relative to CIVs in April 2020, one might expect lower $\Delta CO/\Delta CO_2$ as well. The $\Delta CO/\Delta CO_2$ analysis presented in Table 4.4 shows no significant trend for all hours, however we observe higher ratios on weekends and during the afternoon rush hour in April 2020 than in previous years. A plausible explanation for this trend is that vehicles emit more CO at high speeds (Hickman et al., 1999; OECD and ECMT, 2006; Wang et al., 2018). With less traffic congestion on roads in April 2020, vehicles were driving 14% faster than usual (Figure 4.4) and likely emitted more CO relative to CO_2.

A statistically significant increase in $\Delta NO_x/\Delta CO_2$ was observed for weekdays, weekends, and during the afternoon rush hour. $\Delta NO_x/\Delta CO_2$ increased by 45.4% ($p<0.05$) on weekends and 52.1% ($p<0.05$) in the afternoon rush hours, compared to 12.7% on weekdays (Table 4.4). Higher $\Delta NO_x/\Delta CO_2$ from CIVs combined with a greater fraction of on-road CIVs likely led to elevated $\Delta NO_x/\Delta CO_2$

(but lower NO_x mixing ratios) in April 2020 compared to the same month in prior years. Gasoline vehicles also exhibit a slight increase in mobile NO_x emissions at high speeds that likely contributes to the higher observed $\Delta NO_x/\Delta CO_2$ in April 2020 (OECD and ECMT, 2006).

4.4 Conclusions

The results in this chapter highlight the significance of traffic flow on BC emissions from diesel trucks. Traffic and ambient pollutant observations were collected at stationary sites along I-95, a major highway in the Eastern US. Strong reductions in on-road vehicle counts in April 2020 relative to prior years resulted in the near-elimination of traffic jams and a 14% increase in the average vehicle speed. Significant improvements in traffic flow led to a ~27% decrease in both $\Delta BC/\Delta CO$ and $\Delta BC/\Delta CO_2$ in April 2020 relative to prior Aprils. The reduction of a factor of ~two in $\Delta BC/\Delta CO$, $\Delta BC/\Delta CO_2$, and the fraction of CIVs from weekdays to weekends is consistent with trucks as the dominant emitter of BC emissions. A likely explanation for the lower $\Delta BC/\Delta CO$ and $\Delta BC/\Delta CO_2$, and thus BC emission, in April 2020 compared to prior years is that diesel trucks emitted far less BC in spring 2020 than under typical, congested traffic conditions with frequent acceleration. Less frequent braking in April 2020 also likely contributed to lower BC emissions from vehicular brake pad wear. These results suggest that elimination of traffic jams could reduce highway BC emissions from diesel trucks by ~70% (i.e., to ~30% level of normal emissions). Further reductions in mobile BC emissions may be possible with diesel engine designs that reduce turbocharger lag.

Peak travel restrictions at the beginning of the COVID-19 pandemic in April 2020 enabled us to study the effects of traffic emissions on air quality. Due to the strong impact of traffic speed on vehicular emissions, a topic for future work is to evaluate models of mobile BC emissions, especially their sensitivity to stop-and-go traffic. The first step would be to modify SMOKE-MOVES to account for the strong decrease in traffic jams on simulated levels of restricted access highway BC emissions. Some preliminary work discussing vehicle speeds and BC emission rates from MOVES3 is discussed in Chapter 5. Assessing how air quality models perform given drastic changes in specific variables such as the number of on-road vehicles or stop-and-go traffic can help to improve the accuracy of future modeling endeavors.

Chapter 5: Conclusions and Future Work

The work presented in this dissertation characterizes vehicular emissions in the near-road environment and examines various elements that affect them. Since vehicles are a major source of NO_x, CO, and BC, understanding how mobile emissions change with weather and traffic has important health and environmental impacts. Mobile emissions were estimated using ambient, NR observations of NO_x, CO, BC, and CO_2 at a stationary monitoring site located along I-95 in the Baltimore-Washington area, while traffic counts along I-95 were used to investigate the impact of changes in the passing vehicle fleet on inferred emissions. The focus of the first part of the dissertation is to improve our understanding of the impact of temperature on mobile emissions. The second part focuses on how changes in the vehicle fleet composition and speed impact emissions.

Discrepancies between measured and modeled atmospheric NO_x, especially in the summertime, have been widely reported in the literature and often attributed to inconsistencies in simulated mobile emissions. This gap in knowledge acts as motivation for the work in Chapter 2, where I discuss a temperature sensitivity in vehicular NO_x emissions as a contributor to the reported discrepancy. To infer highway emissions from ambient NR observations, I used several techniques to isolate influence of traffic from background levels that all led to the same conclusion; vehicular NO_x emissions appear to decrease with rising ambient temperatures. Carbon monoxide and CO_2 do not show much sensitivity to temperature. A smaller change in mobile NO_x with specific humidity is not enough to explain the temperature effect, suggesting that combustion processes and/or

pollution control equipment are likely sensitive to ambient temperature. By using traffic observations and conducting the analysis for various time windows, such as the overnight period when the fraction of on-road trucks is highest, we conclude that NO_x emissions from diesel-powered trucks exhibit a strong dependence on temperature.

Chapter 2 also includes an evaluation of mobile NO_x emissions simulated by MOVES. By comparison to the observations, MOVES underestimates the temperature sensitivity of NO_x emissions, indicating that the default setting used in the temperature adjustment factor for running emissions needs further assessment. Adjusting the temperature settings within MOVES may help to bring observed and modeled NO_x abundances into agreement during the warm season, thus reducing some of the discrepancies reported in the literature. Some preliminary work to incorporate a temperature effect into MOVES has already been accomplished, however more work is needed to translate this modification for use in SMOKE-MOVES. With diesel-powered trucks being the dominant source of BC emissions in the NR environment, the temperature analysis from Chapter 2 was extended in Chapter 3 to include vehicular BC emissions. I evaluated highway emissions of BC using inferred emission ratios at the I-95 NR site. The results of this study suggest that BC emissions vary both seasonally and by temperature. Within the four seasons, with highest emissions occurring during the summer and lowest in the winter, similar to other studies that found a seasonal cycle in BC emissions (Chen et al., 2001; Kondo et al., 2006; Wang et al., 2018). To minimize seasonal differences such as in fuel and traffic, I focused the analysis on the cold season and observed

greater mobile BC emissions at higher temperatures. A strong temperature dependence during the overnight period and on weekdays, when the fraction of trucks is at a maximum, suggests that BC emissions from diesel-powered trucks increase with ambient temperature. One hypothesis worth exploring is that higher temperatures result in lower air density entering the combustion chamber, which in turn leads to elevated BC emissions (Chen et al., 2001; Ghazikhani et al., 2013). These results suggest that improvements in diesel engine design may help to lower BC emissions, especially on hotter days when vehicular BC emissions are elevated, and can improve air quality for populations living close to diesel sources.

Like mobile NO_x emissions, the temperature adjustment for BC emissions in MOVES does not agree with observations. The latest version of the model, MOVES3, makes no adjustment to running BC emissions for ambient temperature. Since on- and off-road diesel-powered vehicles account for the majority of BC emissions (2017 NEI), the lack of a temperature adjustment in MOVES and SMOKE-MOVES suggests that modeled ambient BC levels may not agree well with observations. The absence of a temperature adjustment helps to explain a previous study that found CMAQ modeled BC concentrations consistent with observed winter but not summer concentrations (Appel et al., 2008). The findings for Chapter 3 support incorporating a temperature adjustment for BC emissions in MOVES3 to help improve the accuracy of modeled BC concentrations, especially in areas with high BC emissions from diesel engines.

Near-road observations can also be effectively used to study the impact of traffic patterns on emissions of BC, CO, NO_x, and CO_2. In Chapter 4, I utilize vehicle speed information to determine the impact that changing traffic conditions (both speed and number of vehicles) have on mobile emissions. The total number of on-road vehicles fell significantly in April 2020 due to the strict travel limitations implemented in March 2020. With fewer vehicles on the road, speeds were faster and traffic flow greatly improved. Significantly less stop-and-go traffic on I-95 led to an outsized improvement in BC emissions relative to the reduction in CO emissions resulting from fewer on-road car counts. A similar pattern in weekday-weekend differences in emission ratios and the fraction of trucks suggests that trucks are the dominant source of BC at the NR site. We conclude from these findings that diesel-powered trucks benefit greatly from reduced traffic congestion. Additionally, fewer instances of vehicles braking led to lower BC emissions from brake pads, and this effect may have contributed to lower BC emissions in April 2020. Such insight into the impact of traffic flow on vehicular emissions can help shape policy decision making in further reducing BC emissions.

There are several future projects that expand on the work presented in this dissertation. One area of future study is to test for the presence of brake emissions in the NR environment. While tailpipe emissions are an important source of CO, NO_x, PM, and VOCs, emissions from brake pads contain a variety of other chemicals that are hazardous to human health, such as metals. Future work could focus on evaluating the correlation between ambient BC and other species commonly emitted by brakes, such as copper. The I-95 site does not measure ambient concentrations of

the metals commonly found in brake pads, however other sites do measure these as part of the EPA-network of monitors.

An area of consideration is to conduct a full evaluation of inferred VOC emissions at the NR observations and the impact of ambient temperature on vehicular VOC emissions. While this dissertation discussed CO, NO_x, and BC, VOCs represent a large group of compounds emitted by vehicles through exhaust and evaporative emissions. The I-95 monitoring site samples 56 VOCs via grab canisters once per week. A preliminary analysis of several VOCs emitted by vehicles suggests that several, including propene, ethene, 1-butene, and benzene exhibit decreasing emissions as temperatures increase (Figure D1), similar to the trend observed in mobile NO_x emissions. Future work should provide insight into the specific processes by which vehicles emit VOCs at the NR site by grouping VOCs by tailpipe (propene and benzene, for example) and evaporative emissions (n-pentane and butane, for example).

A preliminary analysis of methane (CH_4) observations at the I-95 site suggest that vehicles also produce CH_4. Figure D3 depicts a strong correlation between CH_4 and CO_2 ($r^2 = 0.98$) at the I-95 site during winter months (December, January, and February) from December 2016 through December 2018. The $\Delta CH_4/\Delta CO_2$ emission ratio, estimated by the slope value of the best-fit to the observations, is 2.47 ppbv/ppmv at the NR site (Figure D3). While vehicles are known to emit some CH_4, future work could focus on using the observed NR emission ratio in combination with CO_2 inventories from the on-road sector to quantify vehicular CH_4 emissions.

This is especially important because on-road vehicles, both diesel and gasoline, generate ~34% of CO_2 emissions reported in the 2017 NEI.

Certain vehicles emit ethane, specifically those using natural gas fuel. A scatterplot of 24-hour average ethane and methane at the NR site for October 2016 through December 2018 shows a correlation between the two species with a slope of 0.022 $ppbv_{ethane}/ppbv_{methane}$ and $r^2 = 0.46$ (Figure D4). This emission ratio is lower than that observed in aircraft observations collected over the Baltimore-Washington area (0.033 to 0.043 ppbv/ppbv) by Ren et al. (2018), and should be studied further to examine tailpipe emissions of ethane at the NR site.

Another area of future work may focus on improving MOVES by adjusting parameters controlling the impact of temperature and humidity on vehicular NO_x and BC emissions within the simulator. The goal of this is to better represent the behavior of real-world vehicular emissions and assess the implications of these changes to future surface ozone attainment strategies. Using the temperature dependence in mobile emissions at the I-95 NR observations (Chapters 2 and 3), one could develop an appropriate modification to the temperature adjustment factor for running emissions of NO_x and BC within MOVES. Since the SMOKE-MOVES modeling platform is used to prepare vehicular emissions for use in air quality models, the temperature adjustment developed for MOVES must also be compatible for use in SMOKE-MOVES to produce the observed temperature effect. I have made some progress in developing a preliminary temperature adjustment for vehicular NO_x emissions within MOVES based on the observations, however future work should focus on developing a similar adjustment for BC emissions and then

including these modifications into SMOKE-MOVES. One could alter the base emission rates within MOVES (g NO_x/mile) to reflect the observed temperature dependence by adding a multiplicative adjustment factor to NO_x emissions

$$multiplicative\ factor = 1 - 0.0179 \cdot (T - 75)$$

where T is the ambient temperature in °F, however this would only be applicable to interstate highways such as I-95. Figure D5 shows a comparison of unadjusted NO_x, CO, and CO_2 emission rates from MOVES output, as well as model output obtained from a simulation using identical model input but including the temperature modification shown above. MOVES output from a simulation with the temperature adjustment show nearly a 50% decrease in NO_x emission rates from −5 to 25°C, consistent with NR observations. Incorporating the impact of temperature on NO_x and BC emissions within SMOKE-MOVES will ultimately allow air quality models to better represent mobile emissions inferred from real-world measurements.

Investigating how vehicular BC emissions respond to stop-and-go traffic in MOVES3 (and SMOKE-MOVES) would also be interesting. For a preliminary look into the response of BC emission rates to vehicle speeds in MOVES, I ran MOVES3 using Howard County input data and again using Baltimore County input (input data compiled and provided by MDE). Because of the proximity of Baltimore County to the downtown Baltimore area, we would expect to see higher BC emission rates due to vehicles driving slower (Chapter 4) in urban areas. Figure D shows that emission rates in both counties are similar and that BC emission rates in Baltimore County are generally not higher than in Howard County. This brief study suggests that more work is necessary is to evaluate the effect of speed (and traffic congestion) on

vehicular emissions, perhaps by varying the speed information that is used by MOVES, similar to how the meteorology input data was modified to study the impact of temperature on emissions (Chapters 2 and 3).

The emissions studied in this dissertation are representative of typical highway conditions. An interesting topic for future work is to expand the work on temperature and stop-and-go traffic to other types of roadways, including non-highway monitoring sites such as in suburban locations, like Baltimore County. Doing so would allow us to better understand vehicular emissions in areas that are largely residential in nature and could provide important insight to help strengthen existing public health policies.

Appendix A: Supplemental Information for Chapter 2

A1. Map of I-95 near-road site and 2011 DISCOVER-AQ aircraft campaign

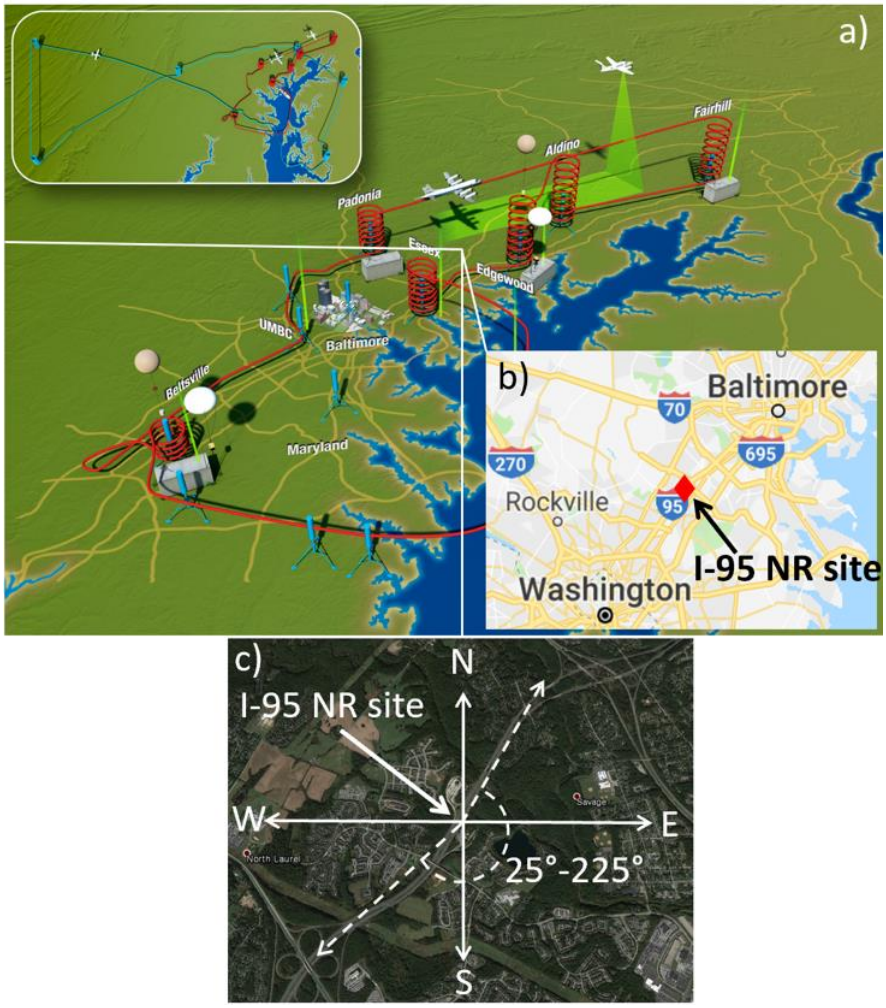

Figure A1. Map of DISCOVER-AQ aircraft campaign over the Baltimore-Washington region in July 2011 (a). The upper-left panel shows the Cessna and P3 flight tracks with respect to the entire state of Maryland, while the right inset shows the overlap between the DISCOVER-AQ campaign and the location of the near-road monitoring site along I-95 used in this study (b). The bottom image shows a close-up view of the I-95 NR site (c; images from Google Earth and Google Maps). DISCOVER-AQ image publicly available at https://discover-aq.larc.nasa.gov/multimedia.html.

A2. Measurement details and analyzer specifications

The DISCOVER-AQ flight campaign was carried out in Maryland over 14 flight days and included segments flown over I-95, an eight-lane interstate highway with heavy truck traffic (Anderson et al., 2014). Carbon monoxide was measured using a diode laser spectrometer and [NO_y] was measured using a four-channel chemiluminescent instrument.

Measurements of meteorological data, [CO], and [NO_x] at the I-95 site were collected using instruments similar to those stationed at other EPA Air Quality System (AQS) sites. Observations of [CO], [NO_x], and meteorological variables at the I-95 site were made every 10 seconds, and for [CO_2] every 2 s. One-minute averages were calculated from the 10- and 2-second values.

Meteorological variables including temperature, relative humidity, pressure, wind direction, and wind speed were measured using a Vaisala WXT 520. A Teledyne Advanced Pollution Instrumentation (API) Model 300 U analyzer was used to determine [CO] based on infrared radiation absorption. According to the manufacturer's specifications, the drift in the zero readings of the CO analyzer may be up to 20 ppbv over 24 hours with noise of up to 10 ppbv, as measured by the root mean square of the zero (API, 2017). Routine quality control checks performed twice a month show that the mean relative accuracy, defined as the average percentage difference between calibration standards and analyzer readings during regular quality control checks using one-minute data, for [CO] was 2.3% at 500 ppbv, calculated from the difference between measured and known concentrations. We consider observations of [CO] less than 100 ppbv to be below the regional

background. The one-minute measurements at I-95 used in this analysis contain up to 1% of measurements for which [CO] was below 100 ppbv; however, these data have passed the official quality control filters mandated by the US EPA for all AQS sites and excluding them would introduce a high bias. We attribute measurements of [CO] below 100 ppbv to total instrument noise, which suggests that ~1% of the measurements are farther than ±3 sigma from the mean. Our analysis includes these data; omitting them does not have a significant impact on any of the scientific conclusions.

NO_x concentrations were measured by a Teledyne API Model 200 U analyzer based on chemiluminescence. The analyzer contains two channels, one in which the mixing ratio of NO ([NO]) in ambient air is measured directly by its reaction with O_3. The other channel indicates [NO_2], and other oxidized reactive nitrogen species, by first converting to NO on hot molybdenum at 315° and then reacting with O_3 (API, 2018; Fontijn et al., 1970). The difference between these two measurements (i.e. [NO_x] − [NO]) approximates [NO_2]. The chemiluminescence technique for measurements of [NO_2] is sensitive to other reactive nitrogen species such as HONO, HNO_3, and peroxyacetyl nitrate (PAN), as noted by, for example, Dickerson et al. (2019), Dunlea et al. (2007,) Fehsenfeld et al. (1987). We assume all emitted NO_y species were detected because air parcels were sampled within ~12 m of a dominant source of NO_x, with little time to lose reactive nitrogen to dry deposition. Mixing ratios of NO_X measured with the NO/NO_2/NO_X analyzer exhibit a zero drift of up to 0.1 ppbv in a 24 hour period, noise at the zero level of up to 25

parts per trillion by volume (pptv; 1σ), and a relative accuracy of 4.7% for abundances between 9 and 12 ppbv (API, 2013).

Measurements of [CO_2] were acquired at the I-95 site using a Los Gatos Research (LGR) Fast Greenhouse Gas Analyzer (FGGA) with the Enhanced Performance option (Los Gatos Research, 2013). The LGR FGGA uses off-axis Integrated Cavity Output Spectroscopy (ICOS) in the Near-Infrared Region (NIR) and has been described previously (Baer et al., 2002; Martin et al., 2017). The manufacturer's specified precision for measurements of [CO_2] collected at a temporal resolution of 1 Hz is 0.3 ppmv (Los Gatos Research, 2013). The maximum drift over 24 hours is 0.3 ppmv, while the drift in the analyzer over a 1-month period has been discussed elsewhere and is ~1.2 ppmv (~0.3%) over a 30-day period (Los Gatos Research, 2013; Martin et al., 2017). The relative accuracy as calculated by comparison of the analyzer readings to known concentrations based on the NIST-standard is 0.089% at 516 ppmv.

A3. Vehicle fleet composition at the I-95 near-road site

Table A1. Summary of vehicle types passing the I-95 near-road site.

% of total vehicles		Average hourly number of vehicles	
Motorcycles	0.10	Motorcycles	7.00
Passenger cars	76.0	Passenger cars	6620
Passenger trucks	10.9	Passenger trucks	954
Buses	1.78	Buses	121
Single-unit trucks	3.16	Single-unit trucks	204
Combination-unit trucks	8.06	Combination-unit trucks	349

[1] Single-unit trucks are a collection of Federal Highway Administration (FHWA) vehicle classes 5–7.

[2] Combination-unit trucks are a collection of FHWA vehicle classes 8–13.

[3] More details regarding traffic classes can be found at https://www.fhwa.dot.gov/publications/research/infrastructure/pavements/ltpp/13091/002.cfm.

A4. Creating meteorology input for MOVES

The impact of temperature in MOVES was investigated by using the correlation between ambient specific humidity and temperature at the I-95 NR site in Howard County, MD, the county for which MOVES was run. We used the relationship between ambient temperature and specific humidity, instead of relative humidity, in preparing the meteorology input for MOVES because combustion temperatures respond to specific, not relative, humidity, following a method similar to Choi et al. (2010).

We first converted observed one-minute relative humidity measurements to specific humidity, then used the exponential equation given in Figure A2 to estimate

the ambient specific humidity for each degree Celsius between −5°C and 24°C. Since MOVES requires temperature and relative, not specific, humidity as input for the meteorology, we convert the specific humidity values estimated from Figure A2 back to relative humidity for use in the model. Results are presented in detail in Chapter 2 of the dissertation and Figure A12. In general, there is a slight decrease in NO_x emissions (11%), and an increase of 23% in CO and 3.5% in CO_2 with rising temperature between −5°C and 24°C within MOVES (Figure A12).

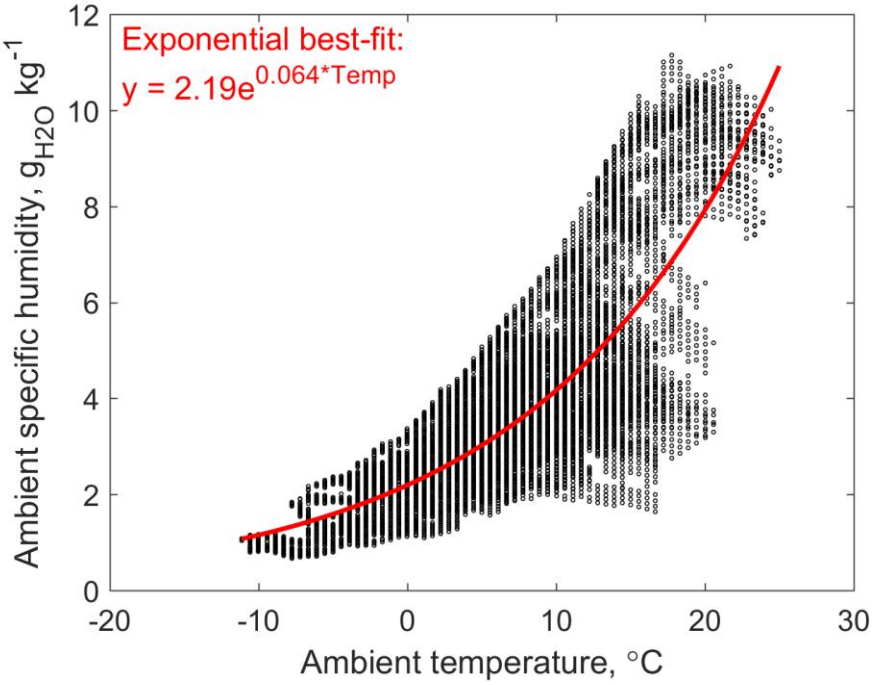

Figure A2. The correlation between observed ambient temperature and specific humidity observations collected at the I-95 NR site in Howard County, MD. The red line represents an exponential best-fit to the one-minute measurements, with the equation $y = 2.19 \cdot e^{0.064 \cdot temp}$.

To analyze the impact of specific humidity on $\Delta CO/\Delta NO_x$, $\Delta CO_2/\Delta NO_x$, and $\Delta CO_2/\Delta CO$ in MOVES, we performed additional model runs setting the input temperature range as −5°C to 25°C and adjusting the relative humidity at each

temperature so that for the entire temperature range the humidity was constant at 1, 2, 4, 6, 8, or 10 g kg^{-1}. To determine the sensitivity of emissions to specific humidity, we then took an average across the temperature range (−5° to 25°C) at each specific humidity level. There is an increase in $\Delta CO/\Delta NO_x$ and $\Delta CO_2/\Delta NO_x$ of 16% and 14% in MOVES, with no change in $\Delta CO_2/\Delta CO$ (Figure A13).

A5. Use of potential temperature in DISCOVER-AQ analysis

Potential temperature was used in the DISCOVER-AQ aircraft analysis because this measure of temperature has the benefit of remaining constant as an unsaturated air parcel moves vertically. The objective is to determine $\Delta CO/\Delta NO_y$ for the appropriate surface temperature. Thus, in a dry adiabatic process where there is no net change of energy in the closed system or any phase changes of water, potential temperature represents the temperature of the air parcel at 1000 hPa where most pollutants are emitted. During DISCOVER-AQ, θ was observed to be nearly constant over a given profile in the planetary boundary layer (PBL), as expected.

The $\Delta CO/\Delta NO_x$ emission ratios were estimated from measurements of CO and NO_x collected during spirals and vertical profiles within the PBL of the aircraft flights. The PBL height was approximated as 0.7 km in the morning and 1.5 km in the afternoon. Figure A3 shows the fraction of free troposphere air within the PBL estimated using Equation A1, where $[CO]_{PBL}$ represents the CO mixing ratio at the bottom of each airplane profile, $[CO]_{obs}$ is the measured value of CO, $[CO]_{ft}$ the CO mixing ratio within the free troposphere, and F_{ft} is the fraction of air from the free troposphere. This supports our approximation of the PBL height as the fraction of

free troposphere air entrained in the PBL is close to 0 below 1 km altitude and less than 20% below 1.5 km.

Equation A1. Simple mixing line calculation used to estimate fraction of free troposphere air within the PBL during aircraft spirals.

$$[CO]_{obs} = [CO]_{PBL} \cdot (1 - F_{ft}) + [CO]_{ft} \cdot F_{ft}$$

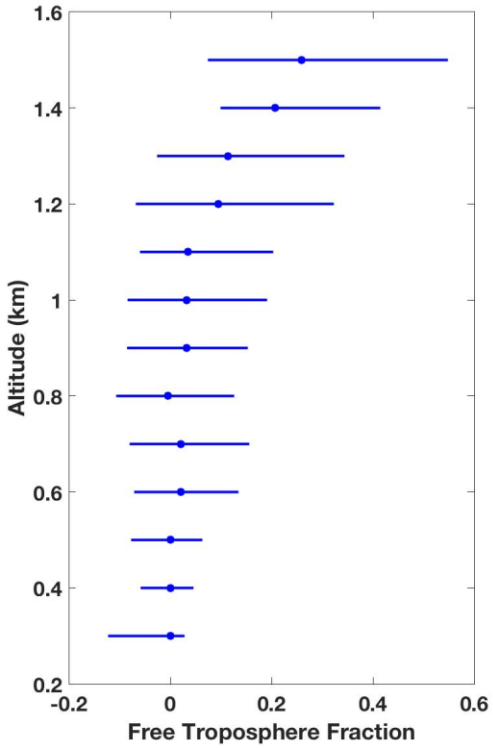

Figure A3. Estimates of the fraction of free tropospheric air entrained within the PBL as a function of altitude during the 2011 DISCOVER-AQ aircraft campaign over the BWR. The filled blue circles represent the median free troposphere fraction in each altitude bin, while the endpoints of the horizontal lines correspond to the 25th and 75th percentiles in each bin.

A6. Average July temperatures for Washington, DC

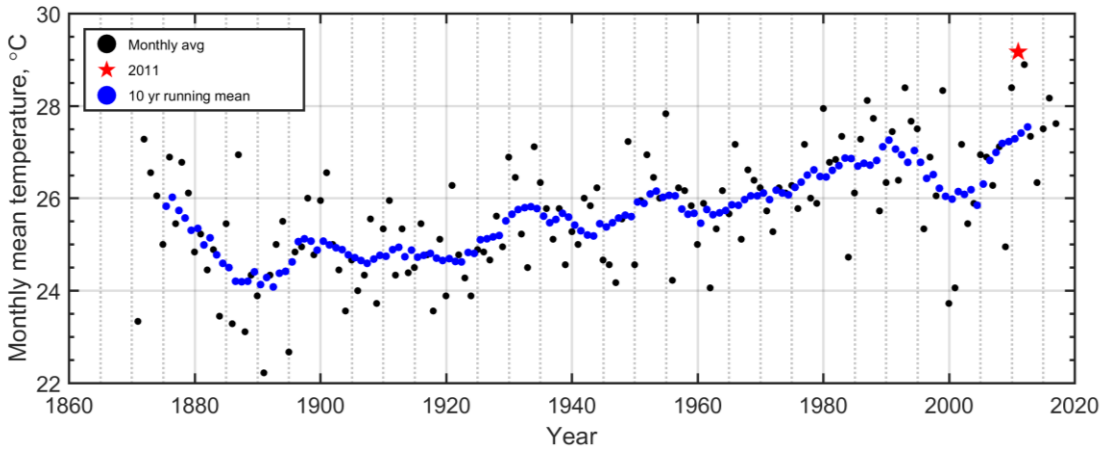

Figure A4. Temperature history for the month of July in Washington, DC. The black dots represent the monthly averaged temperatures, the blue dots the ten-year running mean of the monthly temperatures, and the red star the average temperature in July 2011, the year of the DISCOVER-AQ aircraft campaign over the Baltimore-Washington region. Data obtained from https://www.weather.gov/media/lwx/climate/dcatemps.pdf.

A7. I-95 ambient pollutant concentrations as a function of wind direction

The ambient mixing ratios of CO, NO_x, and CO_2 as a function of the wind direction at the I-95 NR site for November 2016 and February, November, and December 2017 are shown in Figure A5.

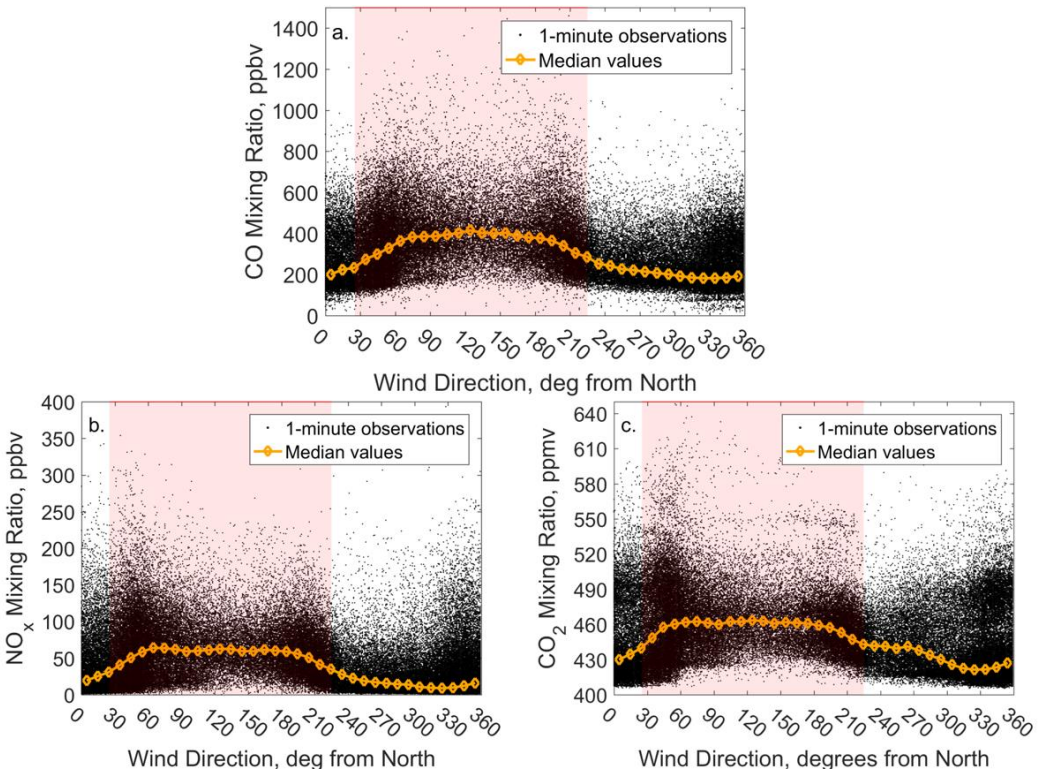

Figure A5. CO, NO_x, and CO_2 mixing ratios as a function of wind direction at the I-95 NR site during the cold season in 2016 and 2017. Highway angles are defined as 25° through 225°Compass and are marked by the red-shaded rectangle. The rest area located North/Northwest of the monitoring site, which has more parking spaces for passenger cars and trucks than the rest area located Southeast of the site, predominantly influences ambient pollutant measurements when winds were from between 310° and 360°Compass. The median mixing ratios when the wind blew from the highway were elevated by 160 ppbv (86%) for CO, 43 ppbv (400%) for NO_x, and 34 ppmv (8%) for CO_2, relative to the median mixing ratios when the wind came from the Northwestern rest area.

A8. Temperature dependence of $\Delta CO/\Delta NO_x$, $\Delta CO_2/\Delta NO_x$, and $\Delta CO_2/\Delta CO$ using the interquartile range to define outliers

We repeated the analysis using the interquartile range (IQR) rather than the 2 standard deviation method to define outliers prior to calculating the geometric mean regressions every hour. Based on this definition, outliers are defined as points that are less than the 25th percentile − 1.5xIQR and points that are greater than the 75th

percentile + 1.5xIQR. This change does not impact our main conclusion that NO_x emissions decrease with increasing temperatures.

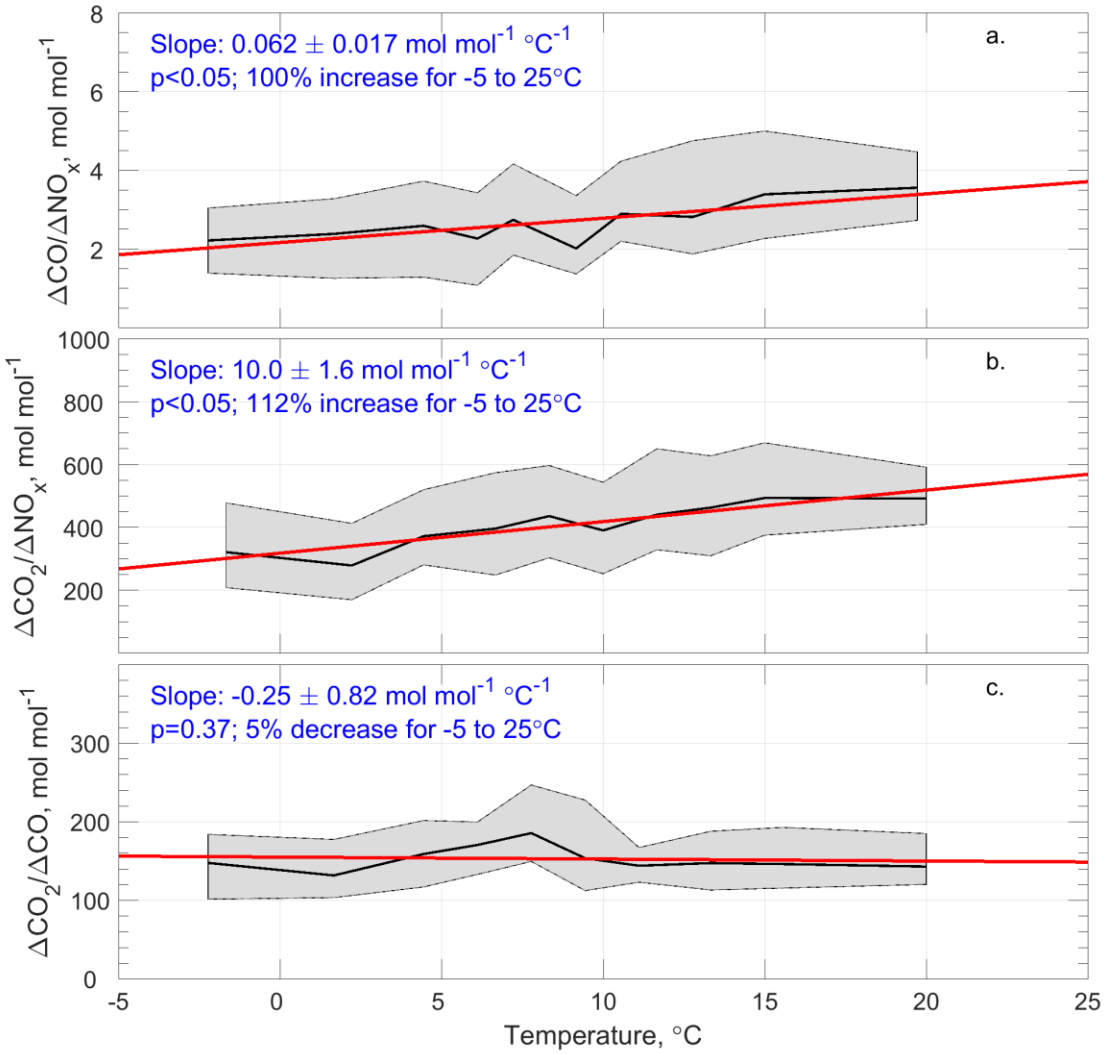

Figure A6. Hourly $\Delta CO/\Delta NO_x$ (a), $\Delta CO_2/\Delta NO_x$ (b), and $\Delta CO_2/\Delta CO$ (c) for all hours of the day and all values of specific humidity shown by the light gray dots, as a function of ambient temperature. Emission ratios were estimated from one-minute data collected at the I-95 NR site in Howard County, MD for November 2016 and February, November, and December 2017. Outliers, defined by the interquartile range rather than the two standard deviation method in Chapter 2, were removed prior to estimating each hourly regression. Data were placed into ten bins, each containing an equal number of points. The black lines correspond to the median emission ratios in each bin, bounded by the 25th and 75th percentiles of the bins represented by the light gray lines. The solid red lines represent ordinary, linear least-squares regression fits of the binned median emission ratios. The uncertainty of

the slope parameter of each trend was estimated using a Method of Maximum Likelihood, following Bevington and Robinson (2002).

A9. Temperature dependence of $\Delta CO/\Delta NO_x$, $\Delta CO_2/\Delta NO_x$, and $\Delta CO_2/\Delta CO$ using robust regression rather than geometric mean regression

We also repeated the analysis using the robust regression technique instead of the geometric mean regression method when calculating hourly emission ratios. The robust regression assigns less weight to outliers, or points that are farther from the best-fit line, and therefore we did not exclude any points prior to calculating the hourly regressions.

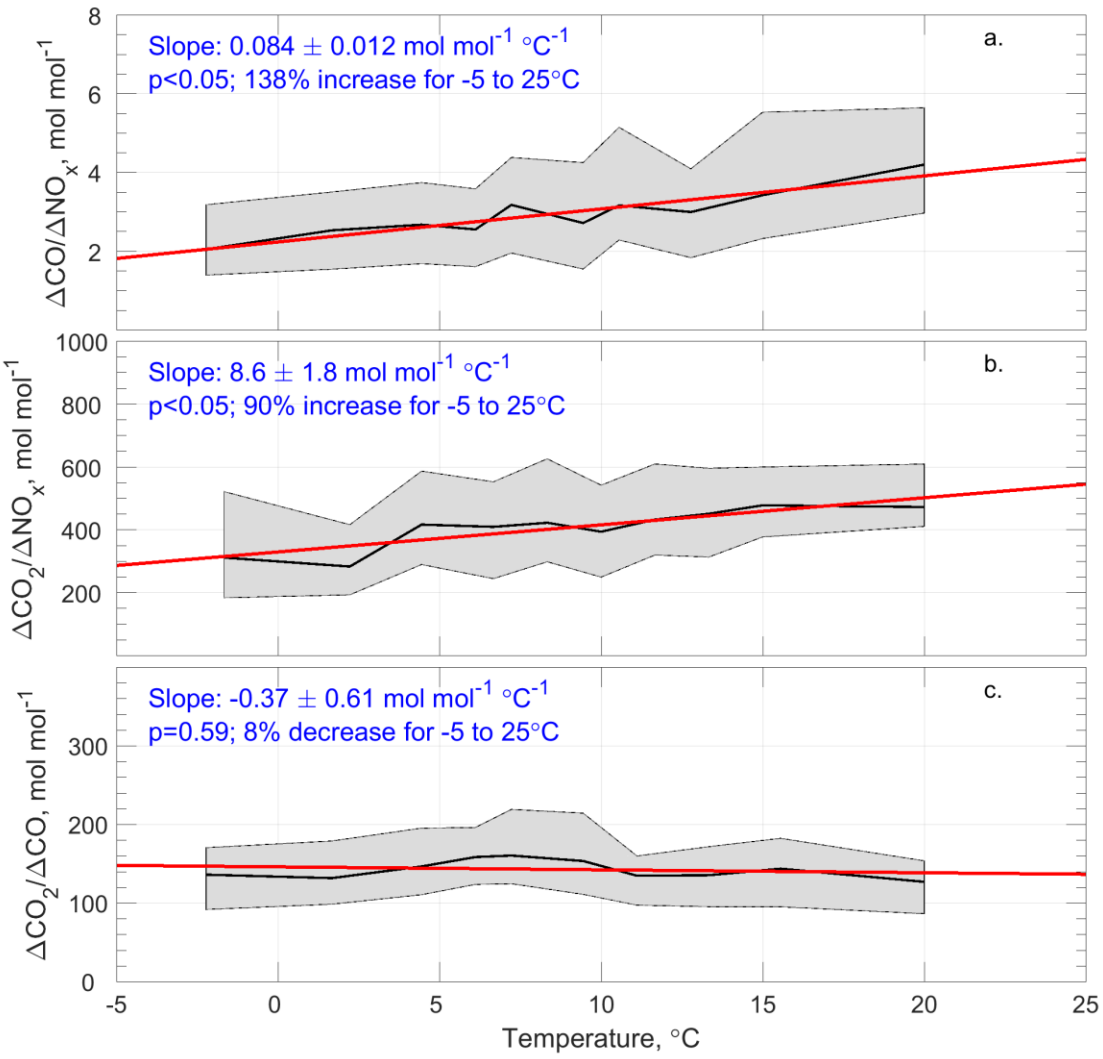

Figure A7. Hourly $\Delta CO/\Delta NO_x$ (a), $\Delta CO_2/\Delta NO_x$ (b), and $\Delta CO_2/\Delta CO$ (c) for all hours of the day and all values of specific humidity shown by the light gray dots, as a function of ambient temperature. Emission ratios were estimated from one-minute data collected at the I-95 NR site in Howard County, MD for November 2016 and February, November, and December 2017. Hourly emission ratios were estimated using a robust regression, including outliers, rather than a geometric mean regression as in Chapter 2. Data were placed into 10 bins, each containing an equal number of points. The black lines correspond to the median emission ratios in each bin, bounded by the 25th and 75th percentiles of the bins represented by the light gray lines. The solid red lines represent ordinary, linear least-squares regression fits of the binned median emission ratios. The uncertainty of the slope parameter of each trend was estimated using a Method of Maximum Likelihood, following Bevington and Robinson (2002).

A10. Temperature dependence of ΔCO/ΔNO$_x$, ΔCO$_2$/ΔNO$_x$, and ΔCO$_2$/ΔCO as a function of daily maximum temperature

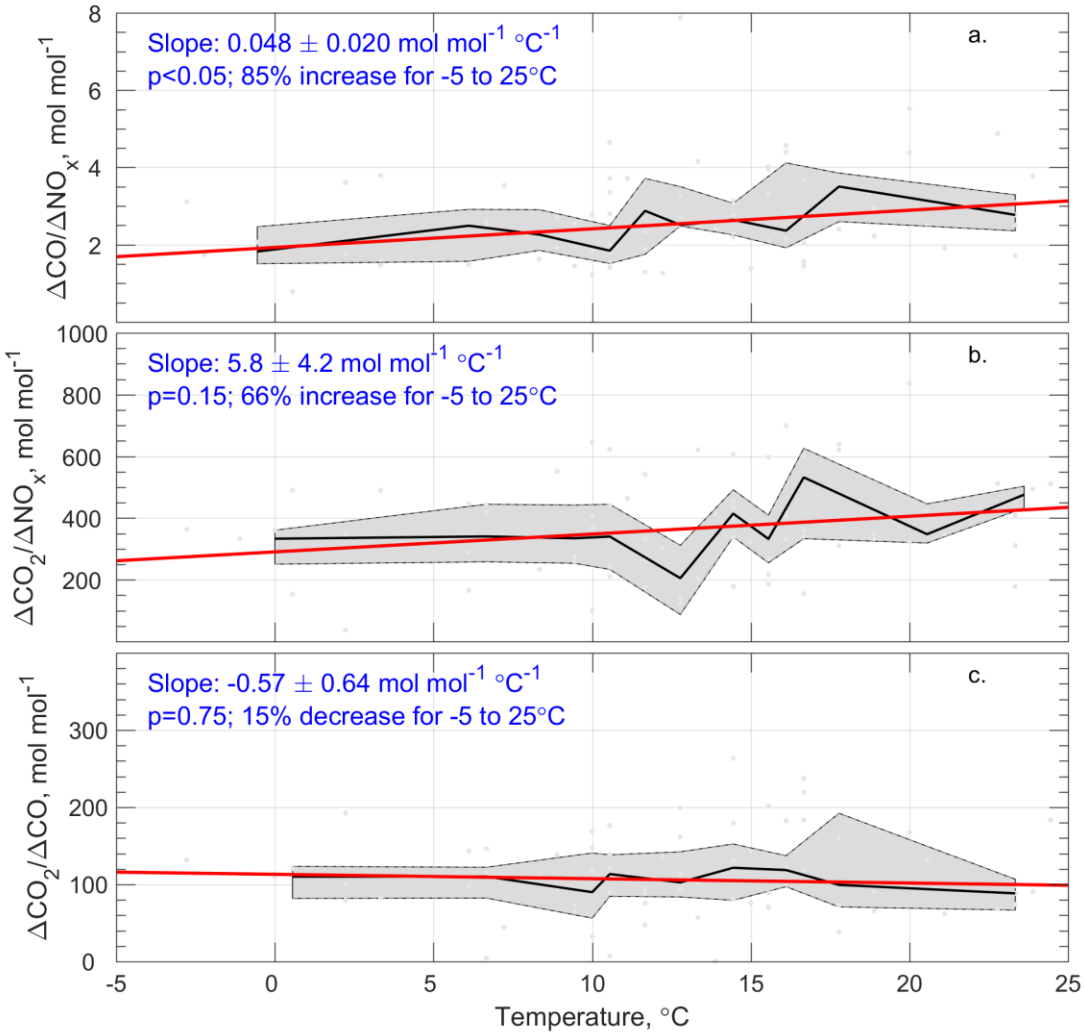

Figure A8. Daily-averaged hourly ΔCO/ΔNO$_x$ (a), ΔCO$_2$/ΔNO$_x$ (b), and ΔCO$_2$/ΔCO (c) for all values of specific humidity shown by the light gray dots, as a function of daily maximum temperature. Hourly emission ratios were estimated from one-minute data collected at the I-95 NR site in Howard County, MD for November 2016 and February, November, and December 2017, then averaged daily. Data were placed into ten bins, each containing an equal number of points. The black lines correspond to the median emission ratios in each bin, bounded by the 25th and 75th percentiles of the bins represented by the light gray lines. The solid red lines represent ordinary, linear least-squares regression fits of the binned median emission ratios. The uncertainty of the slope parameter of each trend was estimated using a Method of Maximum Likelihood, following Bevington and Robinson (2002).

A11. Estimating the temperature dependence on emission ratios from one-minute observations at the I-95 NR site using an alternate technique

In addition to the technique described in Chapter 2 for calculating hourly emission ratios of $\Delta CO/\Delta NO_x$, $\Delta CO_2/\Delta NO_x$, and $\Delta CO_2/\Delta CO$ from one-minute observations, a second method using sets of ten one-minute observations was used for comparison. Linear regression analyses were performed for every ten one-minute observations and emission ratios were estimated by the slope parameters. Only emission ratios from I-95 highway angles (25° to 225°) were used in the analysis. As discussed in Chapter 2, $\Delta CO/\Delta NO_x$ and $\Delta CO_2/\Delta NO_x$ exhibit an increase with rising temperature, while $\Delta CO_2/\Delta CO$ does not show a discernible trend.

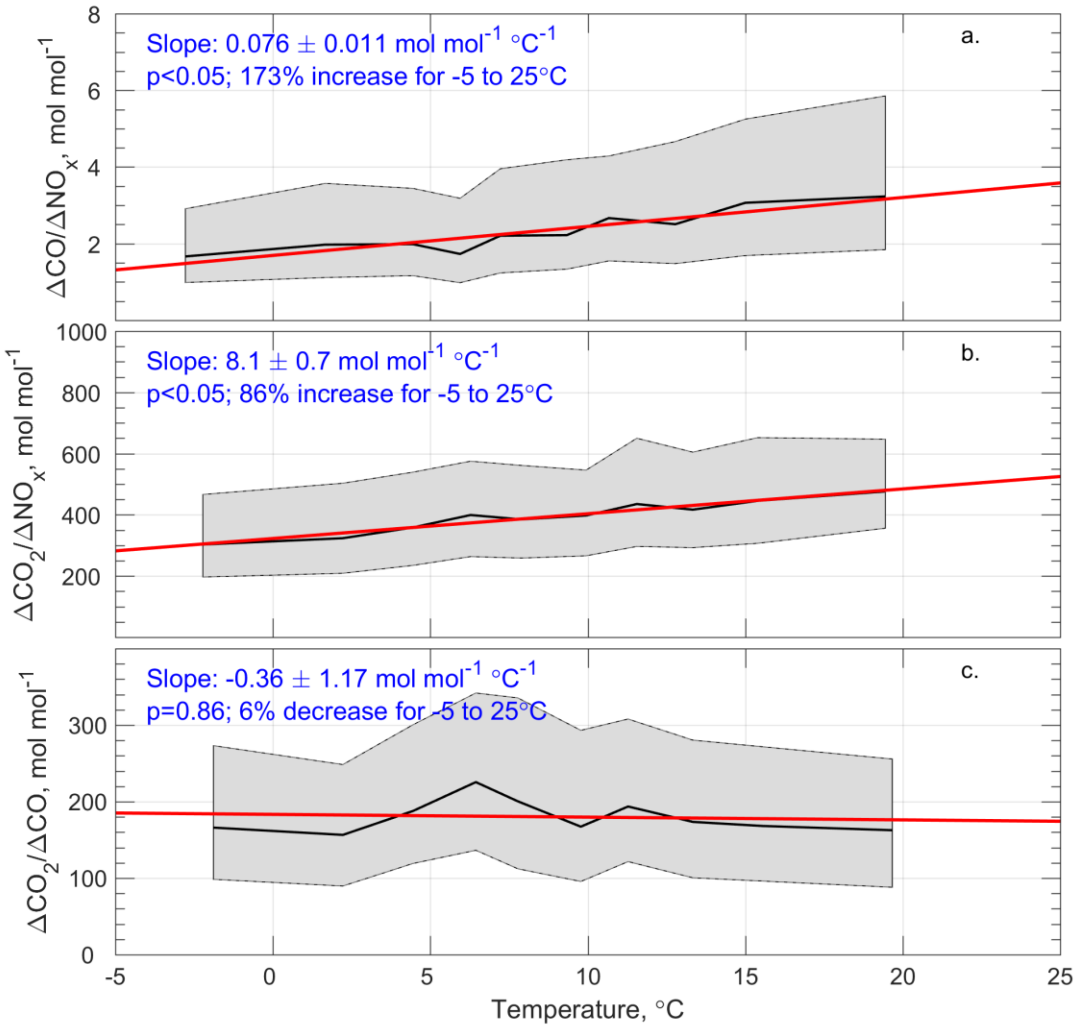

Figure A9. $\Delta CO/\Delta NO_x$ (a), $\Delta CO_2/\Delta NO_x$ (b), and $\Delta CO_2/\Delta CO$ (c) estimated from the slope parameters of linear regressions for every ten one-minute observations as a function of the average temperature of each corresponding ten one-minute set. Observations of CO, NO_x, CO_2, and meteorological variables were collected from November 1, 2016 through February 28, 2017 and November 1, 2017 through December 31, 2017 at the I-95 NR site.

A12. Temperature dependence of ΔCO/ΔNO$_x$ using various methods of estimating the background in calculating hourly emission ratios at I-95 near-road site

Three different methods of calculating background concentrations of [CO] and [NO_x] were used to estimate $\Delta CO/\Delta NO_x$ at the I-95 NR site to test for the sensitivity of the temperature trends to the method of background determination. In the first method, the background was calculated as the 5th percentiles of hourly [CO] and [NO_x] for November 1, 2016 through February 28, 2017 and November 1, 2017 through December 31, 2017. In the second method, averaged [CO] and [NO_x] from wind directions 270° to 330° (not intersecting the highway) represented the background. In the third, a geometric mean fit was found for a scatterplot of [CO] and [NO_x], where the background [NO_x] was the minimum [NO_x] for the entire time period and the background [CO] was the y-value of the best-fit line at the minimum [NO_x]. The background [CO] used in each method was 192 ppb (5th percentile), 193 ppb (upwind method), and 150 ppb (scatterplot method). The background [NO_x] used was 19 ppb (5th percentile), 15 ppb (upwind method), and 4.5 ppb (scatterplot method). These background values were then subtracted from each value of [CO] or [NO_x] and the emission ratio estimated by the ratio of their differences ($\Delta CO/\Delta NO_x$). These hourly emission ratios were placed into ten bins, each bin containing an equal number of data points, and the median, 25th, and 75th percentiles calculated for each bin and plotted in Figure A10. The average trend in emission ratio with temperature between the three methods was 0.10±0.017 mol mol^{-1} °C^{-1}, similar in magnitude to the slope calculated in Chapter 2.

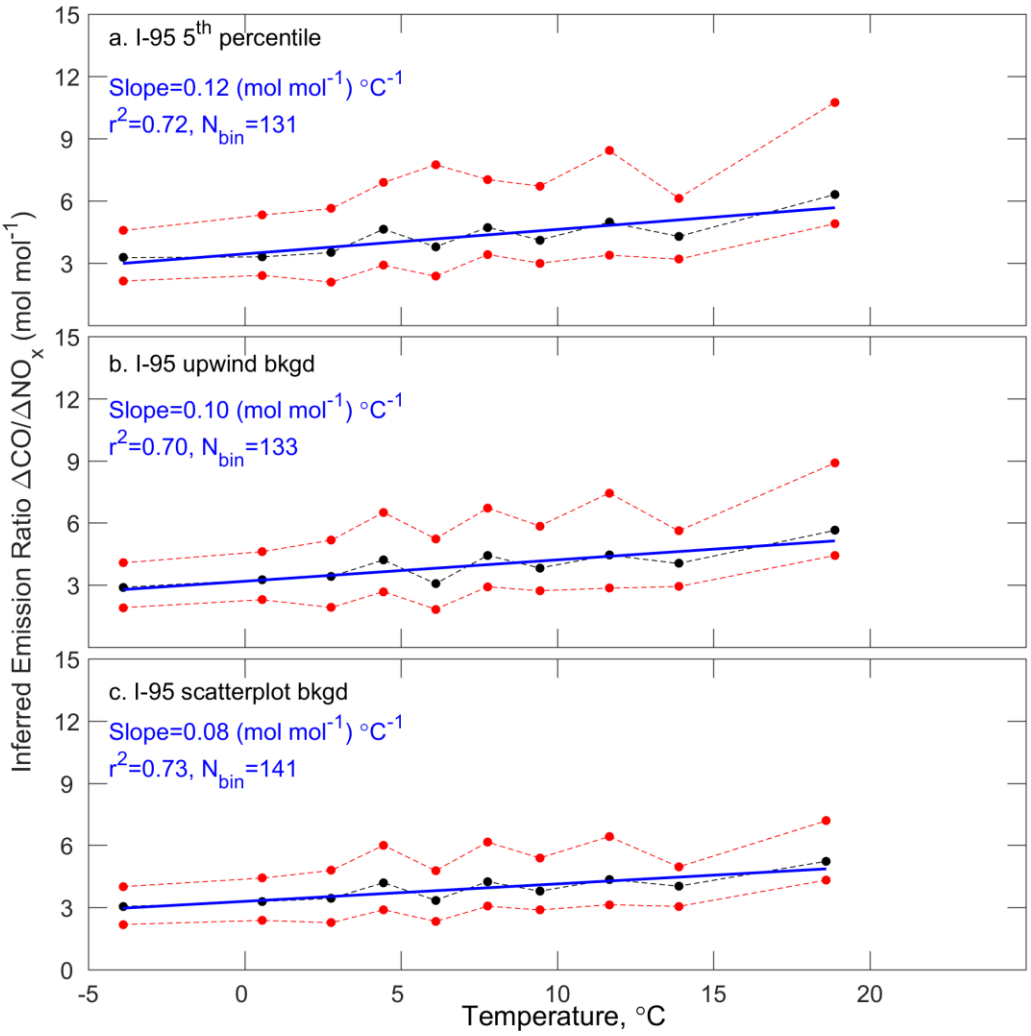

Figure A10. Binned $\Delta CO/\Delta NO_x$ as a function of temperature at the I-95 NR site for November 1, 2016 through February 28, 2017 and November 1, 2017 through December 31, 2017 using three different background methods to calculate emissions. The black line represents the median of ten bins, each containing an equal number of points, while the lower red line represents the 25th percentiles and the upper red line the 75th percentiles. The median was fit with an ordinary least-squares regression that is shown by the blue line.

In addition to the three background methods discussed above, we also used a background site located ten km south/southwest of the I-95 NR site in determining the hourly $\Delta CO/\Delta NO_x$ at the NR site. Hourly [CO] and [NO_x] measured at the Beltsville site were subtracted from those measured at the NR site to determine the

enhancement of [CO] and [NO_x] (i.e., $\Delta CO = CO_{I\text{-}95NR} - CO_{Beltsville}$ and $\Delta NO_x = NO_{x,I\text{-}95NR} - NO_{x,Beltsville}$). The ratio of these enhancements, $\Delta CO/\Delta NO_x$, were divided into ten bins, each containing an equal number of points, that were sorted by ascending ambient temperature and plotted as a function of temperature (Figure A11). The slope of $\Delta CO/\Delta NO_x$ as a function of temperature using the Beltsville site as a background was 0.09 (mol mol^{-1}) $°C^{-1}$, similar to the slope values shown in Figure A10.

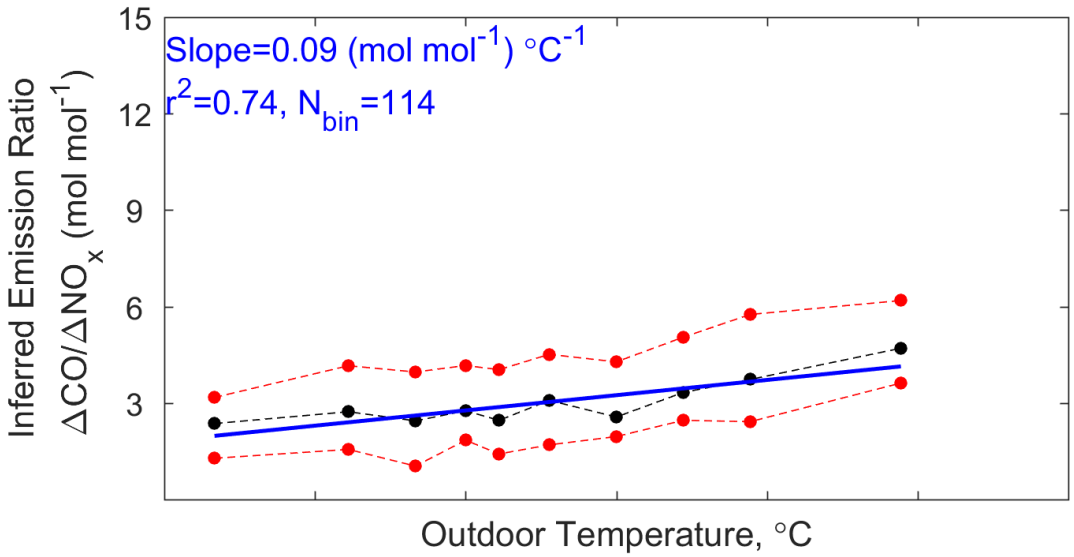

Figure A11. Binned $\Delta CO/\Delta NO_x$ as a function of temperature at the I-95 NR site for November 1, 2016 through February 28, 2017 and November 1, 2017 through December 31, 2017. The hourly emission ratios were calculated by subtracting the hourly concentrations of CO and NO_x at a background site in Beltsville, MD from those at the I-95 NR site to yield hourly values of CO and NO_x enhancement at the NR site. The black line represents the median of ten equal-sized bins, while the lower red line represents the 25th percentiles and the upper red line the 75th percentiles. The median values were fit with an ordinary least-squares regression that is shown by the blue line.

A13. CO production from biogenic oxidation

Recent work by Marvin et al. (2017) has shown that formaldehyde production from isoprene oxidation can be underestimated in the CB05 chemical mechanism used in CMAQ. This result indicates that the CO produced from isoprene oxidation would also be underestimated and may have been partially balanced by an overestimate of anthropogenic CO emissions in the NEI in Anderson et al. (2014), which led to the author's conclusion that the CMAQ modeled CO mixing ratios were in reasonable agreement with the observations (the NEI was 15% higher). This overestimate in CO emissions from the NEI within the BWR has been confirmed by Salmon et al. (2018), who reported that emission rates of CO are a factor of 2 higher in the NEI compared to wintertime aircraft observations. However, vehicular cold-start emissions of CO from the urban area may have impacted this finding by (Salmon et al., 2018) since the study took place in the wintertime.

As shown in Figure A12, CO emissions modeled by MOVES increase at higher temperatures due to a multiplicative A/C factor while NO_x emissions decrease only slightly (11%). This could explain part of an overestimate of CO and NO_x by CMAQ at higher temperatures since the NR observations show a decrease of a factor of two in inferred emissions of NO_x and relatively constant emissions of CO with increasing temperature. In comparison to the NR sites, there still appears to be a large temperature sensitivity of emissions of NO_x that is not captured by MOVES with default settings.

A14. Impacts of excluding slow wind speeds on temperature and humidity sensitivity

Table A2. Slope values of unbinned $\Delta CO/\Delta NO_x$, $\Delta CO_2/\Delta NO_x$, and $\Delta CO_2/\Delta CO$ as a function of temperature (mol mol^{-1} C^{-1}) and specific humidity (mol mol^{-1} $(g_{H2O}$ $kg^{-1})^{-1}$) at the I-95 NR site in Howard County, MD. Hourly wind speed observations of less than 0.5 m s^{-1} were excluded in this experiment. The data have been divided into three Eastern Local Time windows. Values of statistical significance are shown in bold. The percentages of SIV and CIV are indicated in each time window.

Slope as a Function of temperature, mol mol^{-1} $°C^{-1}$	All day 0–23:59 ET 87% SIV 13% CIV	0–4:59 ET 74% SIV 26% CIV	5–10:59 ET 88% SIV 12% CIV	15–20:59 ET 94% SIV 6% CIV
$\Delta CO/\Delta NO_x$	**0.072±0.018 (p<0.05)**	−0.047±0.042 (p=0.60)	**0.048±0.027 (p<0.05)**	0.044±0.042 (p=0.12)
$\Delta CO_2/\Delta NO_x$	**8.7±2.5 (p<0.05)**	**4.9±4.7 (p<0.05)**	**7.6±3.7 (p<0.05)**	7.7±5.3 (p=0.06)
$\Delta CO_2/\Delta CO$	−1.4±0.85 (p=0.15)	1.5±1.5 (p=0.24)	-0.11±0.80 (p=0.85)	−0.95±0.71 (p=0.34)
Slope as a Function of specific humidity, mol mol^{-1} $(g\ kg^{-1})^{-1}$	All day 0–23:59 ET 87% SIV 13% CIV	0–4:59 ET 74% SIV 26% CIV	5–10:59 ET 88% SIV 12% CIV	15–20:59 ET 94% SIV 6% CIV
$\Delta CO/\Delta NO_x$	0.11±0.058 (p=0.28)	0.022±0.10 (p=0.72)	0.097±0.069 (p=0.087)	0.84±0.10 (p=0.35)
$\Delta CO_2/\Delta NO_x$	8.2±4.0 (p=0.11)	−3.7±12 (p=0.47)	9.5±9.6 (p=0.13)	−2.2±12 (p=0.87)
$\Delta CO_2/\Delta CO$	−3.3±1.8 (p=0.15)	0.88±3.9 (p=0.63)	−1.4±2.1 (p=0.86)	−1.0±1.7 (p=0.35)

A15. Estimating I-95 weighted average ΔCO/ΔNO$_x$, ΔCO$_2$/ΔNO$_x$, and ΔCO$_2$/ΔCO from MOVES output as a function of temperature and specific humidity

The weighted average $\Delta CO_2/\Delta NO_x$ and $\Delta CO_2/\Delta CO$ were estimated from MOVES output to reflect traffic at the I-95 site. The contribution of each vehicle type on the weighted average emission rates and ratios was estimated by multiplying the emission rate of a specific vehicle type by a weighting factor, calculated by the product of the fraction of the vehicle type (Table A1) and the NO_x or CO emission rate (mol mile^{-1}) of that vehicle type in MOVES. This ensured that the large contribution of NO_x emissions from combination unit trucks was reflected in the average $\Delta CO_2/\Delta NO_x$ despite these trucks making up only a small fraction of the total number of vehicles passing the site. A similar procedure was followed to calculate the weighted average $\Delta CO/\Delta NO_x$, except an average was taken of $\Delta CO/\Delta NO_x$ weighted by NO_x and CO emissions separately.

A16. Calculating heat index within MOVES

Equation A2. Heat index calculation within MOVES

$$Heat\ Index = -42.378 + 2.04901523 \cdot T + 10.14333127 \cdot RH - 0.22475541 \cdot T \cdot RH - 6.83783 \cdot 0.001 \cdot T^2 - 5.481717 \cdot 0.01 \cdot RH^2 + 1.22874 \cdot 0.001 \cdot T^2 \cdot RH + 8.5282 \cdot 0.0001 \cdot T \cdot RH^2 - 1.99 \cdot 0.000001 \cdot T^2 \cdot RH^2$$

T is temperature in degrees Fahrenheit
RH is the relative humidity in percent
Source: https://www.epa.gov/moves/moves-algorithms

A17. MOVES CO, NO_x, and CO_2 as a function of temperature and specific humidity

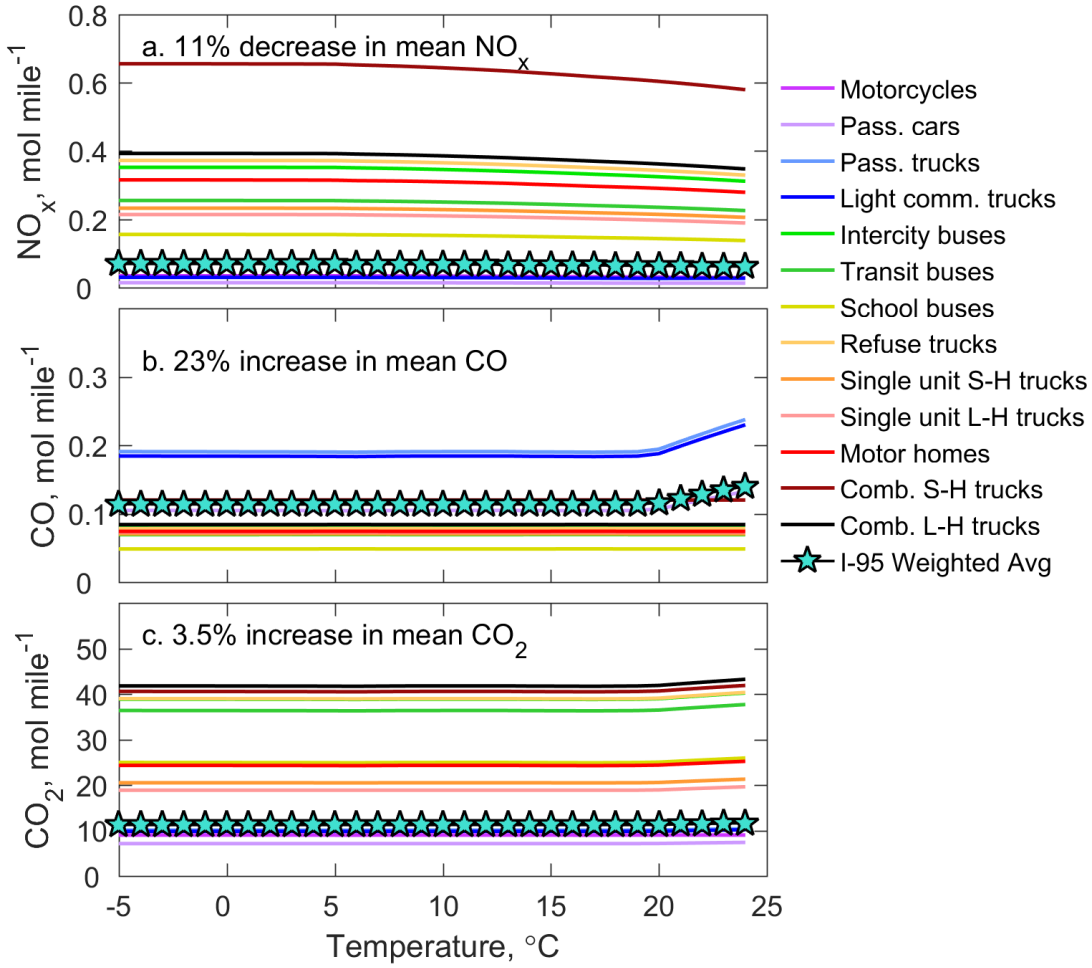

Figure A12. Rates of CO, NO_x, and CO_2 emissions calculated from average emission ratios weighted by vehicle speed and model year from MOVES output for Howard County, MD, using December 2014 input data. Plotted are the emission rates as a function of temperature sorted by vehicle source type for weekdays on rural restricted roads. Each point represents an emission rate at the indicated temperature or the specific humidity calculated from Figure A2, an exponential best-fit of the observed specific humidity values at the I-95 site. Passenger cars, passenger trucks, motorcycles, and light commercial trucks are assumed to run on gasoline (based on county vehicle fuel data), whereas all other vehicle types operate on diesel. Turquoise stars represent a weighted average of each pollutant using I-95 vehicle fractions from traffic counts.

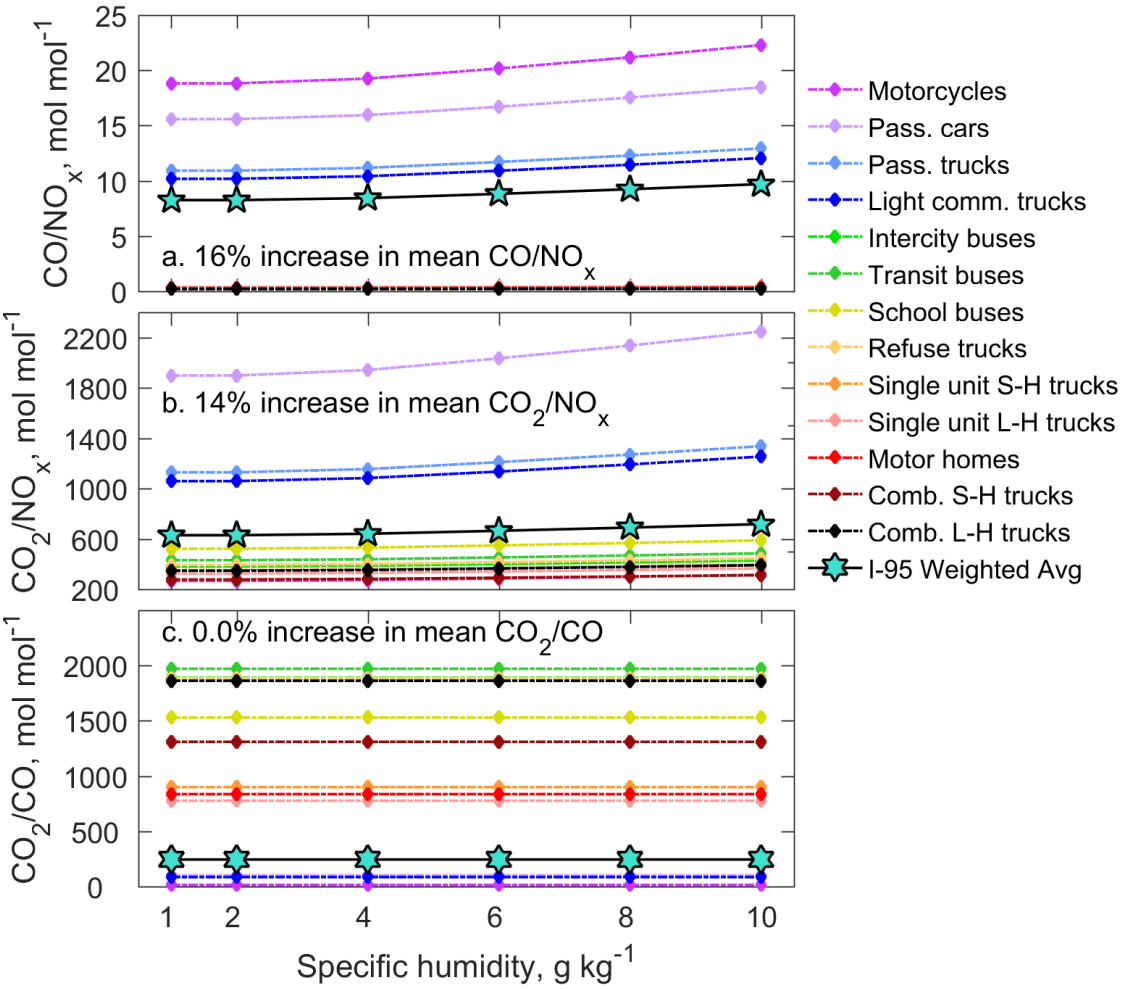

Figure A13. $\Delta CO/\Delta NO_x$, $\Delta CO_2/\Delta NO_x$, and $\Delta CO_2/\Delta CO$ calculated from average emission ratios weighted by vehicle speed and model year from MOVES output for Howard County, MD, using December 2014 input data. Plotted are the emission ratios as a function of specific humidity sorted by vehicle source type for weekdays on rural restricted roads. Each point represents an emission rate averaged over −5°C to 24ºC, similar to the range of temperature seen in the observations. Passenger cars, passenger trucks, motorcycles, and light commercial trucks are assumed to run on gasoline (based on county vehicle fuel data), whereas all other vehicle types operate on diesel. Essentially all vehicles (98%) fall into the categories of passenger cars and trucks and SH plus LH trucks. Turquoise stars represent a weighted average of each pollutant using I-95 vehicle fractions from traffic

Appendix B: Supplemental Information for Chapter 3

B1. I-95 ambient BC and CO abundances by time of day and month

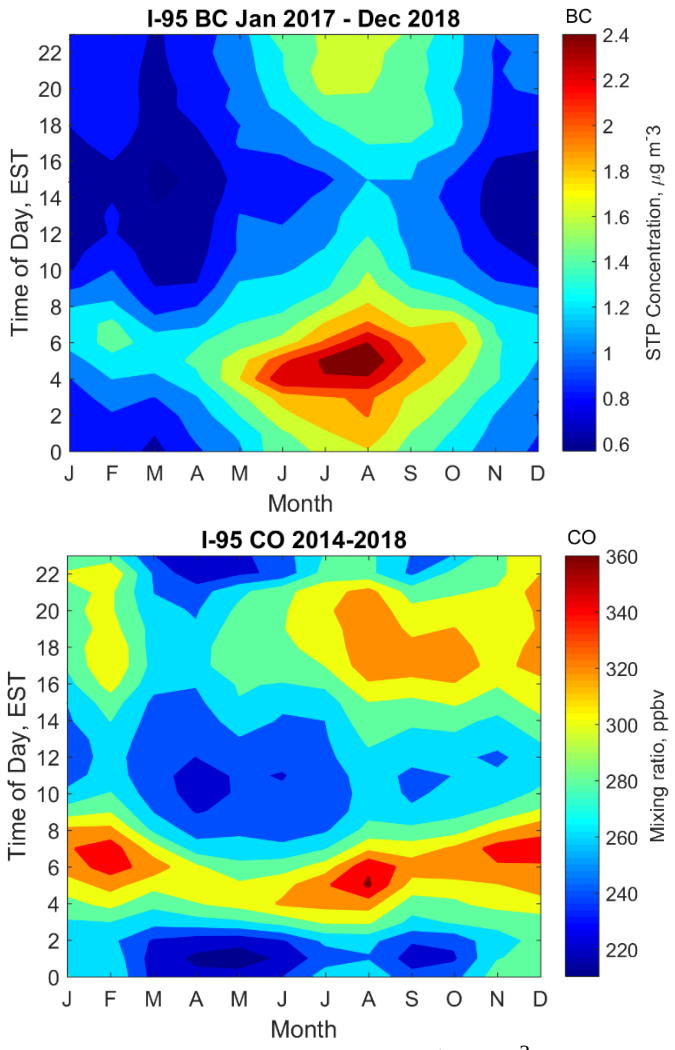

Figure B1. Contrast maps showing ambient BC (μg m^{-3}) and CO (ppbv) abundance measurements collected at the I-95 NR site as a function of time of day and by month, using all available data through December 2018.

Appendix C: Supplemental Information for Chapter 4

C1. Time series of total vehicle counts along I-95

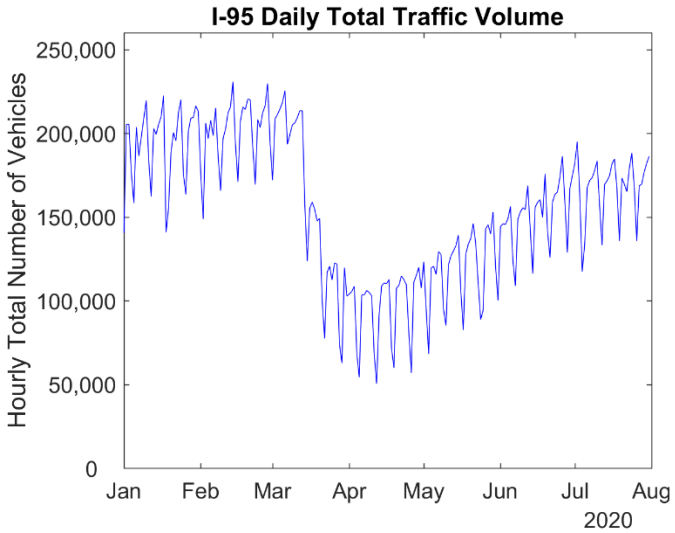

Figure C1. Daily total number of vehicles passing the I-95 NR site in Howard County, MD, from January through July 2020.

Appendix D: Supplemental Information for Chapter 5

D1. Preliminary VOC analysis at I-95 NR site

a. Propene

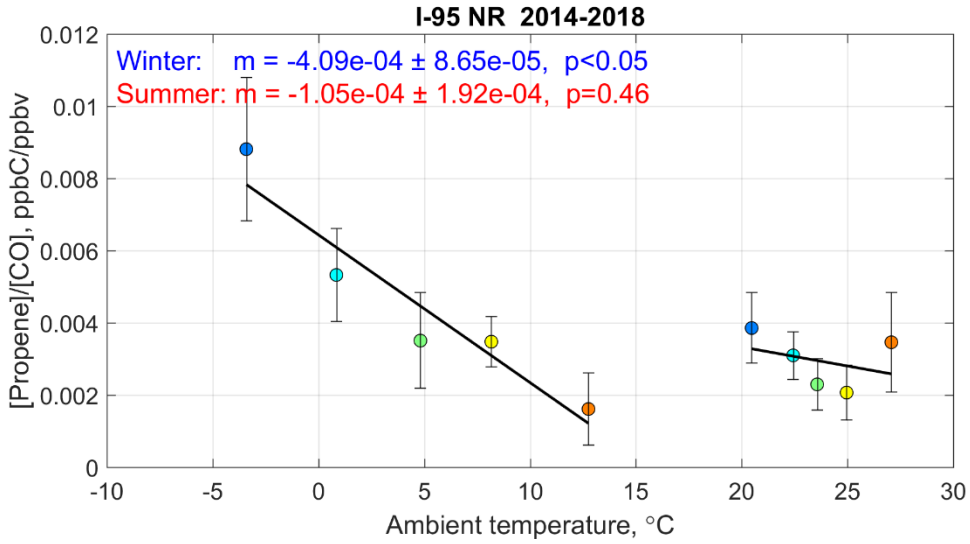

b. Ethene

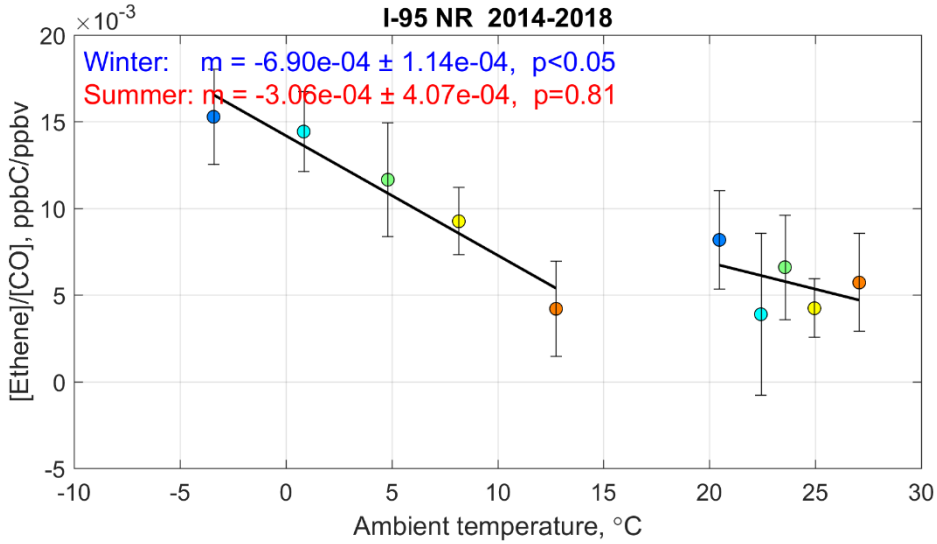

c. 1-Butene

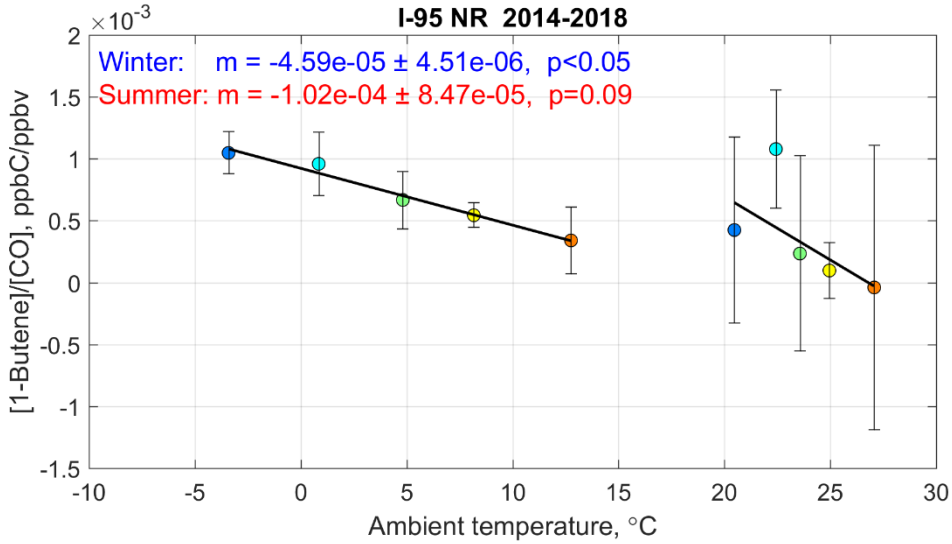

d. Benzene

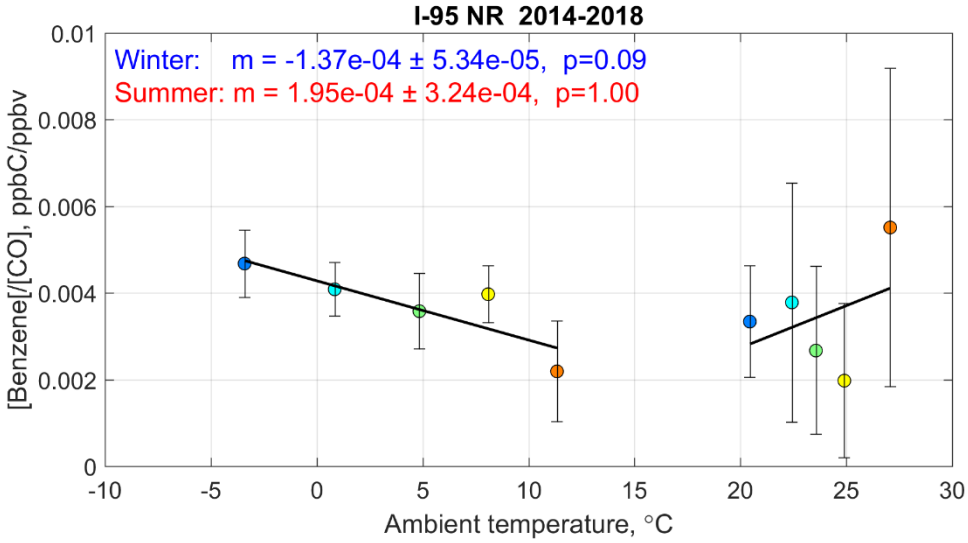

Figure D1. Preliminary analysis of VOC temperature dependence at the I-95 NR site in Maryland. Suppliers change the composition of fuel with ambient temperature. VOC measurements in each season (winter or summer) were sorted into five bins, each containing an equal number of points. The average of each bin is plotted as the filled, round circles, with the bars representing ±1σ from the average. A linear geometric mean regression was fit to the binned values, with the regression parameters in winter and summer provided in the top left corner of each figure.

D2. Vehicular emissions of methane at the I-95 NR site

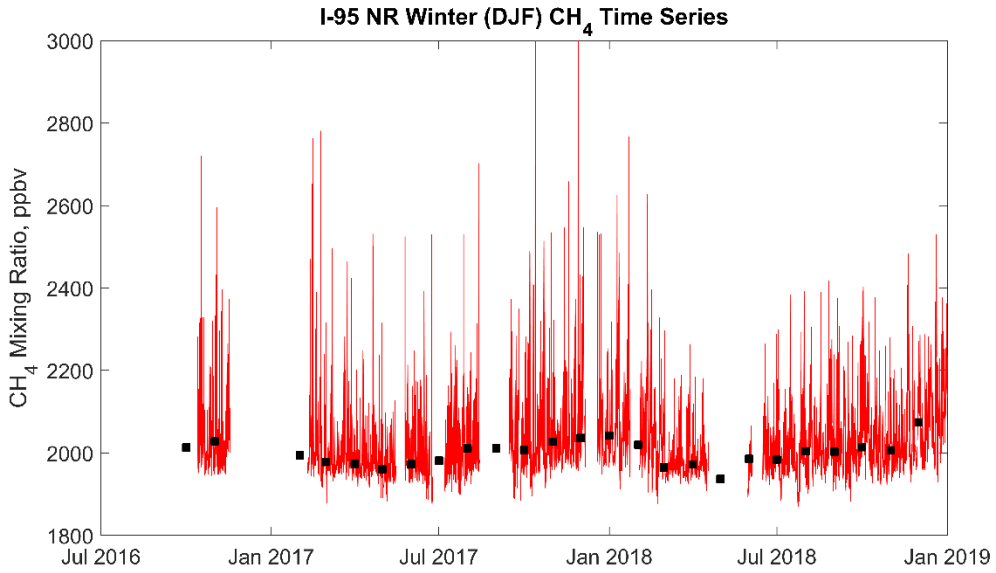

Figure D2. Time series of one-minute CH_4 observations at the I-95 NR site from October 2016 through December 2018. Black squares represent the monthly median values.

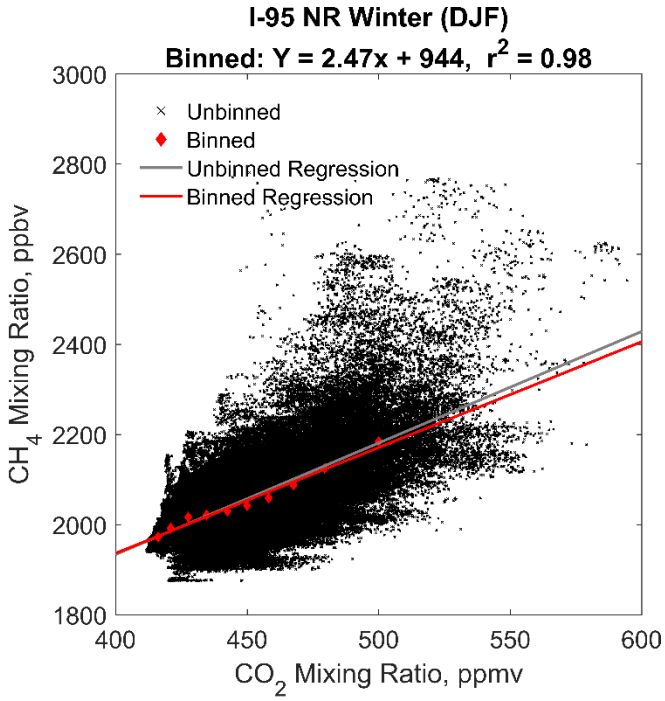

Figure D3. Ambient CH_4 and CO_2 mixing ratios collected at the I-95 NR site during the months of December, January, and February from December 2016 through December 2018. Black points show one-minute observations and red diamonds represent the median binned values after the observations were placed into ten equal-

sized bins. The binned values were fit with an ordinary least-squares regression, shown by the red line.

D3. Vehicular emissions of ethane at the I-95 NR site

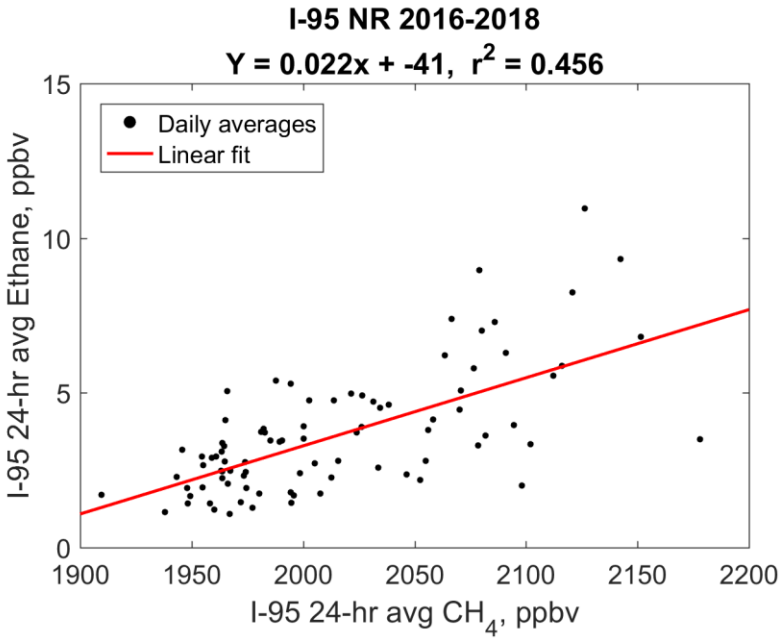

Figure D4. 24-hour average ethane and methane observations collected at the I-95 site from October 2016 through December 2018. Ethane was measured via grab canisters and CH_4 with the LGR analyzer. The flow rate of intake air into the canisters was controlled so that the intake shut off after 24 hours, so that the final measurement represents 24 hours of sampled air. Canisters were replaced at the site ~once per week. The red line represents an ordinary least-squares fit to the daily averages.

D4. MOVES2014b output incorporating a temperature adjustment

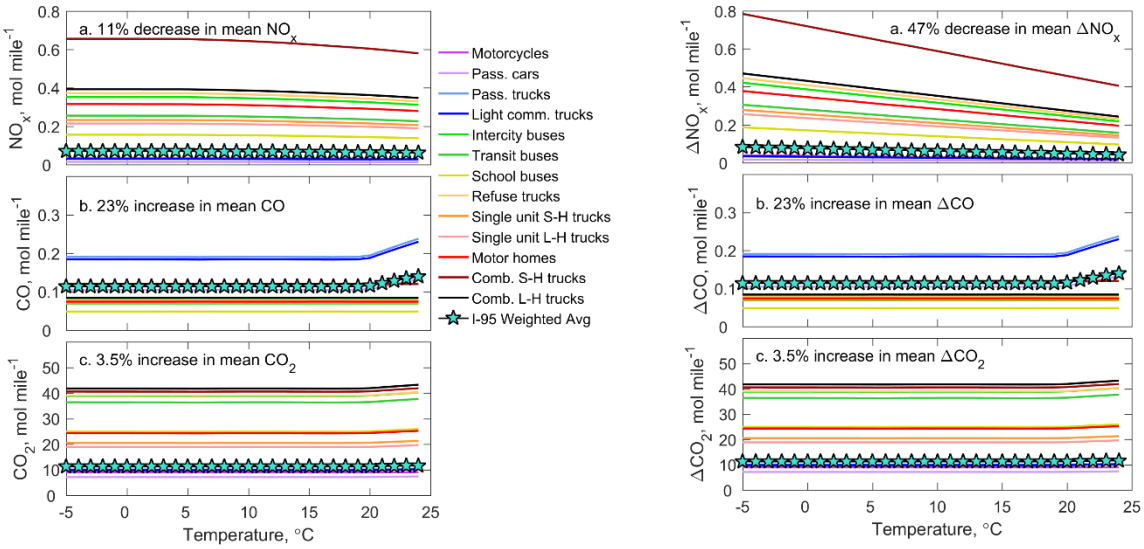

Figure D5. MOVES2014b output for Howard County, MD, with default settings (left) and incorporating a temperature adjustment for NO_x emissions (right), as described in Chapter 5.

D5. Baltimore County, MD, MOVES3 modeling

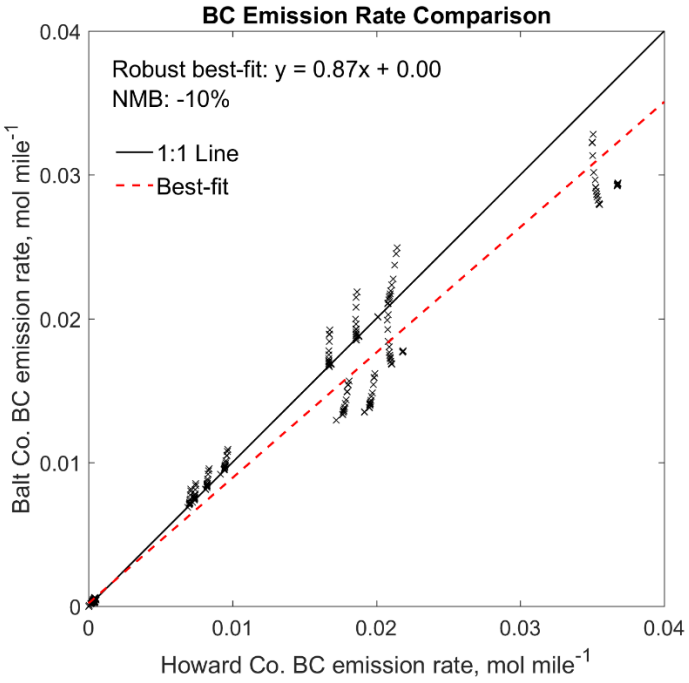

Figure D6. Comparison of wintertime BC emission rates (mol/mile) using Baltimore County and Howard County input data for 2014 supplied by the MOVES team at MDE. The one-to-one line is shown by the solid black line. Emission rates were fit using a robust least-squares regression (dashed red line).

Bibliography

Ammoura, L., Xueref-Remy, I., Vogel, F., Gros, V., Baudic, A., Bonsang, B., Delmotte, M., Té, Y., Chevallier, F., 2016. Exploiting stagnant conditions to derive robust emission ratio estimates for CO_2, CO and volatile organic compounds in Paris. Atmos. Chem. Phys. 16, 15653–15664. https://doi.org/10.5194/acp-16-15653-2016

Anderson, D.C., 2016. Photochemistry and Transport of Tropospheric Ozone and its Precursors in Urban and Remote Environments.

Anderson, D.C., Loughner, C.P., Diskin, G., Weinheimer, A., Canty, T.P., Salawitch, R.J., Worden, H.M., Fried, A., Mikoviny, T., Wisthaler, A., Dickerson, R.R., 2014. Measured and modeled CO and NO_y in DISCOVER-AQ: An evaluation of emissions and chemistry over the eastern US. Atmos. Environ. 96, 78–87. https://doi.org/10.1016/j.atmosenv.2014.07.004

API, T., 2018. Operation Manual Model T200 NO/NO2/NOx Analyzer [WWW Document].

API, T., 2017. Manual Appendum Model T300U CO Analyzer with Auto-Reference [WWW Document]. URL http://www.teledyne-api.com/prod/Downloads/06864D - T300%26T300M Manual.pdf (accessed 1.10.19).

API, T., 2013. Manual Addendum Ultra Sensitivity Model T200U NO/NO_2/NO_x [WWW Document]. URL http://www.teledyne-api.com/prod/Downloads/T200U Manual Addendum - 06861.pdf (accessed 1.10.19).

Appel, W.K., Bhave, P. V., Gilliland, A.B., Sarwar, G., Roselle, S.J., 2008. Evaluation of the community multiscale air quality (CMAQ) model version 4.5: Sensitivities impacting model performance; Part II-particulate matter. Atmos. Environ. 42, 6057–6066. https://doi.org/10.1016/j.atmosenv.2008.03.036

Baer, D.S., Paul, J.B., Gupta, M., O'Keefe, A., 2002. Sensitive absorption measurements in the near-infrared region using off-axis integrated-cavity-output spectroscopy. Appl. Phys. B Lasers Opt. 75, 261–265. https://doi.org/10.1007/s00340-002-0971-z

Ban-Weiss, G.A., McLaughlin, J.P., Harley, R.A., Lunden, M.M., Kirchstetter, T.W., Kean, A.J., Strawa, A.W., Stevenson, E.D., Kendall, G.R., 2008. Long-term changes in emissions of nitrogen oxides and particulate matter from on-road gasoline and diesel vehicles. Atmos. Environ. 42, 220–232. https://doi.org/https://doi.org/10.1016/j.atmosenv.2007.09.049

Barone, T., Storey, J., Domingo, N., 2010. An Analysis of Field-Aged Diesel

Particulate Filter Performance: Particle Emissions before, during, and after Regeneration. J. Air Waste Manage. Assoc. 60, 968–976. https://doi.org/10.3155/1047-3289.60.8.968

Bellucci, P., Cipriani, E., 2010. Data accuracy on automatic traffic counting: the SMART project results. Eur. Transp. Res. Rev. 2, 175–187. https://doi.org/10.1007/s12544-010-0039-9

Bevington, P.R., Robinson, D.K., 2002. Least-Squares Fit to a Straight Line, in: Data Reduction and Error Analysis for the Physical Sciences. McGraw-Hill Education - Europe.

Bishop, G.A., Stedman, D.H., 2008. A decade of on-road emissions measurements. Environ. Sci. Technol. 42, 1651–1656. https://doi.org/10.1021/es702413b

Book, E.K., Snow, R., Long, T., Fang, T., Baldauf, R., 2015. Temperature effects on particulate emissions from DPF-equipped diesel trucks operating on conventional and biodiesel fuels. J. Air Waste Manage. Assoc. 65, 751–758. https://doi.org/10.1080/10962247.2014.984817

Brent, L.C., Thorn, W.J., Gupta, M., Leen, B., Stehr, J.W., He, H., Arkinson, H.L., Weinheimer, A., Garland, C., Pusede, S.E., Wooldridge, P.J., Cohen, R.C., Dickerson, R.R., 2015. Evaluation of the use of a commercially available cavity ringdown absorption spectrometer for measuring NO_2 in flight, and observations over the Mid-Atlantic States, during DISCOVER-AQ. J. Atmos. Chem. 72, 503–521. https://doi.org/10.1007/s10874-013-9265-6

Briedis, P., Trueman, H., Samuels, S., 2010. The Accuracy of Inductive Loop Detectors, in: 24th Australian Road Research Board Conference. Melbourne, Australia.

Canty, T.P., Hembeck, L., Vinciguerra, T.P., Anderson, D.C., Goldberg, D.L., Carpenter, S.F., Allen, D.J., Loughner, C.P., Salawitch, R.J., Dickerson, R.R., 2015. Ozone and NO_x chemistry in the eastern US: Evaluation of CMAQ/CB05 with satellite (OMI) data. Atmos. Chem. Phys. 15, 10965–10982. https://doi.org/10.5194/acp-15-10965-2015

Castellanos, P., Marufu, L.T., Doddridge, B.G., Taubman, B.F., Schwab, J.J., Hains, J.C., Ehrman, S.H., Dickerson, R.R., 2011. Ozone, oxides of nitrogen, and carbon monoxide during pollution events over the eastern United States: An evaluation of emissions and vertical mixing. J. Geophys. Res. Atmos. 116. https://doi.org/10.1029/2010JD014540

Chan, T.W., Meloche, E., Kubsh, J., Brezny, R., Rosenblatt, D., Rideout, G., 2013. Impact of ambient temperature on gaseous and particle emissions from a direct injection gasoline vehicle and its implications on particle filtration. SAE Tech. Pap. 2, 350–371. https://doi.org/10.4271/2013-01-0527

Chen, A.L.-W., Doddridge, B., Dickerson, R., Chow, J., Mueller, P., Quinn, J., Butler, W., 2001. Seasonal variations in elemental carbon aerosol, carbon monoxide and sulfur dioxide: Implications for sources. Geophys. Res. Lett. 28, 1711–1714.

Choi, D., Beardsley, M., Brzezinski, D., Koupal, J., Warila, J., 2010. MOVES Sensitivity Analysis : The Impacts of Temperature and Humidity on Emissions. 19th Int. Emiss. Invent. Conf. San Antonio, Texas. https://doi.org/23/32/10190 [pii]

Cipollone, R., Di Battista, D., Vittorini, D., 2017. Experimental assessment of engine charge air cooling by a refrigeration unit. Energy Procedia 126, 1067–1074. https://doi.org/https://doi.org/10.1016/j.egypro.2017.08.226

Crawford, J., 2010. DISCOVER-AQ [WWW Document]. URL https://www-air.larc.nasa.gov/missions/discover-aq/docs/Crawford_DISCOVER-AQ_Overview_05Oct2010.pdf

Crutzen, P., 1973. A discussion of the chemistry of some minor constituents in the stratosphere and troposphere. Pure Appl. Geophys. 106, 1385–1399. https://doi.org/10.1007/BF00881092

Crutzen, P.J., 1973. Gas-phase nitrogen and methane chemistry in the atmosphere, in: McCormac, B.M. (Ed.), Physics and Chemistry of Upper Atmosphere. University of Stockholm, Sweden, pp. 110–124.

Crutzen, P.J., Heidt, L.E., Krasnec, J.P., Pollock, W.H., Seiler, W., 1979. Biomass burning as a source of atmospheric gases CO, H_2, N_2O, NO, CH_3Cl and COS. Nature 282, 253–256. https://doi.org/10.1038/282253a0

Dallmann, T.R., Harley, R.A., 2010. Evaluation of mobile source emission trends in the United States. J. Geophys. Res. Atmos. 115, 1–12. https://doi.org/10.1029/2010JD013862

Dallmann, T.R., Kirchstetter, T.W., DeMartini, S.J., Harley, R.A., 2013. Quantifying On-Road Emissions from Gasoline-Powered Motor Vehicles: Accounting for the Presence of Medium- and Heavy-Duty Diesel Trucks. Environ. Sci. Technol. 47, 13873–13881. https://doi.org/10.1021/es402875u

Day, D.A., Wooldridge, P.J., Dillon, M.B., Thornton, J.A., Cohen, R.C., 2002. A thermal dissociation laser-induced fluorescence instrument for in situ detection of NO_2, peroxy nitrates, alkyl nitrates, and HNO_3. J. Geophys. Res. 107. https://doi.org/10.1029/2001JD000779

de Nevers, N., 2010. Air Pollution Control Engineering, Second. ed. Waveland Press, Long Grove, Illinois.

Dickerson, R.R., Anderson, D.C., Ren, X., 2019. On the use of data from commercial NO_x analyzers for air pollution studies. Atmos. Environ. 214. https://doi.org/10.1016/j.atmosenv.2019.116873

Du, J., Rakha, H.A., Filali, F., Eldardiry, H., 2021. COVID-19 pandemic impacts on traffic system delay, fuel consumption and emissions. Int. J. Transp. Sci. Technol. 10, 184–196. https://doi.org/https://doi.org/10.1016/j.ijtst.2020.11.003

Duncan, B.N., Yoshida, Y., Olson, J.R., Sillman, S., Martin, R. V., Lamsal, L., Hu, Y., Pickering, K.E., Retscher, C., Allen, D.J., Crawford, J.H., 2010. Application of OMI observations to a space-based indicator of NO_x and VOC controls on surface ozone formation. Atmos. Environ. 44, 2213–2223. https://doi.org/10.1016/j.atmosenv.2010.03.010

Dunlea, E.J., Herndon, S.C., Nelson, D.D., Volkamer, R.M., San Martini, F., Sheehy, P.M., Zahniser, M.S., Shorter, J.H., Wormhoudt, J.C., Lamb, B.K., Allwine, E.J., Gaffney, J.S., Marley, N. a., Grutter, M., Marquez, C., Blanco, S., Cardenas, B., Retama, A., Ramos Villegas, C.R., Kolb, C.E., Molina, L.T., Molina, M.J., 2007. Evaluation of nitrogen dioxide chemiluminescence monitors in a polluted urban environment. Atmos. Chem. Phys. 7, 2691–2704. https://doi.org/10.5194/acp-7-2691-2007

Farmer, D.K., Wooldridge, P.J., Cohen, R.C., 2006. Application of thermal-dissociation laser induced fluorescence (TD-LIF) to measurement of HNO_3, Σalkyl nitrates, Σperoxy nitrates, and NO_2 fluxes using eddy covariance. Atmos. Chem. Phys. 6, 3471–3486. https://doi.org/10.5194/acp-6-3471-2006

Fehsenfeld, F.C., Dickerson, R.R., Hübler, G., Luke, W.T., Nunnermacker, L.J., Williams, E.J., Roberts, J.M., Calvert, J.G., Curran, C.M., Delany, A.C., Eubank, C.S., Fahey, D.W., Fried, A., Gandrud, B.W., Langford, A.O., Murphy, P.C., Norton, R.B., Pickering, K.E., Ridley, B.A., 1987. A Ground-Based Intercomparison of NO, NO_x, and NO_y Measurement Techniques. J. Geophys. Res. 92, 14710–14722. https://doi.org/10.1029/JD092iD12p14710

Fontijn, A., Sabadell, A.J., Ronco, R.J., 1970. Homogeneous chemiluminescent measurement of nitric oxide with ozone. Implications for continuous selective monitoring of gaseous air pollutants. Anal. Chem. 42, 575–579. https://doi.org/10.1021/ac60288a034

Fujita, E.M., Campbell, D.E., Zielinska, B., Chow, J.C., Lindhjem, C.E., DenBleyker, A., Bishop, G.A., Schuchmann, B.G., Stedman, D.H., Lawson, D.R., 2012. Comparison of the MOVES2010a, MOBILE6.2, and EMFAC2007 mobile source emission models with on-road traffic tunnel and remote sensing measurements. J. Air Waste Manag. Assoc. 62, 1134–1149. https://doi.org/10.1080/10962247.2012.699016

Georgia Department of Transportation, 1995. Accuracy of Traffic Monitoring Equipment: Chapter 8.

Ghazikhani, M., Ebrahim, M., Mahian, O., Sabazadeh, A., 2013. Effects of Altitude on the Soot Emission and Fuel Consumption of a Light-Duty Diesel Engine 28. https://doi.org/10.3846/16484142.2013.798743

Giakoumis, E.G., Zachiotis, A.T., 2021. A comprehensive comparative investigation of a heavy-duty vehicle's performance, consumption and emissions during eight driving cycles. Int. J. Ambient Energy 42, 29–45. https://doi.org/10.1080/01430750.2018.1525578

Gilbert, R.O., 1987. Statistical Methods for Environmental Pollution Monitoring. Van Nostrand Reinhold, New York.

Goldberg, D.L., Vinciguerra, T.P., Anderson, D.C., Hembeck, L., Canty, T.P., Ehrman, S.H., Martins, D.K., Stauffer, R.M., Thompson, A.M., Salawitch, R.J., Dickerson, R.R., 2016. CAMx ozone source attribution in the eastern United States using guidance from observations during DISCOVER-AQ Maryland. Geophys. Res. Lett. 43, 2249–2258. https://doi.org/10.1002/2015GL067332

Grange, S.K., Farren, N.J., Vaughan, A.R., Rose, R.A., Carslaw, D.C., 2019. Strong Temperature Dependence for Light-Duty Diesel Vehicle NO_x Emissions. Environ. Sci. Technol. 53, 6587–6596. https://doi.org/10.1021/acs.est.9b01024

Grieshop, A., Lipsky, E., Pekney, N., Takahama, S., Robinson, A., 2006. Fine particle emission factors from vehicles in a highway tunnel: Effects of fleet composition and season. Atmos. Environ. 40, 287–298. https://doi.org/10.1016/j.atmosenv.2006.03.064

Grimes, C.D., Dickerson, R.R., 2021. Evaluation of a filter-based black carbon (BC) instrument using a brown carbon (BrC) surrogate as well as pure and coated BC surrogates. Aerosol Sci. Technol. 55, 501–511. https://doi.org/10.1080/02786826.2021.1878096

Haagen-Smit, A.J., Bradley, C.E., Fox, M.M., 1953. Ozone Formation in Photochemical Oxidation of Organic Substances. Ind. Eng. Chem. 45, 2086–2089. https://doi.org/10.1021/ie50525a044

Hall, D.L., Anderson, D.C., Martin, C.R., Ren, X., Salawitch, R.J., He, H., Canty, T.P., Hains, J.C., Dickerson, R.R., 2020. Using near-road observations of CO, NO_y, and CO_2 to investigate emissions from vehicles: Evidence for an impact of ambient temperature and specific humidity. Atmos. Environ. 232, 117558. https://doi.org/10.1016/j.atmosenv.2020.117558

Harkins, C., McDonald, B.C., Henze, D.K., Wiedinmyer, C., 2021. A fuel-based method for updating mobile source emissions during the COVID-19 pandemic.

Environ. Res. Lett. 16. https://doi.org/10.1088/1748-9326/ac0660

Hassler, B., McDonald, B.C., Frost, G.J., Borbon, A., Carslaw, D.C., Civerolo, K., Granier, C., Monks, P.S., Monks, S., Parrish, D.D., Pollack, I.B., Rosenlof, K.H., Ryerson, T.B., Schneidemesser, E. von, Trainer, M., 2016. Analysis of long-term observations of NO_x and CO in megacities and application to constraining emissions inventories. Geophys. Res. Lett. 43, 9920–9930. https://doi.org/10.1002/2016GL069894

He, Hao, Hembeck, L., Hosley, K.M., Canty, T.P., Salawitch, R.J., Dickerson, R.R., 2013. High ozone concentrations on hot days: The role of electric power demand and NO_x emissions. Geophys. Res. Lett. 40, 5291–5294. https://doi.org/10.1002/grl.50967

He, H., Stehr, J.W., Hains, J.C., Krask, D.J., Doddridge, B.G., Vinnikov, K.Y., Canty, T.P., Hosley, K.M., Salawitch, R.J., Worden, H.M., Dickerson, R.R., 2013. Trends in emissions and concentrations of air pollutants in the lower troposphere in the Baltimore/Washington airshed from 1997 to 2011. Atmos. Chem. Phys. 13, 7859–7874. https://doi.org/10.5194/acp-13-7859-2013

Hickman, J., Hassel, D., Joumard, R., Samaras, Z., Sorenson, S., 1999. Methodology for Calculating Transport Emissions and Energy Consumption.

Huang, Y., Surawski, N.C., Zhuang, Y., Zhou, J.L., Hong, G., 2021. Dual injection: An effective and efficient technology to use renewable fuels in spark ignition engines. Renew. Sustain. Energy Rev. 143, 110921. https://doi.org/https://doi.org/10.1016/j.rser.2021.110921

Hudda, N., Simon, M.C., Patton, A.P., Durant, J.L., 2020. Reductions in traffic-related black carbon and ultrafine particle number concentrations in an urban neighborhood during the COVID-19 pandemic. Sci. Total Environ. 742. https://doi.org/https://doi.org/10.1016/j.scitotenv.2020.140931

Joshi, A., James, S., Meckl, P., King, G., Laboratories, R., Jennings, K., 2009. Assessment of Charge-Air Cooler Health in Diesel Engines Using Nonlinear Time Series Analysis of Intake Manifold Temperature. J. Dyn. Syst. Meas. Control 131. https://doi.org/10.1115/1.3023142

Kendall, M.G., 1975. Rank Correlation Methods. Charles Griffin, London.

Kim, E., Hopke, P.K., 2012. Source Apportionment of Fine Particles in Washington, DC, Utilizing Temperature-Resolved Carbon Fractions. J. Air Waste Manage. Assoc. 54, 773–785. https://doi.org/10.1080/10473289.2004.10470948

Ko, J., Myung, C.L., Park, S., 2019. Impacts of ambient temperature, DPF regeneration, and traffic congestion on NO_x emissions from a Euro 6-compliant diesel vehicle equipped with an LNT under real-world driving conditions.

Atmos. Environ. 200, 1–14. https://doi.org/10.1016/j.atmosenv.2018.11.029

Kondo, Y., Komazaki, Y., Miyazaki, Y., Moteki, N., Takegawa, N., Kodama, D., Deguchi, S., Nogami, M., Fukuda, M., Miyakawa, T., Morino, Y., Koike, M., Sakurai, H., Ehara, K., 2006. Temporal variations of elemental carbon in Tokyo. J. Geophys. Res. 111. https://doi.org/https://doi.org/10.1029/2005JD006257

Kota, S.H., Zhang, H., Chen, G., Schade, G.W., Ying, Q., 2014. Evaluation of on-road vehicle CO and NOx national emission inventories using an urban-scale source-oriented air quality model. Atmos. Environ. 85, 99–108. https://doi.org/10.1016/j.atmosenv.2013.11.020

Krotkov, N.A., McLinden, C.A., Li, C., Lamsal, L.N., Celarier, E.A., Marchenko, S. V., Swartz, W.H., Bucsela, E.J., Joiner, J., Duncan, B.N., Folkert Boersma, K., Pepijn Veefkind, J., Levelt, P.F., Fioletov, V.E., Dickerson, R.R., He, H., Lu, Z., Streets, D.G., 2016. Aura OMI observations of regional SO_2 and NO_2 pollution changes from 2005 to 2015. Atmos. Chem. Phys. 16, 4605–4629. https://doi.org/10.5194/acp-16-4605-2016

Li, J., Mao, J., Fiore, A.M., Cohen, R.C., Crounse, J.D., Teng, A.P., Wennberg, P.O., Lee, B.H., Lopez-Hilfiker, F.D., Thornton, J.A., Peischl, J., Pollack, I.B., Ryerson, T.B., Veres, P., Roberts, J.M., Neuman, J.A., Nowak, J.B., Wolfe, G.M., Hanisco, T.F., Fried, A., Singh, H.B., Dibb, J., Paulot, F., Horowitz, L.W., 2018. Decadal changes in summertime reactive oxidized nitrogen and surface ozone over the Southeast United States. Atmos. Chem. Phys. 18, 2341–2361. https://doi.org/10.5194/acp-18-2341-2018

Li, P., Lü, L., 2021. Research on a China 6b heavy-duty diesel vehicle real-world engine out NOx emission deterioration and ambient correction using big data approach. Environ. Sci. Pollut. Res. Int. https://doi.org/10.1007/s11356-021-15778-2

Los Gatos Research, 2018. Greenhouse Gas Analyzer Data Sheet [WWW Document]. URL http://www.lgrinc.com/documents/LGR_FGGA_Datasheet - 20180101.pdf (accessed 1.4.21).

Los Gatos Research, 2013. Greenhouse Gas Analyzer and Fast Greenhouse Gas Analyzer Rackmount – Enhanced Performance User Manual.

Lyu, Y., Olofsson, U., 2020. On black carbon emission from automotive disc brakes. J. Aerosol Sci. 148, 105610. https://doi.org/https://doi.org/10.1016/j.jaerosci.2020.105610

Magee Scientific, 2018. Aethalometer Model AE33 User Manual.

Mann, H.B., 1945. Nonparametric Tests Against Trend. Econometrica 13, 245–259.

Mao, J., Carlton, A., Cohen, R.C., Brune, W.H., Brown, S.S., Wolfe, G.M., Jimenez, J.L., Pye, H.O.T., Lee Ng, N., Xu, L., McNeill, V.F., Tsigaridis, K., McDonald, B.C., Warneke, C., Guenther, A., Alvarado, M.J., de Gouw, J., Mickley, L.J., Leibensperger, E.M., Mathur, R., Nolte, C.G., Portmann, R.W., Unger, N., Tosca, M., Horowitz, L.W., 2018. Southeast Atmosphere Studies: learning from model-observation syntheses. Atmos. Chem. Phys. 18, 2615–2651. https://doi.org/10.5194/acp-18-2615-2018

Martin, C.R., Zeng, N., Karion, A., Dickerson, R.R., Ren, X., Turpie, B.N., Weber, K.J., 2017. Evaluation and environmental correction of ambient CO_2 measurements from a low-cost NDIR sensor. Atmos. Meas. Tech. 10, 2383–2395. https://doi.org/10.5194/amt-10-2383-2017

Marvin, M.R., Wolfe, G.M., Salawitch, R.J., Canty, T.P., Roberts, S.J., Travis, K.R., Aikin, K.C., de Gouw, J.A., Graus, M., Hanisco, T.F., Holloway, J.S., Hubler, G., Kaiser, J., Keutsch, F.N., Peischl, J., Pollack, I.B., Roberts, J.M., Ryerson, T.B., Veres, P.R., Warneke, C., 2017. Impact of evolving isoprene mechanisms on simulated formaldehyde: An inter-comparison supported by in situ observations from SENEX. Atmos. Environ. 164, 325–336. https://doi.org/10.1016/j.atmosenv.2017.05.049

McDonald, B.C., Dallmann, T.R., Martin, E.W., Harley, R.A., 2012. Long-term trends in nitrogen oxide emissions from motor vehicles at national, state, and air basin scales. J. Geophys. Res. 117. https://doi.org/10.1029/2012JD018304

McDonald, B.C., McKeen, S.A., Cui, Y.Y., Ahmadov, R., Kim, S.-W., Frost, G.J., Pollack, I.B., Peischl, J., Ryerson, T.B., Holloway, J.S., Graus, M., Warneke, C., Gilman, J.B., de Gouw, J.A., Kaiser, J., Keutsch, F.N., Hanisco, T.F., Wolfe, G.W., Trainer, M., 2018. Modeling Ozone in the Eastern U.S. using a Fuel-Based Mobile Source Emissions Inventory. Environ. Sci. Technol. 52, 7360–7370.

Miyoshi, A., Washida, S.H.N., 1994. OH radical- initiated photooxidation of isoprene: An estimate of global CO production. J. Geophys. Res. 99, 18779–18787.

Ng, N.L., Kroll, J.H., Chan, A.W.H., Chhabra, P.S., Flagan, R.C., Seinfeld, J.H., 2007. Secondary organic aerosol formation from m-xylene, toluene, and benzene. Atmos. Chem. Phys. 7, 3909–3922. https://doi.org/10.5194/acp-7-3909-2007

O'Driscoll, R., Stettler, M., Molden, N., Oxley, T., Apsimon, H., 2017. Real world CO_2 and NO_x emissions from 149 Euro 5 and 6 diesel, gasoline and hybrid passenger cars. Sci. Total Environ. 621, 282–290. https://doi.org/10.1016/j.scitotenv.2017.11.271

OECD, ECMT, 2006. Speed Management.

Olson, M.R., Victoria Garcia, M., Robinson, M.A., Van Rooy, P., Dietenberger, M.A., Bergin, M., Schauer, J.J., 2015. Investigation of black and brown carbon multiple-wavelength-dependent light absorption from biomass and fossil fuel combustion source emissions. J. Geophys. Res. Atmos. 120, 6682–6697. https://doi.org/https://doi.org/10.1002/2014JD022970

Park, S.S., Kozawa, K., Fruin, S., Mara, S., Hsu, Y.-K., Jakober, C., Winer, A., Herner, J., 2011. Emission Factors for High-Emitting Vehicles Based on On-Road Measurements of Individual Vehicle Exhaust with a Mobile Measurement Platform. J. Air Waste Manage. Assoc. 61, 1046–1056. https://doi.org/10.1080/10473289.2011.595981

Parrish, D.D., Lamarque, J.F., Naik, V., Horowitz, L., Shindell, D.T., Staehelin, J., Derwent, R., Cooper, O.R., Tanimoto, H., Volz-Thomas, A., Gilge, S., Scheel, H.E., Steinbacher, M., Fröhlich, M., 2014. Long-term changes in lower tropospheric baseline ozone concentrations: Comparing chemistry-climate models and observations at northern midlatitudes. J. Geophys. Res. Atmos. 119, 5719–5736. https://doi.org/10.1002/2013JD021435

Picarro, 2019. Picarro CO_2, CH_4, H_2O Data Sheet.

Prati, M.V., Costagliola, M.A., Zuccheroso, A., Napolitano, P., 2019. Assessment of Euro 5 diesel vehicle NO_x emissions by laboratory and track testing. Environ. Sci. Pollut. Res. 26, 10576–10586. https://doi.org/10.1007/s11356-019-04486-7

Preble, C. V., Harley, R.A., Kirchstetter, T.W., 2019. Control Technology-Driven Changes to In-Use Heavy-Duty Diesel Truck Emissions of Nitrogenous Species and Related Environmental Impacts. Environ. Sci. Technol. 53, 14568–14576. https://doi.org/10.1021/acs.est.9b04763

Pusede, S.E., Cohen, R.C., 2012. On the observed response of ozone to NO_x and VOC reactivity reductions in San Joaquin Valley California 1995-present. Atmos. Chem. Phys. 12, 8323–8339. https://doi.org/10.5194/acp-12-8323-2012

Qin, M., Yu, H., Hu, Y., Russell, A.G., Odman, M.T., Doty, K., Pour-Biazar, A., McNider, R.T., Knipping, E., 2019. Improving ozone simulations in the Great Lakes Region: The role of emissions, chemistry, and dry deposition. Atmos. Environ. 202, 167–179. https://doi.org/10.1016/j.atmosenv.2019.01.025

Rakopoulos, C., Giakoumis, E., 2009. Diesel Engine Transient Operation. https://doi.org/10.1007/978-1-84882-375-4

Ramanathan, V., Carmichael, G., 2008. Global and regional climate changes due to black carbon. Nat. Geosci. 1, 221–227. https://doi.org/10.1038/ngeo156

Reff, A., Phillips, S., Eyth, A., Mintz, D., 2020. Preparations of Emissions Inventories for 2017 North American Emissions.

Ren, X., Salmon, O., Hansford, J., Ahn, D., Hall, D., Benish, S., Stratton, P., He, H., Sahu, S., Grimes, C., Heimburger, A., Martin, C., Cohen, M., Stunder, B., Salawitch, R., Ehrman, S., Shepson, P., Dickerson, R., 2018. Methane Emissions From the Baltimore-Washington Area Based on Airborne Observations: Comparison to Emissions Inventories. J. Geophys. Res. Atmos. 123. https://doi.org/10.1029/2018JD028851

Ridley, B.A., Grahek, F.E., 1990. A Small, Low Flow, High Sensitivity Reaction Vessel for NO Chemiluminescence Detectors. J. Atmos. Ocean. Technol. https://doi.org/10.1175/1520-0426(1990)007<0307:ASLFHS>2.0.CO;2

Sachse, G.W., Hill, G.F., Wade, L.O., Perry, M.G., 1987. Fast-Response, High-Precision Carbon Monoxide Sensor Using a Tunable Diode Laser Absorption Technique. J. Geophys. Res. 92, 2071–2081. https://doi.org/10.1029/JD092iD02p02071

Saha, P.K., Khlystov, A., Snyder, M.G., Grieshop, A.P., 2018. Characterization of air pollutant concentrations, fleet emission factors, and dispersion near a North Carolina interstate freeway across two seasons. Atmos. Environ. 177, 143–153. https://doi.org/10.1016/j.atmosenv.2018.01.019

Saliba, G., Saleh, R., Zhao, Y., Presto, A.A., Lambe, A.T., Frodin, B., Sardar, S., Maldonado, H., Maddox, C., May, A.A., Drozd, G.T., Goldstein, A.H., Russell, L.M., Hagen, F., Robinson, A.L., 2017. Comparison of Gasoline Direct-Injection (GDI) and Port Fuel Injection (PFI) Vehicle Emissions: Emission Certification Standards, Cold-Start, Secondary Organic Aerosol Formation Potential, and Potential Climate Impacts. Environ. Sci. Technol. 51, 6542–6552. https://doi.org/10.1021/acs.est.6b06509

Salmon, O.E., Shepson, P.B., Ren, X., He, H., Hall, D.L., Dickerson, R.R., Stirm, B.H., Brown, S.S., Fibiger, D.L., McDuffie, E.E., Campos, T.L., Gurney, K.R., Thornton, J.A., 2018. Top-Down Estimates of NO_x and CO Emissions From Washington, D.C.-Baltimore During the WINTER Campaign. J. Geophys. Res. Atmos. 123, 7705–7724. https://doi.org/10.1029/2018JD028539

Sather, M.E., Cavender, K., 2016. Trends analyses of 30 years of ambient 8 hour ozone and precursor monitoring data in the South Central U.S.: progress and challenges. Environ. Sci. Process. Impacts 18, 819–831. https://doi.org/10.1039/C6EM00210B

Schauer, J.J., Christensen, C.G., Kittelson, D.B., Johnson, J.P., Watts, W.F., 2008. Impact of Ambient Temperatures and Driving Conditions on the Chemical Composition of Particulate Matter Emissions from Non-Smoking Gasoline-Powered Motor Vehicles. Aerosol Sci. Technol. 42, 210–223. https://doi.org/10.1080/02786820801958742

Sher, E. (Ed.), 1998. Chapter 10: Combustion-Related Emissions in CI Engines, in:

Handbook of Air Pollution from Internal Combustion Engines: Pollutant Formation and Control. Academic Press.

Silvern, R.F., Jacob, D.J., Mickley, L.J., Sulprizio, M.P., Travis, K.R., Marais, E.A., Cohen, R.C., Laughner, J.L., Choi, S., Joiner, J., Lamsal, L.N., 2019. Using satellite observations of tropospheric NO_2 columns to infer long-term trends in US NO_x emissions: the importance of accounting for the free tropospheric NO_2 background. Atmos. Chem. Phys. Discuss. 8863–8878. https://doi.org/10.5194/acp-2019-168

Simon, H., Valin, L.C., Baker, K.R., Henderson, B.H., Crawford, J.H., Pusede, S.E., Kelly, J.T., Foley, K.M., Chris Owen, R., Cohen, R.C., Timin, B., Weinheimer, A.J., Possiel, N., Misenis, C., Diskin, G.S., Fried, A., 2018. Characterizing CO and NO_y Sources and Relative Ambient Ratios in the Baltimore Area Using Ambient Measurements and Source Attribution Modeling. J. Geophys. Res. Atmos. 123, 3304–3320. https://doi.org/10.1002/2017JD027688

Souri, A.H., Choi, Y., Jeon, W., Li, X., Pan, S., Diao, L., Westenbarger, D.A., 2016. Constraining NO_x emissions using satellite NO_2 measurements during 2013 DISCOVER-AQ Texas campaign. Atmos. Environ. 131, 371–381. https://doi.org/10.1016/j.atmosenv.2016.02.020

Statistics, B. of T., 2018. Estimated National Average Vehicle Emissions Rates per Vehicle by Vehicle Type Using Gasoline and Diesel [WWW Document]. URL https://www.bts.gov/content/estimated-national-average-vehicle-emissions-rates-vehicle-vehicle-type-using-gasoline-and

Travis, K.R., Jacob, D.J., Fisher, J.A., Kim, P.S., Marais, E.A., Zhu, L., Yu, K., Miller, C.C., Yantosca, R.M., Sulprizio, M.P., Thompson, A.M., Wennberg, P.O., Crounse, J.D., St Clair, J.M., Cohen, R.C., Laughner, J.L., Dibb, J.E., Hall, S.R., Ullmann, K., Wolfe, G.M., Pollack, I.B., Peischl, J., Neuman, J.A., Zhou, X., 2016. Why do models overestimate surface ozone in the Southeast United States? Atmos. Chem. Phys. 16, 13561–13577. https://doi.org/10.5194/acp-16-13561-2016

Tucker, W.G., 2000. An overview of $PM_{2.5}$ sources and control strategies. Fuel Process. Technol. 65, 379–392.

U.S. Department of Energy, 2021. Alternative Fuels Data Center - Fuel Properties Comparison.

US Department of Transportation Federal Highway Administration, 2014. Verification, Refinement, and Applicability of Long-Term Pavement Performance Vehicle Classification Rules.

US Department of Transportation Federal Highway Administration, 2006. Traffic Detector Handbook: Third Edition-Volume I.

US EPA, 2021a. Evolution of the Clean Air Act [WWW Document]. URL https://www.epa.gov/clean-air-act-overview/evolution-clean-air-act (accessed 10.1.22).

US EPA, 2021b. NAAQS Table for Criteria Air Pollutants [WWW Document]. URL https://www.epa.gov/criteria-air-pollutants/naaqs-table (accessed 10.1.22).

US EPA, 2021c. Ozone Trends [WWW Document]. URL https://www.epa.gov/air-trends/ozone-trends (accessed 10.1.22).

US EPA, 2021d. Regional Fuels and the Fuel Wizard in MOVES3.

US EPA, 2021e. Particulate Matter (PM) Basics [WWW Document]. URL https://www.epa.gov/pm-pollution/particulate-matter-pm-basics#effects

US EPA, 2021f. Basics of Climate Change [WWW Document]. URL https://www.epa.gov/climatechange-science/basics-climate-change#aerosols

US EPA, 2020a. The 2019 EPA Automotive Trends Report.

US EPA, 2020b. Emission Adjustments for Temperature, Humidity, Air Conditioning and Inspection and Maintenance for Onroad Vehicles in MOVES3 [WWW Document]. URL https://nepis.epa.gov/Exe/ZyPDF.cgi?Dockey=P1010M29.pdf

US EPA, 2020c. Emission Adjustments for Temperature , Humidity , Air Conditioning , and Inspection and Maintenance for On - road Vehicles in MOVES3.

US EPA, 2016. Fuel Supply Defaults: Regional Fuels and the Fuel Wizard in MOVES2014.

US EPA, 2015a. MOVES2014a User Guide.

US EPA, 2015b. Emission Adjustments for Temperature , Humidity , Air Conditioning , and Inspection and Maintenance for On - road Vehicles in MOVES2014.

US EPA, 2010a. Diesel Oxidation Catalyst General Information.

US EPA, 2010b. Highway Vehicle Temperature, Humidity, Air Conditioning, and Inspection and Maintenance Adjustments.

Wang, J.M., Jeong, C.H., Hilker, N., Shairsingh, K.K., Healy, R.M., Sofowote, U., Debosz, J., Su, Y., McGaughey, M., Doerksen, G., Munoz, T., White, L., Herod, D., Evans, G.J., 2018. Near-Road Air Pollutant Measurements: Accounting for Inter-Site Variability Using Emission Factors. Environ. Sci. Technol. 52, 9495–9504. https://doi.org/10.1021/acs.est.8b01914

Wang, X., Khlystov, A., Ho, K., Campbell, D., Chow, J.C., Kohl, S.D., Watson, J.G., Lee, S.F., Chen, L.A., Lu, M., Sai, S., Ho, H., 2019. Real-World Vehicle Emissions Characterization for the Shing Mun Tunnel in Hong Kong and Fort McHenry Tunnel in the United States. Boston, MA: Health Effects Institute.

Wang, Z., Du, H., Li, K., Miao, J., Li, M., Xu, B., 2021. Experimental Research on Distribution Characteristics of NO_x Conversion Efficiency of a Diesel Engine SCR Catalyst. ACS omega 6, 23083–23089. https://doi.org/10.1021/acsomega.1c02396

Weber, C., Sundvor, I., Figenbaum, E., 2019. Comparison of regulated emission factors of Euro 6 LDV in Nordic temperatures and cold start conditions : Diesel- and gasoline direct-injection. Atmos. Environ. 206, 208–217. https://doi.org/10.1016/j.atmosenv.2019.02.031

Wooldridge, P.J., Perring, A.E., Bertram, T.H., Flocke, F.M., Roberts, J.M., Singh, H.B., Huey, L.G., Thornton, J.A., Wolfe, G.M., Murphy, J.G., Fry, J.L., Rollins, A.W., Lafranchi, B.W., Cohen, R.C., 2010. Total Peroxy Nitrates (PNs) in the atmosphere: The Thermal Dissociation-Laser Induced Fluorescence (TD-LIF) technique and comparisons to speciated PAN measurements. Atmos. Meas. Tech. 3, 593–607. https://doi.org/10.5194/amt-3-593-2010

World Health Organization, 2022. Air Quality and Health - Types of Pollutants [WWW Document]. URL https://www.who.int/teams/environment-climate-change-and-health/air-quality-and-health/health-impacts/types-of-pollutants (accessed 10.1.22).

Xu, L., Kollman, M.S., Song, C., Shilling, J.E., Ng, N.L., 2014. Effects of NOx on the Volatility of Secondary Organic Aerosol from Isoprene Photooxidation. Environ. Sci. Technol. 48, 2253–2262. https://doi.org/10.1021/es404842g

Yang, J., Wen, Y., Wang, Y., Zhang, S., Pinto, J.P., Pennington, E.A., Wang, Z., Wu, Y., Sander, S.P., Jiang, J.H., Hao, J., Yung, Y.L., Seinfeld, J.H., 2021. From COVID-19 to future electrification: Assessing traffic impacts on air quality by a machine-learning model. Proc. Natl. Acad. Sci. 118. https://doi.org/10.1073/pnas.2102705118

Yu, S., Mathur, R., Pleim, J., Pouliot, G., Wong, D., Eder, B., Schere, K., Gilliam, R., Rao, S.T., 2012. Comparative evaluation of the impact of WRF/NMM and WRF/ARW meteorology on CMAQ simulations for PM2.5 and its related precursors during the 2006 TexAQS/GoMACCS study. Atmos. Chem. Phys. 3, 149–162. https://doi.org/10.5194/acp-12-4091-2012

Zeldovich, Y.B., 1946. The Oxidation of Nitrogen in Combustion Explosions. Acta Physicochim. 21, 577–628.

Zeng, N., Han, P., Liu, Zhiqiang, Liu, D., Oda, T., Martin, C., Liu, Zhu, Yao, B., Sun, W., Wang, P., Cai, Q., Dickerson, R., Maksyutov, S., 2021. Global to local impacts on atmospheric CO_2 from the COVID-19 lockdown, biosphere and weather variabilities. Environ. Res. Lett. 17, 15003. https://doi.org/10.1088/1748-9326/ac3f62

Zimmerman, N., Wang, J.M., Jeong, C.H., Wallace, J.S., Evans, G.J., 2016. Assessing the Climate Trade-Offs of Gasoline Direct Injection Engines. Environ. Sci. Technol. 50, 8385–8392. https://doi.org/10.1021/acs.est.6b01800